# Refining the physical and temporal record of metamorphism during the Delamerian Orogeny

Thesis submitted in accordance with the requirements of the University of Adelaide for an Honours Degree in Geology

Melissa Danielle Stinear

November 2017

THE UNIVERSITY
of ADELAIDE

# REFINING THE PHYSICAL AND TEMPORAL RECORD OF METAMORPHISM DURING THE DELAMERIAN OROGENY

## RUNNING TITLE

Refining the record of metamorphism during the Delamerian Orogeny.

## ABSTRACT

The Delamerian Orogen formed via convergence against the southeastern margin of the Gawler Craton during the Late Cambrian and is characterised by low-P, high-T metamorphism. The evolution of the Delamerian Orogen has been extensively studied by several authors through U-Pb zircon and Sm/Nd geochronology, but lacks fundamental characterisation of its thermal history. Metamorphic studies, of where there are few, suggest an 'anticlockwise' P-T evolution for the Delamerian Orogen. Garnet-staurolite-andalusite-bearing and sillimanite-bearing metapelites in this study were investigated using U-Pb LA-ICP-MS and have metamorphic monazite ages between 514-480Ma. Calculated phase equilibria modelling constrains metamorphism in the andalusite-staurolite-bearing schists to ~4.6kbar and 570°C, to 3.7kbar and 635°C in the sillimanite-bearing schists, and 1.0-4.4kbar and 790-860°C in the highest-grade parts of the orogen. The coupled $^{206}Pb/^{238}U$ monazite ages and phase equilibria modelling suggest that the crust deformed in temporal association with the repeated intrusions of granitic material that weakened the comparatively rigid mid-upper crust, leading to the formation of temporally discrete 'anticlockwise' P-T paths. Older metamorphic ages on Kangaroo Island and younger ages on mainland South Australia indicate that the thermal locus moved northwards over time, resulting in a metamorphic terrain that gives the appearance of a patchwork orogen of discrete metamorphic sub-domains, with the highest-grades surrounding granitic intrusions which occur late in the evolution of the Delamerian Orogen.

## KEYWORDS

Delamerian Orogeny, metamorphism, monazite, U-Pb geochronology, P-T pseudosection

**TABLE OF CONTENTS**

## LIST OF FIGURES AND TABLES

**INTRODUCTION**

The southern Adelaide Fold Belt forms part of the Delamerian Orogen (Fig. 1), which formed via convergence along the southeastern margin of the Gawler Craton during the Late Cambrian (Foden *et al*, 1999). The orogen encompasses the Adelaide Hills, the Fleurieu Peninsula and into Kangaroo Island, and forms part of an extensive orogenic system that extends down into Tasmania and further south to the Transantarctic Mountains in Antarctica, where it is known as the Ross Orogen (Foden *et al*, 2006; Boger & Miller, 2004). Deformation was immediately preceded by deposition of the Cambrian Normanville and Kanmantoo groups, which was accompanied by mafic volcanism, suggesting an extensional tectonic regime (Foden *et al*, 1999). The onset of Delamerian-aged convergence at terminated Kanmantoo Group sedimentation and initiated inversion and deformation of the basin (Alias et al, 2002; Flottman *et al*, 1995; Weinberg *et al*, 2013).

A large number of studies have focused on the deformational, metamorphic and igneous evolution of the Delamerian Orogen. However, few studies have provided quantitative thermobarometry coupled with age data. The Delamerian Orogen is characterized by low pressure, high temperature metamorphism (Foden *et al*, 2002; Sandiford et al, 1992). Foden *et al* (2006) argued that convergent deformation ceased by $493 \pm 1$Ma. That age constraint on the end of deformation primarily comes from igneous relationships. However, there have been essentially no studies that directly date the minerals that grew during peak metamorphism in different areas of the orogen. Recent U-Pb monazite data from an orthopyroxene-cordierite bearing granulite in the eastern Mt Lofty Ranges gives an age of $483 \pm 4$Ma (Bockmann unpublished, 2016), an

age that it significantly younger than the inferred end of convergence. Further south on Kangaroo Island, Weinberg *et al* (2013) used monazite geochronology to date granitic rocks from within the diaxtexites on Kangaroo Island. They found that both samples have a similar extent of continuous ages from 495-465Ma, and suggest that this continuous age range is indicative of a large single partial melting event, lasting between 495-465Ma.

In the central Mount Lofty Ranges, closely spaced metamorphic isograds show increasing metamorphic grade southward toward region dominated by granitic magmatism (Cartwright, Vry & Sandiford, 1995; Dymocke & Sandiford, 1992; Sandiford *et al*, 1995). The age of the isograds is unknown and based on the broad age constraints of the orogen, can range in age between 515-485Ma. Furthermore, it is not known whether the isograd sequence represents a single metamorphic progression or is the result of two superimposed events with the second being of higher intensity to the south. Therefore, the quantitative characterization of the thermal (metamorphic) history of the Delamerian Orogen is unknown. This results in an overall lack of understanding of the thermal character of the orogen.

In this study, metasedimentary rocks are used to constrain the thermal structure of the Delamerian Orogen. Calculated P-T pseudosections for metapelites throughout the orogen are coupled with U-Pb LA-ICP-MS geochronology of in-situ monazite to constrain the P-T history. Collectively, these results offer insight into the metamorphism and geodynamics of the Delamerian Orogen.

**GEOLOGICAL SETTING**

The Ross-Delamerian Orogen formed along Gondwana's Pacific margin, and marks a change from a passive to active margin when convergence and subduction were initiated at ~560-540Ma (Boger & Miller, 2004; Foden $et$ $al$, 2006). U-Pb zircon dating of volcaniclastic rocks from the Ross Orogen indicates that convergent tectonism began at this time. Initiation of subduction is proposed to have been due to a continent-arc collision; however, subduction was not pervasive along Gondwana's Pacific margin (Boger & Miller, 2004). Instead, extension continued along the continental margin of what is now South Australia until ~515Ma (Boger & Miller, 2004). The early compressional phase of the Delamerian Orogeny involved west-vergent thrusts (Flottman $et$ al, 1995; Foden $et$ al, 2002) ($D_1$), and the development of a low-angle $S_1$ fabric, which was then overprinted by tight to open upright folds ($D_2$ and $D_3$) (Offler $et$ $al$, 1968; Oliver & Zakowski, 1995).
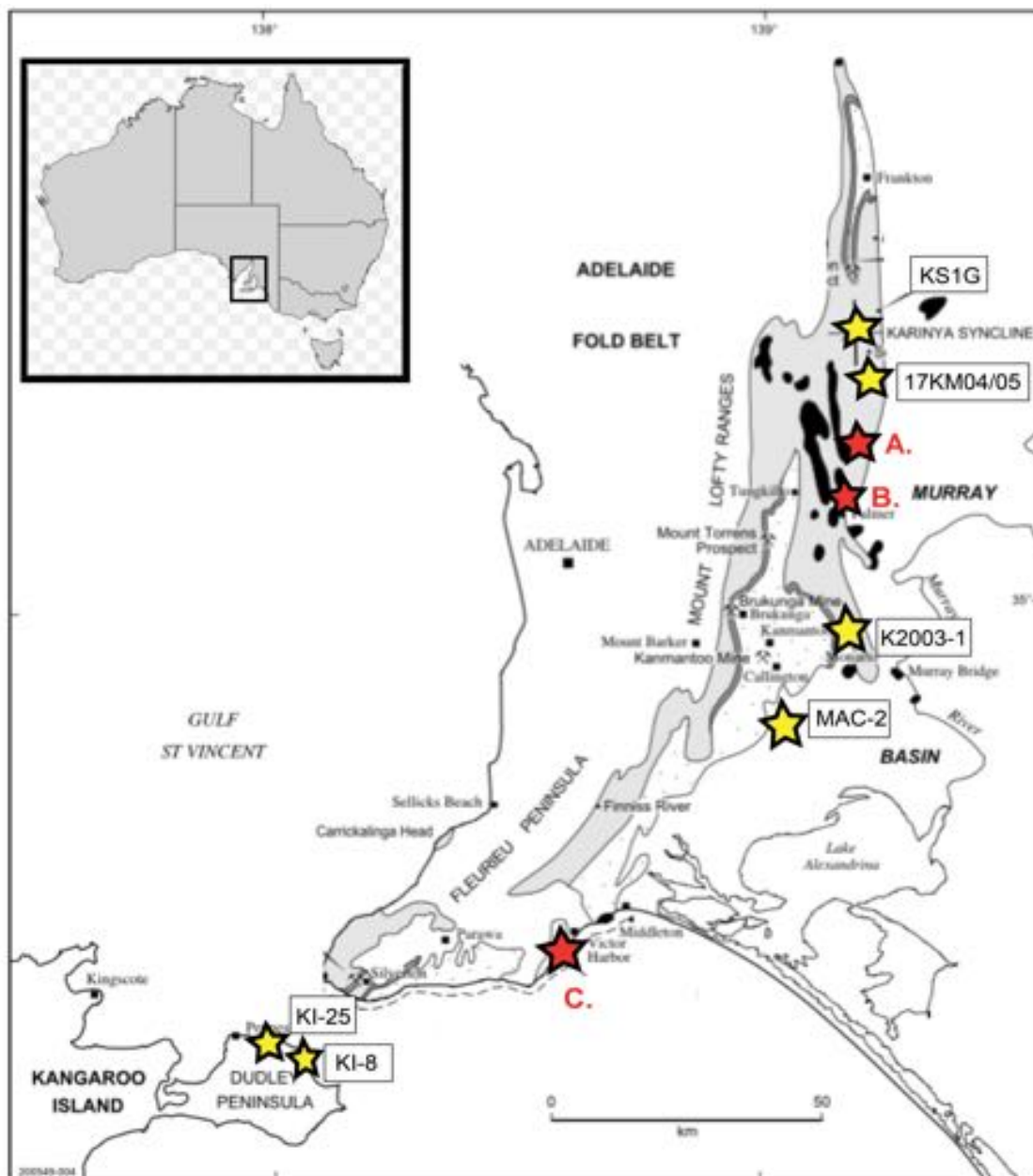
**Figure 1: Sample location map adapted from Jago et al (2003). Yellow stars: sample locations from this study. Red stars – sample locations from previous work. (A) Rathjen Gneiss dated at 514 ±4Ma (Foden et al, 2006). (B) Orthopyroxene-cordierite bearing granulite from Reedy Creek dated at 483±4Ma (Bockmann, unpublished, 2016). (C) Petrel Cove – anticlockwise P-T path interpreted (Alias et al, 2002).**

The southern Adelaide fold-thrust belt consists of four principal lithotectonic units; Mesoproterozoic crystalline basement (granitoid, gneiss and schist units), the Adelaidean supersequence (Neoproterozoic), Cambrian metasediments and volcanics and the Delamerian-aged granitoids (Marshak & Flottmann, 1996).

## Basement

The Mesoproterozoic basement of the Adelaide Fold-Thrust Belt consists of 1.75-1.6Ga granitoids, gneiss and schist units (Marshak & Flottmann, 1996; Morrisey *et al*, 2013).

## Adelaidean Supersequence

The late Proterozoic (~850-600Ma) Adelaidean-aged sediments were deposited in a series of relatively shallow water basins within, or on the margin of the basement of the Gawler Craton (Sandiford *et al*, 1992; Turner *et al*, 1994).  The rocks are unmetamorphosed to very low grade sandstones, mudstones and diamictons with some carbonates and volcanic tuffs, and thickens from the south to the north (Marshak & Flottmann, 1996; Boger & Miller, 2004).

## Cambrian rocks

A second or renewed phase of sedimentation occurred during the early Cambrian, where the basal Normanville Group and overlying Kanmantoo Group were deposited in the Stansbury Basin (Alessio *et al*, 2017; Foden *et al*, 2006).  The Normanville Group consists of deformed limestones, shales, sandstones and the Truro Volcanics.  Zircon dating of a volcanic tuff layer places the beginning of this phase of sedimentation at 526 ± 4Ma (Cooper *et al*, 1992).  Overlying this unit is the highly deformed Kanmantoo Group, which consists of thick (up to 8km) clastic strata, including deep-water turbiditic

sequences of greywacke and shale (Marshak & Flottmann, 1996; Haines & Flottman, 1998; Turner *et al*, 1994). Deposition of the Kanmantoo Group has been dated to ~522Ma, and is proposed to have been deposited rapidly, as the earliest intruded granitic pluton is dated to 514 ±4Ma (Foden *et al*, 2006). Deposition of the Normanville and Kanmantoo groups immediately preceded the onset of the Delamerian Orogeny, and have been variably deformed and metamorphosed during convergence. The Kangaroo Island Group is a fine-grained shallow water sequence that overlies the southern margin of the Gawler Craton, and is confined to northern Kangaroo Island (Haines & Flottman, 1998; Flottmann *et al*, 1995). The external foreland of the orogen (W/NW margin) is characterized by low-grade metasedimentary rocks (subgreenschist to greenschist facies) whereas the internal parts of the belt (E/SE margin) are characterized by higher metamorphic grades (greenschist to amphibolite facies) with abundant felsic magmatic rocks (Alias *et al*, 2002).

**Delamerian granitoids**

The onset of the Delamerian Orogeny is marked by the inversion of late Proterozoic and early-Cambrian extensional basins. The earliest granitic intrusions marks the onset of Delamerian-aged convergence is the Rathjen Gneiss at 514±4Ma (Foden *et al*, 2006), which intrudes the Kanmantoo Group (Turner *et al*, 2009). Two distinct granitic phases are recognized in the southern Adelaide fold-belt. The first is an older, dominantly I-type (transitioning through to S-type) granitic suite. These syntectonic granites have ages spanning 514Ma-490Ma, and thus appear to have been generated through the convergent deformation history (Sandiford *et al*, 1992). Sandiford *et al* (1995) suggest that these deformed syntectonic intrusives, including the Rathjen Gneiss and Reedy Creek Granodiorite, may have provided some of the heat for metamorphism due to

concentric zoning of isograds surrounding the intrusive bodies. The cessation of

convergence is marked by a change in granitic composition, from the I- to S-type

syntectonic granites to an undeformed, post-tectonic suite of bimodal A-type granites,

dated to 490-480Ma (Foden *et al*, 2006).
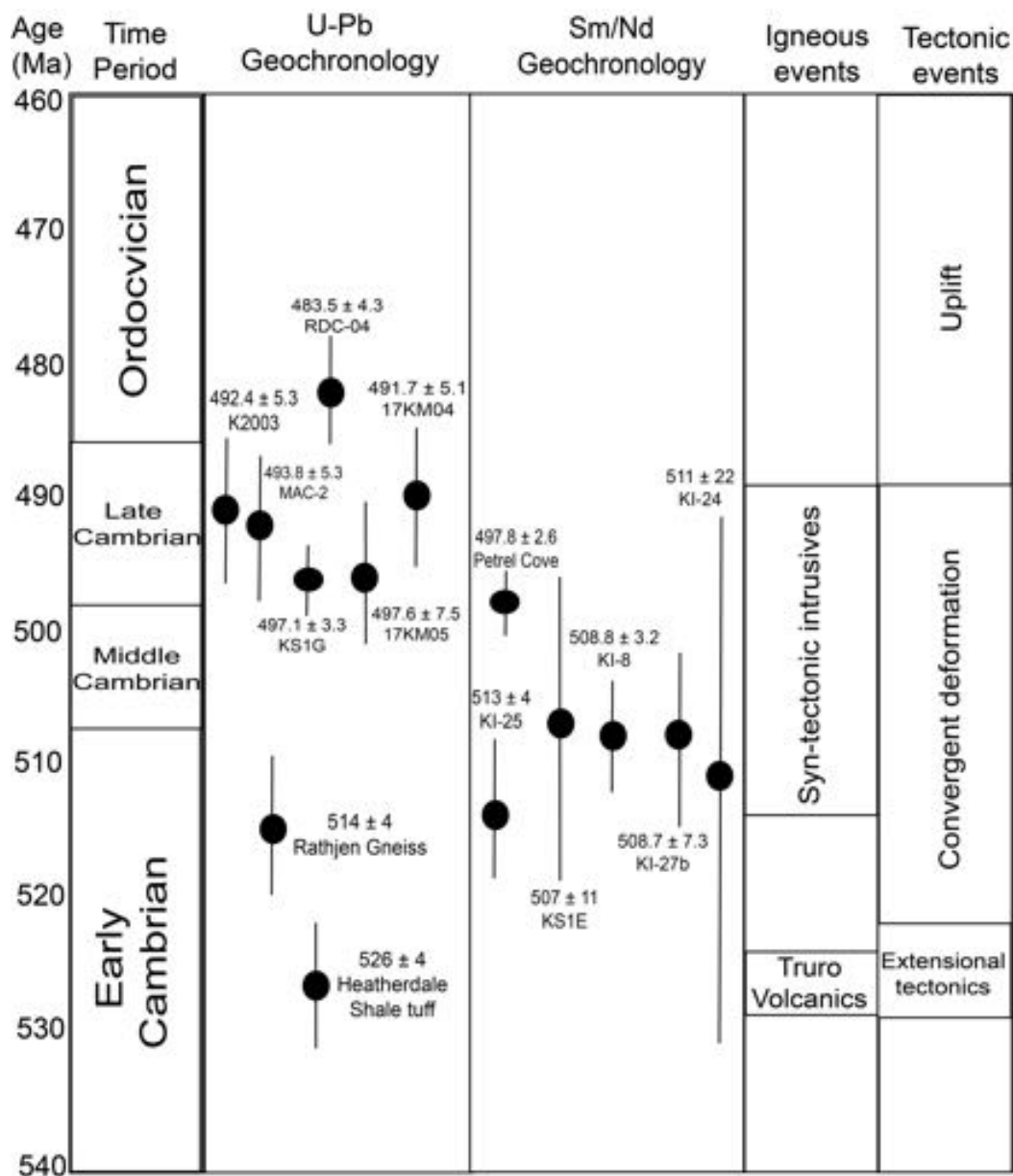


**Figure 2: Time-space plot compiled for the current literature. Rathjen Gneiss age: Foden *et al*, 2006. Heatherdale Shale Tuff age: Cooper *et al*, 1992. Sm/Nd data provided by Hand, unpublished, pers comms.**

## Metamorphism

Within the Kanmantoo Group, metamorphism in the Delamerian Orogen is low-pressure, high temperature, with migmatite zones developed around syn-tectonic intrusive plutons (Dymocke & Sandiford, 1992; Jenkins & Sandiford, 1991). Metamorphic grade increases to the east, from chlorite facies to andalusite- to sillimanite-bearing assemblages, and migmatite zones (Direen *et al*, 2005). Dymocke & Sandiford (1992) suggest that the peak temperature was attained later in lower
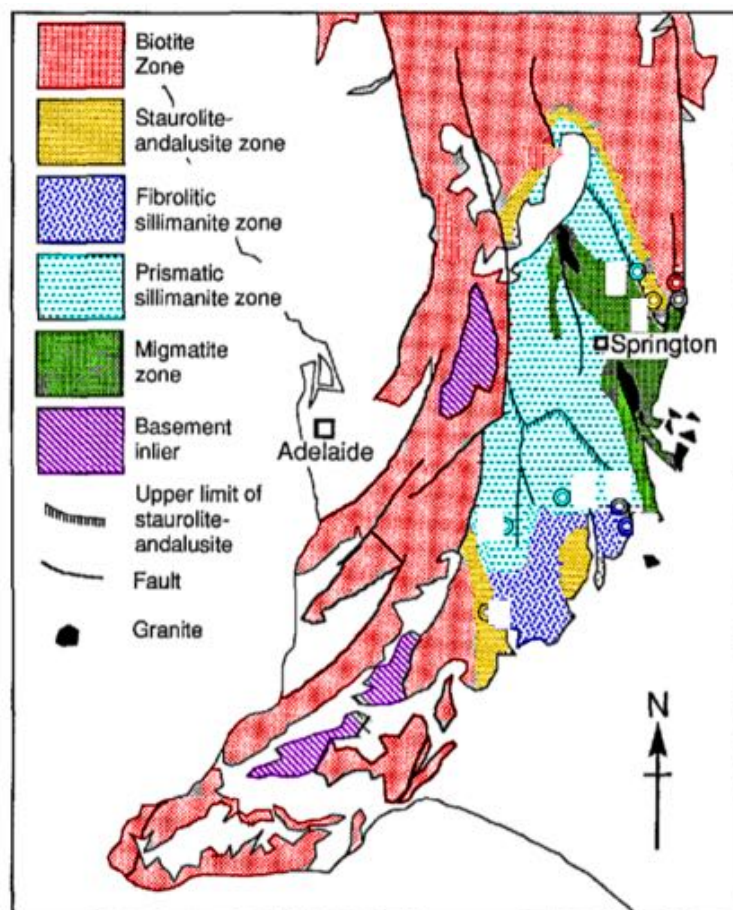


**Figure 3: Geological map of the Adelaide Fold Belt showing the regional metamorphic zonation adapted from Dymocke & Sandiford (1992).**

grade regions than higher-grade regions due to lateral heat transfer away from granitic intrusions based on the regional arrangement of isograds (Fig. 3). They also suggest that the isograd arrangements reflect an essentially isobaric metamorphic field gradient with maximum temperature gradients of around 10°C/km. The only quantitative thermobarometric work done on the Delamerian Orogen is from Alias *et al* (2002) for aluminosilicate-cordierite-staurolite-bearing schists from Petrel Cove, within the thermal aureole Victor Harbour Granite, concluding that the rocks at Petrel Cove followed an anticlockwise P-T path.

SAMPLE PETROGRAPHY

In the following descriptions, the logic that peak minerals are coarser grained and/or defines a fabric and that retrograde minerals define either no fabric and are finer-grained is applied.  The modal abundance ('mode') of porphyroblasts in each sample are provided in Table 1 because this data is used to constrain P-T conditions.

MAC-2

Matrix minerals consist of biotite (*tabular)*, muscovite (*tabular)* and quartz.  The dominant fabric of the sample is defined by biotite and muscovite, with $S_1$ and $S_2$ fabrics observed throughout (Fig. 4a).  Porphyroblasts of garnet and staurolite are typically separated.  Garnet contains inclusions of quartz.  Staurolite contains inclusions of quartz, biotite and some muscovite.  Accessory minerals include monazite and zircon, and less commonly xenotime, which mainly occur within the dominant fabric and less commonly, as inclusions in garnet.  The interpreted peak assemblage is biotite + muscovite + garnet + staurolite + ilmenite. Two generations of chlorite occur, the first being obliquely oriented to the dominant fabric, and is interpreted to be retrograde in origin.  The second is observed parallel to $S_2$, and is interpreted to have grown as $S_2$ continued to develop. Staurolite and garnet both occur within the retrograde foliation, thus some staurolite and garnet is interpreted to have been stable during the retrograde history.

KS1G

Matrix minerals consist of biotite (*tabular*), muscovite (*tabular)* and quartz.  Biotite and muscovite weakly define the primary fabric throughout the sample.  Andalusite poikiloblasts contain inclusions of quartz, biotite and garnet (Fig. 4b).  Staurolite

12

porphyroblasts contain inclusions of quartz and biotite. Accessory minerals, monazite, zircon, occur throughout the sample within the dominant fabric and as inclusions in andalusite. The interpreted peak assemblage is garnet + biotite + staurolite + quartz + muscovite + ilmenite. Chlorite grains occur perpendicular to the dominant fabric, and are interpreted to be retrograde in origin. Some muscovite is also interpreted to be retrograde, for the same argument presented above for chlorite.

K2003-1

The matrix consists of tabular biotite and muscovite, quartz and ilmenite (Fig. 4c). The dominant fabric in the sample is defined by biotite and muscovite. Porphyroblasts of garnet, staurolite and andalusite are separated and the foliation wraps around them. Garnet porphyroblasts contain inclusions of quartz. Staurolite is poikiloblastic and has typically euhedral, equant grains, with numerous inclusions of quartz, muscovite and biotite. Andalusite grains are poikiloblastic, subhedral and contain inclusions of quartz, biotite and ilmenite. Garnet grains are commonly fractured with fine-grained biotite and chlorite. Accessory minerals include monazite, zircon and xenotime, which mainly occur in the dominant fabric and as inclusions in andalusite, staurolite and garnet. The interpreted peak assemblage is garnet + staurolite + andalusite + muscovite + quartz + biotite + ilmenite. Retrograde chlorite occurs within the cracks in garnet, and porphyroblasts obliquely and perpendicularly oriented to the dominant fabric.

17KM04

Matrix minerals consist of quartz, biotite, muscovite, potassium feldspar and plagioclase. Biotite, quartz and muscovite define the pervasive foliation. Sillimanite occurs as both prismatic grains and fibrolite (Fig. 4d). Fibrolite replaces relic

andalusite. Accessory minerals include monazite and zircon. The interpreted peak assemblage is quartz + sillimanite + biotite + muscovite + plagioclase + ilmenite. A second morphology of muscovite occurs, growing across the pervasive foliation, and is interpreted to be retrograde in origin.


17KM05

Matrix minerals consist of quartz, biotite, potassium feldspar, muscovite and some plagioclase. Biotite, muscovite and quartz define a pervasive foliation throughout (Fig. 4e). Sillimanite occurs as prismatic grains as well as fibrolite. Accessory minerals include monazite and zircon. The interpreted peak assemblage is quartz + sillimanite + biotite + muscovite + plagioclase + ilmenite. Late muscovite is observed growing across the pervasive foliation.


RDC-02

Sample RDC-02 contains biotite, cordierite, plagioclase and ilmenite. Cordierite and plagioclase are the two primary matrix minerals. There are two morphologies of biotite. Some biotite grains are aligned to define a weak foliation, whereas other biotite grains are randomly oriented (Fig. 4f). Biotite grains contain inclusions of accessory minerals monazite and zircon, as well as ilmenite. The peak assemblage is interpreted to be plagioclase + biotite + cordierite + ilmenite.


KI-25

Sample KI-25 contains biotite, andalusite, staurolite, muscovite, garnet, chlorite, plagioclase, quartz and ilmenite. Matrix minerals include quartz, plagioclase, ilmenite and biotite. Biotite, muscovite and quartz define the strong pervasive foliation, which

wraps around andalusite porphyroblasts.  There are two morphologies of muscovite, the first within the foliation and one which cross cuts the foliation and is hence interpreted to be retrograde.  Retrograde chlorite cross cuts the foliation and grows aligned to the rim of some andalusite porphyroblasts.  Staurolite is localised to two locations, the first on the rim of an andalusite porphyroblast and the second within a portion of the foliation (Fig. 4g).  Garnet contains inclusions of quartz and ilmenite.  Andalusite contains inclusions of biotite and quartz. The interpreted peak assemblage is therefore andalusite + biotite + muscovite + plagioclase + ilmenite + quartz.

**Table 1: Summary of mineral modal proportions for each sample.  Mineral abbreviations used throughout this study include; g (garnet), st (staurolite), and (andalusite), mu (muscovite), bi (biotite), k-spar (potassium feldspar), pl (plagioclase), chl (chlorite), sill (sillimanite), q (quartz).**

| SAMPLE | MINERAL PROPORTION | | | | | | | | TOTAL |
|---|---|---|---|---|---|---|---|---|---|
|  | g | st | and | sill | bi | mu | q | chl | |
| **K2003-1** | <1% | 2.6% | 4.2% | - | ~34% | ~21% | ~33% | 2.6% | 98.4% |
| **MAC-2** | <1% | 4.8% | - | - | ~29% | ~25% | ~36% | 3.3% | 99.1% |
| **KS1G** | 1.1% | 2.4% | 5.9% | - | ~32% | ~22% | ~32% | 3.2% | 98.6% |
| **17-KM-04** | - | - | - | 5.3% | ~36% | ~19% | ~38% | - | 98.3% |
| **17-KM-05** | - | - | <1% | 3.5% | ~35% | ~20% | ~39% | - | 98.5% |
| **KI-25** | <1% | <1% | 6.6% | - | ~34% | ~19% | ~36% | 1.2% | 98.8% |
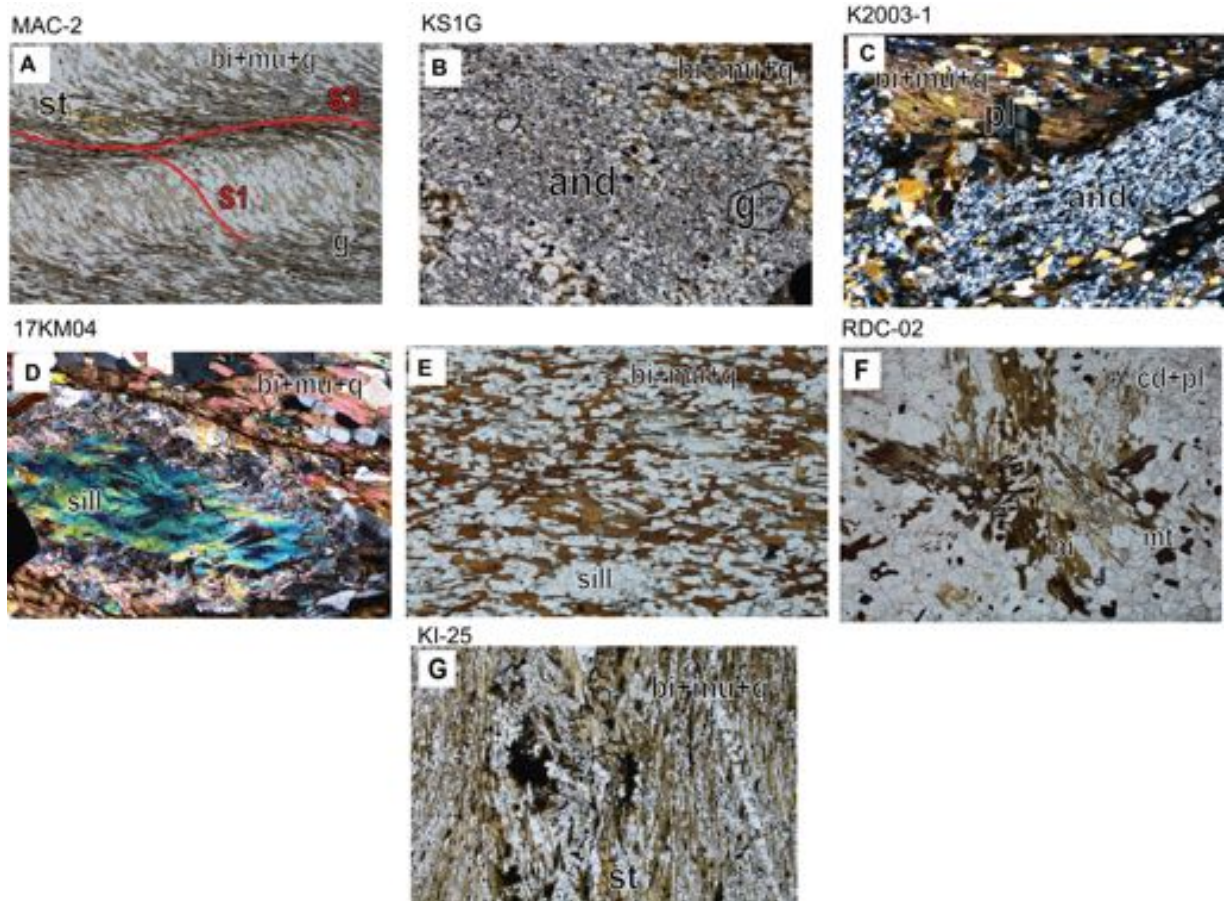
**Figure 4: Photomicrographs of samples used in this study: (A) S$_1$/S$_2$ fabric defined by biotite, muscovite and quartz. S$_1$ domains are quartz-rich. S$_2$ fabrics are defined primarily by biotite and muscovite. Chlorite occurs parallel to S$_2$ as S$_2$ developed; (B) Andalusite porphyroblasts coexisting with garnet; (C) Fine-grained plagioclase within biotite + muscovite fabric; (D) Sillimanite porphyroblasts occurring as fibrolite; (E) Pervasive biotite + muscovite foliation; (F) Randomly oriented biotite + magnetite in a cordierite + plagioclase matrix (G) Localised staurolite growing within biotite + muscovite + quartz foliation.**

## METHODS

## U-Pb geochronology

U-Pb monazite ages were acquired from samples MAC-2, KS1G, K2003-1, 17-KM-04, 17-KM-05 and RDC-02 and RDC-04 (data collected by Kiara Aleisso, unpublished, 2016) by LA-ICP-MS at Adelaide Microscopy for the purpose of dating metamorphism. Sample preparation and operational procedures for this technique is detailed in Appendix A.

**Electron Microprobe Analyses**

Mineral composition element analyses were undertaken at Adelaide Microscopy, using

a CAMECA SXFive electron microprobe.  Operational procedures are presented in

Appendix E.

**Phase equilibria forward modelling**

Phase equilibria calculations were performed using the software program

THERMOCALC in the model chemical system $MnO$-$Na_2O$-$CaO$-$K_2O$-$FeO$-$Mg$-$O$-

$Al_2O_3$-$SiO_2$-$H_2O$-$TiO_2$-$O$ (MnNCKFMASHTO), where 'O' is a proxy for $Fe_2O_3$, using

the latest internally-consistent thermodynamic dataset 'ds6' for Macintosh (filename tc-

dxmn.txt; Holland & Powell, 2011) and activity-composition models (Powell et al,

2014; White et al, 2014a; White el al, 2014b).  THERMOCALC calculations are using a

user-specified initial stable assemblage and calculating field boundaries and points.  The

diagram is built up from that initial stable assemblage, involving many trial and error

calculations in order to determine the phases that disappear or appear as a function of

pressure, temperature or composition.  The most uncertain compositional variables and

$Fe_2O_3$ and $H_2O$ (Kelsey & Hand, 2015), requiring that these be constrained with T-M

diagrams (where M refers to the amount of an oxide component) prior to the calculation

of the P-T pseudosection.  $T$-$M_o$ diagrams were calculated to assess the oxidation state

of the samples and are provided in Appendix F.  The pressure at which the $T$-$M_o$

diagram calculations were based on was determined by estimating the pressure at which

the observed peak metamorphic assemblage is stable; in this case, 3.5kbar.

Compositions chosen along the x-axis from the peak fields of the T-Mo diagrams for P-

T modelling were selected based on modal proportions of minerals that best estimated

the estimated modes.  Contouring of the phase equilibria models for the normalised

abundances (mode) of phases was calculated using automated software TCInvestigator v2.0 (Pearce *et al*, 2015).  The bulk compositions are presented as insets in the diagrams in 1 atom normalized to 100%.

## RESULTS

### Monazite U-Pb LA-ICP-MS geochronology

SAMPLE K2003-1

Thirty-eight analyses were collected from 38 individual in-situ monazite grains.  Of the thirty-eight analyses, sixteen analyses were excluded from age calculations due to discordance.  Of the twenty-two concordant analyses, three analyses were rejected based on their significant deviation from the dominant spread (monazite grains 8, 26 and 32).  The remaining nineteen analyses define a weighted average $^{206}Pb/^{238}U$ age of 492.4±5.3Ma (MSWD = 4.2, 95% conf.).

SAMPLE KS1G

Thirty-five analyses were collected from 35 individual in-situ monazite grains.  Of the thirty-five analyses, twenty-four analyses were excluded from age calculations.  The remaining data defines a concordia age of $^{206}Pb/^{238}U$ 497.1 ± 3.3 Ma (n = 11, MSWD = 8.2).  A linear probability plot for the analyses used to define the concordia age shows the spread of $^{206}Pb/^{238}U$ ages (i.e. between 488.1-507.6 Ma).

SAMPLE MAC-2

Thirty-four analyses were collected from 34 individual in-situ monazite grains.  Of the thirty-four analyses, nine analyses were excluded from age calculations due to discordance.  Of the twenty-five concordant analyses, the two oldest were rejected due to their significant deviation from the dominant spread (monazite grains 9 and 34).  The

remaining twenty-three analyses define a weighted average age of $^{206}Pb/^{238}U$

493.8±5.3Ma (MSWD = 4.4, 95% conf.).


SAMPLE 17-KM-04

Fifty-nine analyses were collected from 34 individual in-situ monazite grains.  Of those

fifty-nine analyses, forty-two analyses were excluded from age calculations due to

discordance.  The remaining seventeen analyses define a weighted average age of

$^{206}Pb/^{238}U$ 491.7±5.1Ma (MSWD = 5.2, 95% conf.).


SAMPLE 17-KM-05

Forty-three analyses were collected from 25 individual in-situ monazite grains.  Of

those forty-three analyses, twenty-eight analyses were excluded from age calculations

due to discordance.  Of the remaining fourteen analyses, two analyses were rejected due

to their significant deviation from the dominant spread (analyses 13 and 21).  The

remaining twelve analyses define a weighted average age of $^{206}Pb/^{238}U$ 497.6±7.5Ma

(MSWD = 8.2, 95% conf.).


SAMPLE RDC-02

Eleven analyses were taken from 8 individual in-situ monazite grains.  A linear

probability plot for the analyses shows the spread of $^{206}Pb/^{238}U$ ages.  The spread of this

data defines two groups occurring between 523.6-507.0 Ma and 466.3-423 Ma.  Three

data points define a concordia age of $^{206}Pb/^{238}U$ 515.1 ± 16Ma (n = 3, MSWD = 11.8).

SAMPLE RDC-04

Data collected by Kiara Bockmann from the University of Adelaide in 2016.  Thirty-five data points define a concordia age of $^{206}Pb/^{238}U$ 483.5 ± 4.3Ma (n = 35, MSWD = 2.6, 95% conf).  There is a continuous spread of data from 440-560Ma.
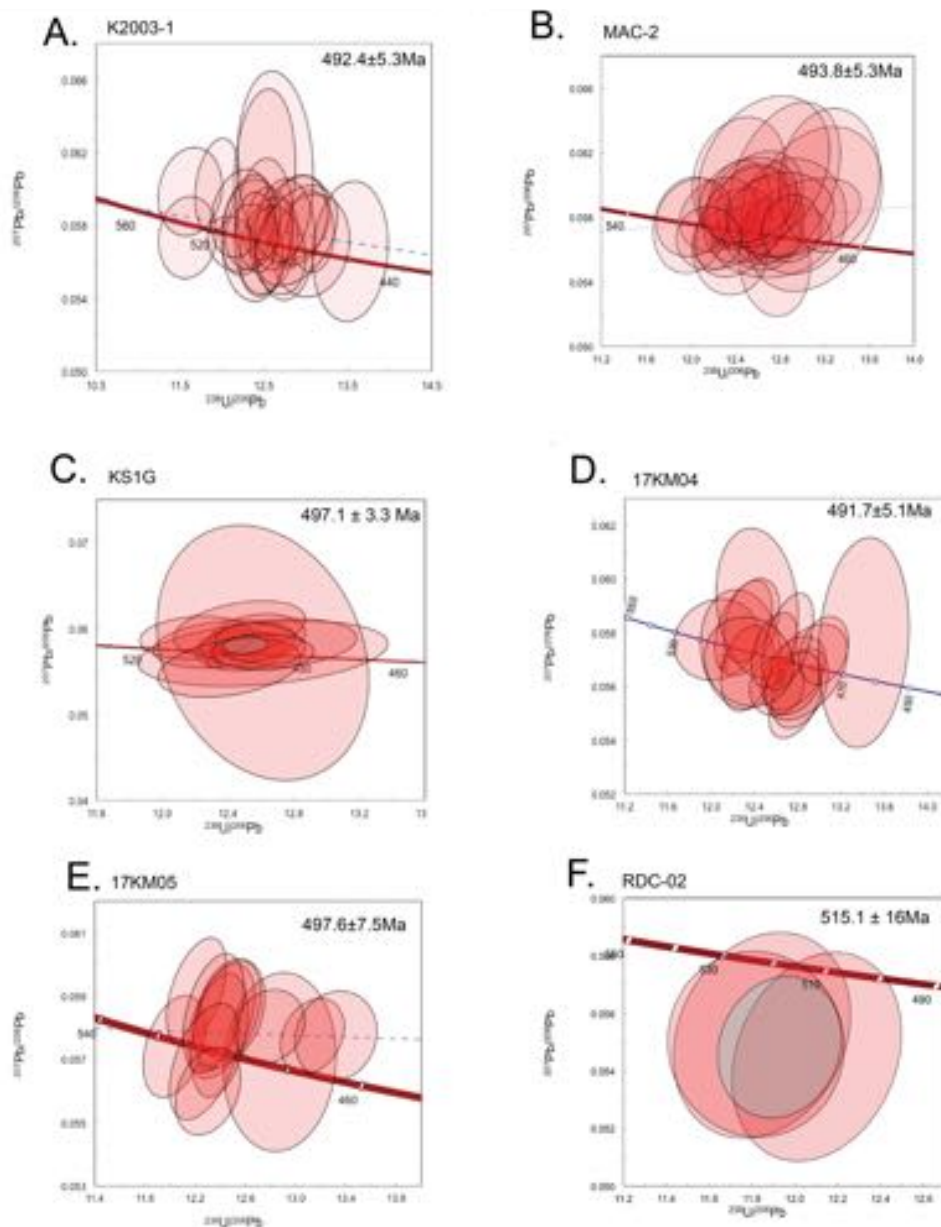


**Figure 5: Terra-Wasserburg concordia plots for monazite age data for all samples studied in this thesis.**
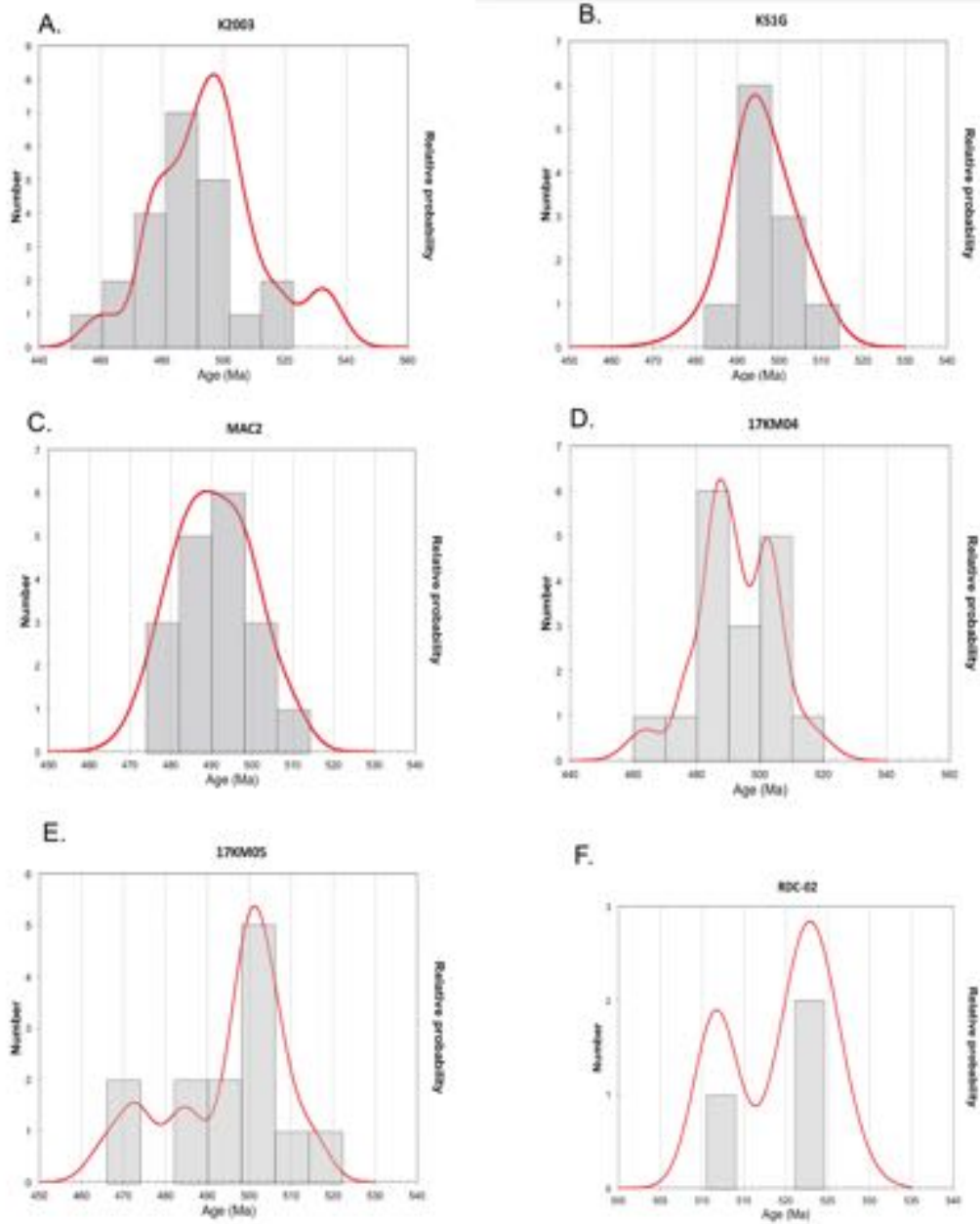
**Figure 6: Probability density plots of concordant monazite U-Pb LA-ICP-MS analyses.**
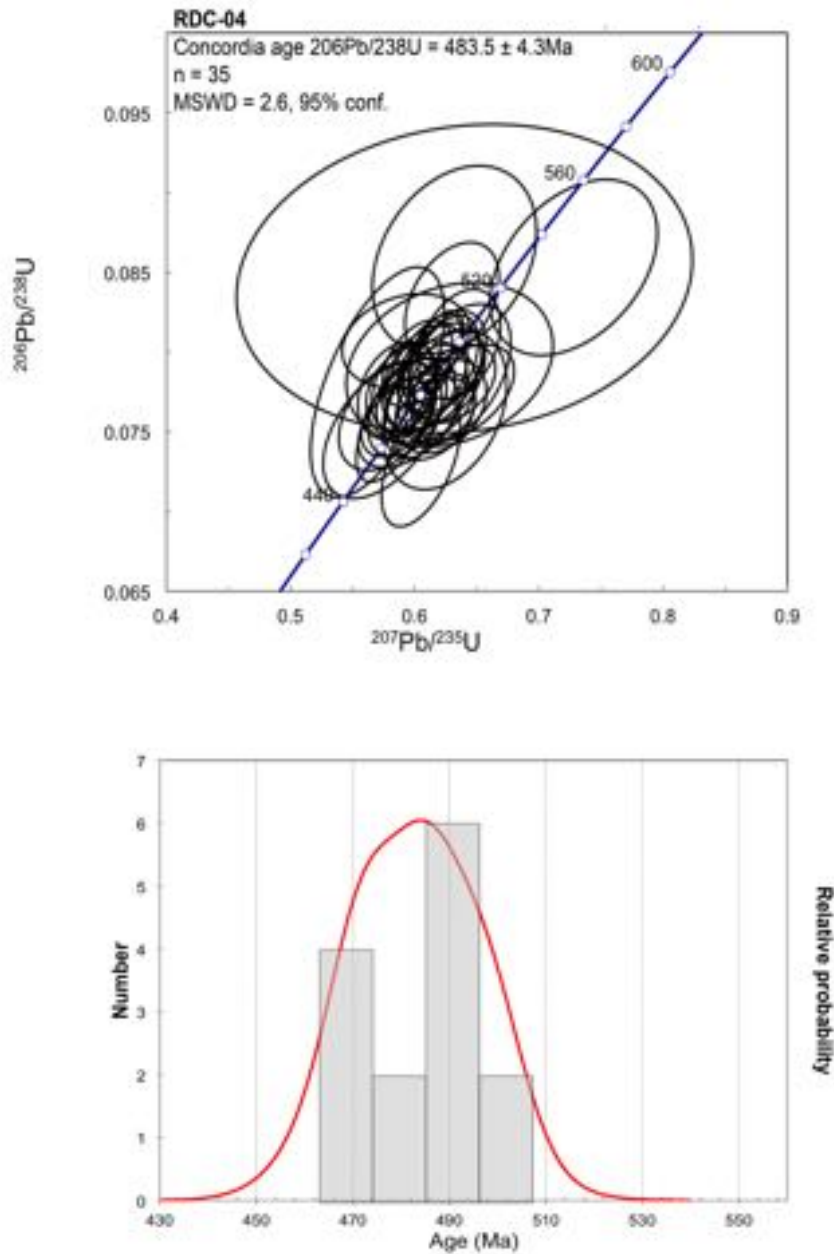
**Figure 7: (Top): Terra-Wasserburg concordia plot for sample RDC-04 compiled by Kiara Bockmann, unpublished, pers comms, defining a concordia age of 483.5 ± 4.3Ma (n = 35, MSWD = 2.6). (Bottom): Probability density plot of concordant monazite.**

## Monazite yttrium content

Concentrations for yttrium in monazite were collected for garnet-bearing samples

KS1G, K2003-1 and MAC-2 because yttrium (Y) is known to be a sensitive recorder of

the respective timing of garnet and monazite in metamorphic rocks (Foster *et al*, 2000;

Spear & Pyle, 2002; Williams *et al*, 2007). Monazites in sample K2003-1 have the

highest yttrium content (up to 11200 ppm) whereas monazites in sample MAC-2 have

the lowest yttrium content.
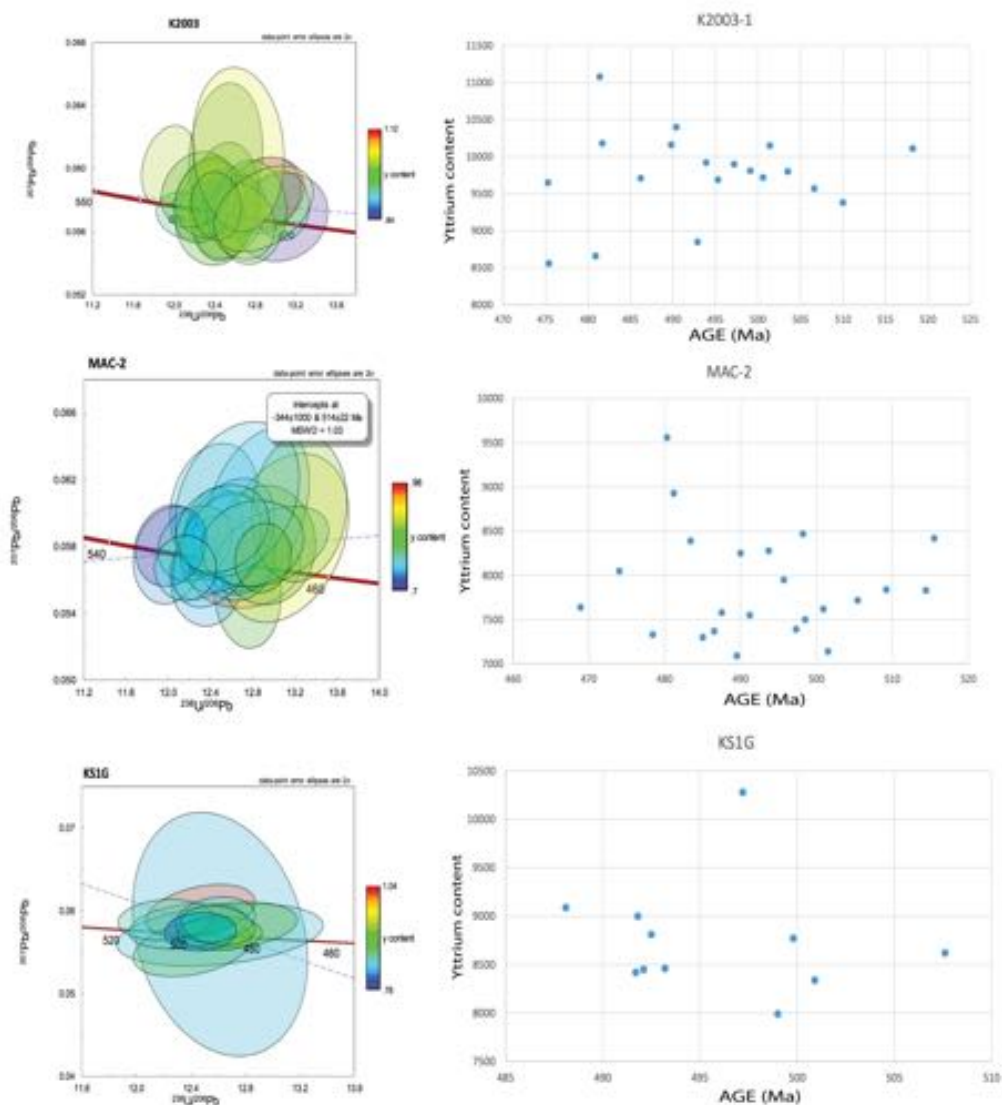


**Figure 8: Age vs yttrium content for garnet-bearing samples.**

## Sm/Nd geochronology

Sm/Nd dating was done on six samples from the Delamerian Orogen; KI-8, KI-14, KI-

25, KI-27b, Petrel Cove and KS1E (rock types summarized in Table 2, data from Hand,

unpublished pers com). Whole rock and garnet Sm-Nd results are shown in Table 2.

The Sm-Nd whole rock isochron for Petrel Cove yielded a younger age of 497.8 ±

2.6Ma (Fig. 9e) compared to all other samples. Kangaroo Island samples yield the

oldest ages, ranging from 508.7 ± 7.3Ma to 513 ± 4Ma.
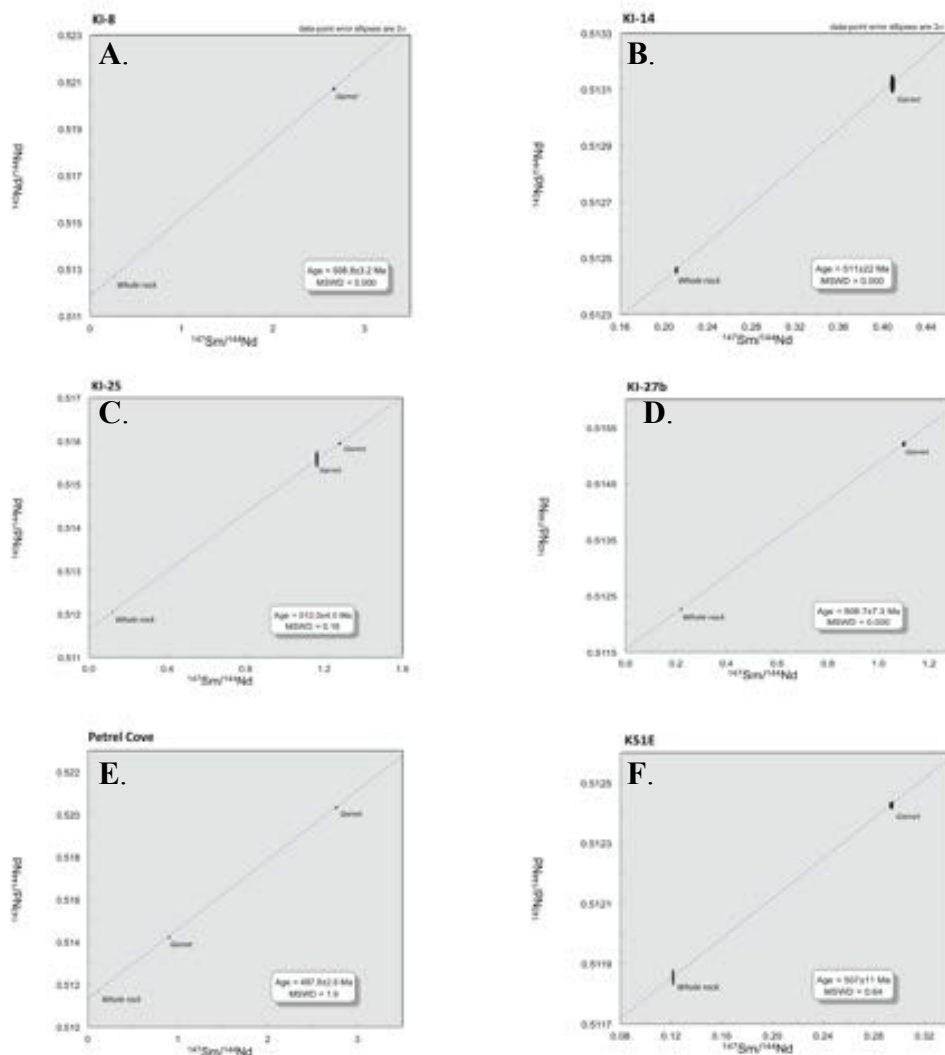


**Figure 9: Sm/Nd isochrons for samples KI-8, KI-14, KI-25, KI-27b, Petrel Cove and KS1E.**

**Table 2: Sm/Nd data obtained from Hand pers comms.  WR = whole rock**

| Sample | Rock type | | $^{147}Sm/^{144}Nd$ | ± | $^{143}Nd/^{144}Nd$ | ± | Initial $^{143}Nd/^{144}Nd$ | Age |
|---|---|---|---|---|---|---|---|---|
| **KI 8** | **Metased** | WR | 0.2753 | 0.00092 | 0.5127602 | 0.0000120 | 0.511843 ± 0.000015 | 508.8 ± 3.2 Ma |
| | | gt | 2.6586 | 0.00886 | 0.5207032 | 0.0000403 | | |
| **KI 14** | **Deformed pegmatitie vein** | WR | 0.211 | 0.00070 | 0.5124609 | 0.0000100 | 0.511753 ± 0.000035 | 511 ± 22 Ma |
| | | gt | 0.408 | 0.00136 | 0.5131201 | 0.0000260 | | |
| **KI 25** | **Metased** | WR | 0.122 | 0.00041 | 0.5120624 | 0.0000199 | 0.511651 ± 0.000022 | 513 ± 4 Ma |
| | | | 1.278 | 0.00426 | 0.5159435 | 0.0000164 | | |
| | | gt1 | 1.249 | 0.00416 | 0.5160064 | 0.0000473 | | |
| | | gt2 | 1.162 | 0.00387 | 0.5155871 | 0.0001532 | | |
| | | gt3 | | | | | | |
| | | WR | 0.122 | 0.00041 | 0.5120624 | 0.0000199 | | |
| | | gt1 | 1.278 | 0.00426 | 0.5159435 | 0.0000194 | | |
| | | gt3 | 1.162 | 0.00387 | 0.5155871 | 0.0001532 | | |
| **KI 27B** | **Undeformed pegmatitie** | WR | 0.221 | 0.00074 | 0.5122846 | 0.0000240 | 0.511547 ± 0.000031 | 508.7 ± 7.3 Ma |
| | | gt | 1.099 | 0.00366 | 0.5152076 | 0.0000330 | | |
| **Petrel Cove** | **Metased** | WR | 0.127 | 0.00042 | 0.5117500 | 0.0000209 | 0.511333 ± 0.000021 | 497.8 ± 2.6 Ma |
| | | gt1 | 0.908 | 0.00303 | 0.5142550 | 0.0000570 | | |
| | | gt2 | 2.758 | 0.00919 | 0.5203305 | 0.0000278 | | |
| **KS1E** | **Garnet-Staurolite schist** | WR | 0.1218 | 0.000405857 | 0.51185445 | 0.000009 | 0.511452 ± 0.000014 | 507 ± 11 Ma |
| | | WR 2 | 0.1217 | 0.000405682 | 0.51186442 | 0.000016 | | |
| | | gt | 0.2932 | 0.000977274 | 0.51242573 | 0.00001 | | |
| | | gt2 | 0.1218 | 0.00040586 | 0.51185445 | 0.000018 | | |

## Phase equilibria forward modelling

Temperature-Molar oxidation (T-$M_o$) (see Appendix G) and pressure-temperature (P-T) pseudosections were calculated for samples MAC-2, K2003-1, KS1G, 17KM04 and KI-25.  The objective of phase equilibria modelling was to constrain the P-T conditions for the five samples, hence developing the thermal framework for their metamorphic evolution.  The principle uncertainty in pseudosection modelling is in the determination of effective composition, particularly $Fe_2O_3$ (Kelsey & Hand, 2015) in this study.  The appropriate oxidation state, as $Fe_2O_3$ vs FeO amount for the P-T pseudosection was constrained for each of the five samples by calculating T-$M_o$ pseudosections first.  A fixed pressure is required for this calculation, which in this study was 3.5kbar based on

the observed mineral assemblages and is in within the range of pressures inferred from previous studies (eg. Alias *et al*, 2002).

SAMPLE MAC-2

The calculated P-T pseudosection is shown in Fig. 10. The interpreted peak assemblage is quartz + biotite + muscovite + plagioclase + garnet + staurolite + ilmenite. Obliquely and perpendicularly oriented chlorite and muscovite are interpreted to be retrograde in origin. The chosen oxidation state corresponds to the composition at Mo = 0.080 (Appendix G) on the basis that modal proportions of porphyroblasts estimated in Table 1 coincide with calculated modes of phases. The peak field in the calculated P-T pseudosection (Fig. 10) is constrained to conditions of ~4.7 kbar and 570 degrees (Fig. 10f). This field is bound by the occurrence of sillimanite up-temperature and chlorite down-temperature. The retrograde path is defined by the appearance of chlorite (Fig. 10c) and increasing mode of muscovite (Fig. 11e), defining a decreasing P-T evolution.

SAMPLE KS1G

The calculated P-T pseudosection is shown in Fig. 12. The interpreted peak assemblage is quartz + biotite + muscovite + plagioclase + garnet + staurolite + ilmenite. The chosen oxidation state corresponds to the composition at $M_o = 1.000$ on the basis that modal proportions estimated in Table 1 coincides with calculated modes of phases of porphyroblasts (Appendix G). The peak field in the calculated P-T pseudosection (Fig. 12) is constrained to conditions of ~4.6 kbar and 560 degrees (Fig. 13e). This field is bound by the occurrence of sillimanite up-temperature and chlorite down-temperature.

The retrograde path is defined by the appearance of chlorite (Fig. 13c) and increasing mode of muscovite (Fig. 13e).


SAMPLE K2003-1

The calculated P-T pseudosection is shown in Fig. 14.  The interpreted peak assemblage is quartz + biotite + muscovite + plagioclase + garnet + staurolite + ilmenite.   The chosen oxidation state corresponds to the composition at $M_o$ = 1.000 on the basis that modal proportions of porphyroblasts estimated in Table 1 coincides with calculated modes of phases (Appendix G).  The peak field in the calculated P-T pseudosection (Fig. 14) is constrained to conditions of ~4.8 kbar and 575 degrees (Fig. 15e).  This field is bound by the occurrence of sillimanite up-temperature and chlorite down-temperature.  The retrograde path is defined by the appearance of chlorite (Fig. 15c) and increasing abundance in muscovite (Fig. 15e).


SAMPLE 17-KM-04

The calculated P-T pseudosection is shown in Fig. 16.   The interpreted peak assemblage is biotite + muscovite + plagioclase + sillimanite + ilmenite + quartz.  The chosen oxidation state corresponds to the composition at $M_o$ = 0.070 on the basis that modal proportions estimated in Table 1 coincides with calculated modes of phases.  The peak field in the calculated P-T pseudosection (Fig. 16) is constrained to conditions of ~3.7 kbar and 635 degrees (Fig. 17e).  This field is bound by the occurrence of staurolite down-temperature and andalusite down-temperature.  The retrograde path is defined by the increasing mode of muscovite (Fig. 17a).

SAMPLE KI-25

The calculated P-T pseudosection is shown in Fig. 18. KI-25 has lower silica content than all other samples. The interpreted peak assemblage is garnet + staurolite + biotite + muscovite + + chlorite + ilmenite + quartz. The retrograde path is defined by the increasing mode of muscovite and chlorite (Fig. 19d).
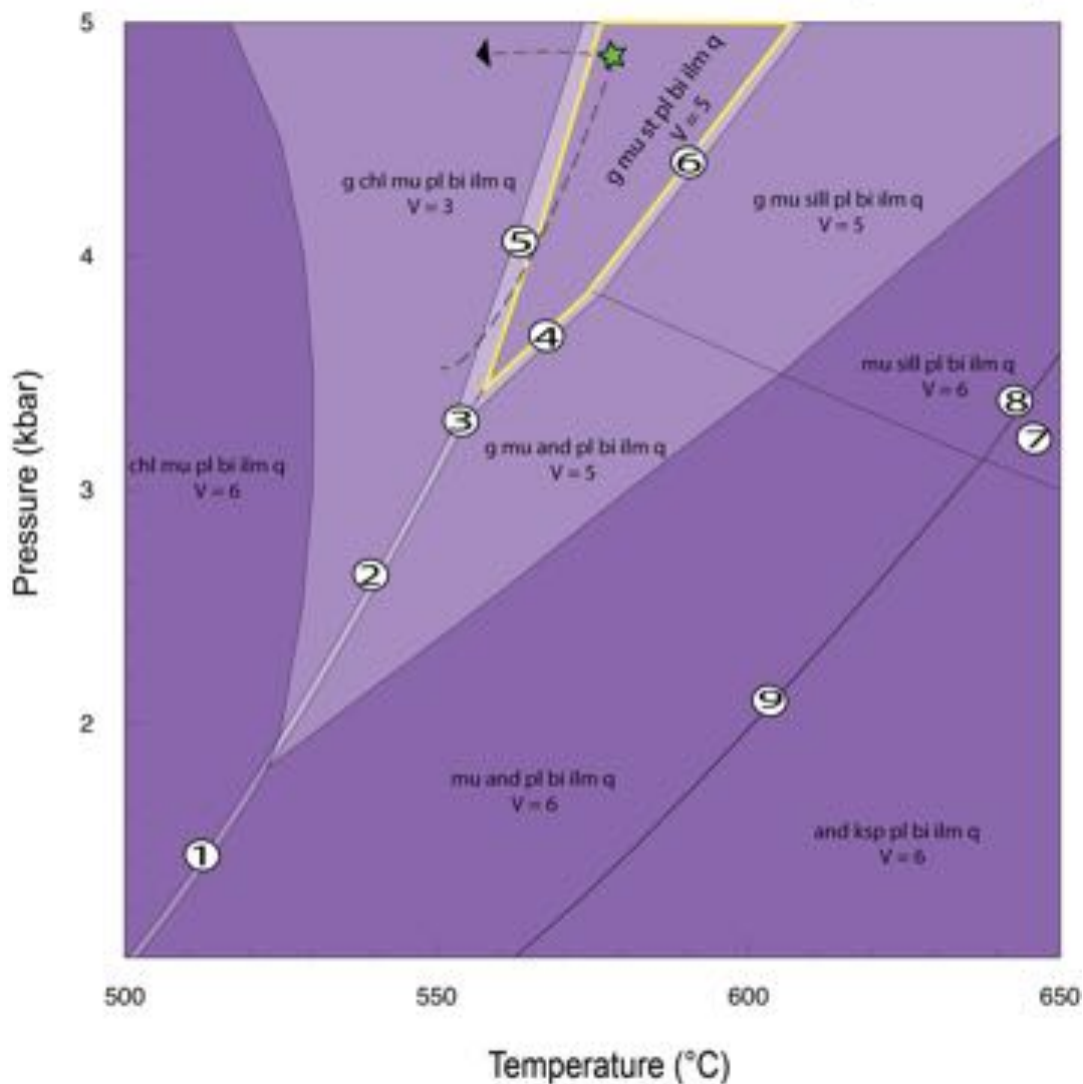
**Figure 10: Calculated P-T pseudosection for sample MAC-2. All fields in the diagram additionally contain water, H$_2$O, as part of the equilibrium assemblage. Fields too small to be directly labelled are identified by numbered circles corresponding to the assemblage occurring within the field. Progressively darker tones are representative of increasing variance, V, where V = components – phases + 2 (components = 10). The composition in mole % used to calculate the diagram, corresponding to that at M = 0.080 in Appendix G is provided above the diagram. The dashed line represents the interpreted P-T path. FeO* = FeO + 2 x 'O'.**
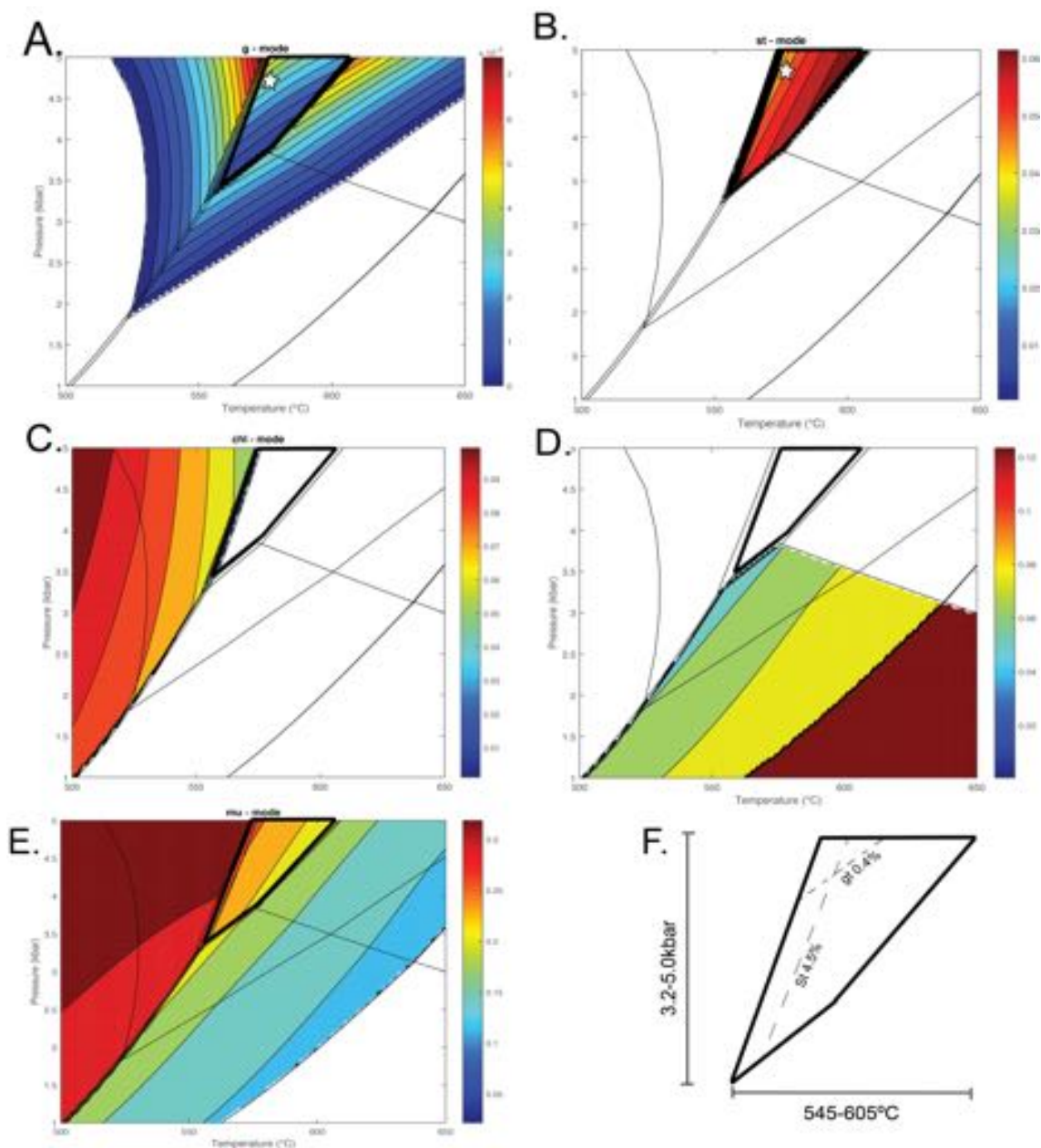
**Figure 11: Calculated P-T pseudosection for sample MAC-2 contoured for the abundance ('mode')
of some minerals.  The calculated abundances of phases in the peak assemblage (bold outline) were
used in conjunction with the estimated abundances of minerals in the sample (Table 1) to constrain
the peak P-T conditions experienced by the rock.  Diagram F shows the detail of the peak
assemblage field with calculated abundances of phase (combination of A and B), to further
constrain the metamorphic conditions within the peak assemblage field.**
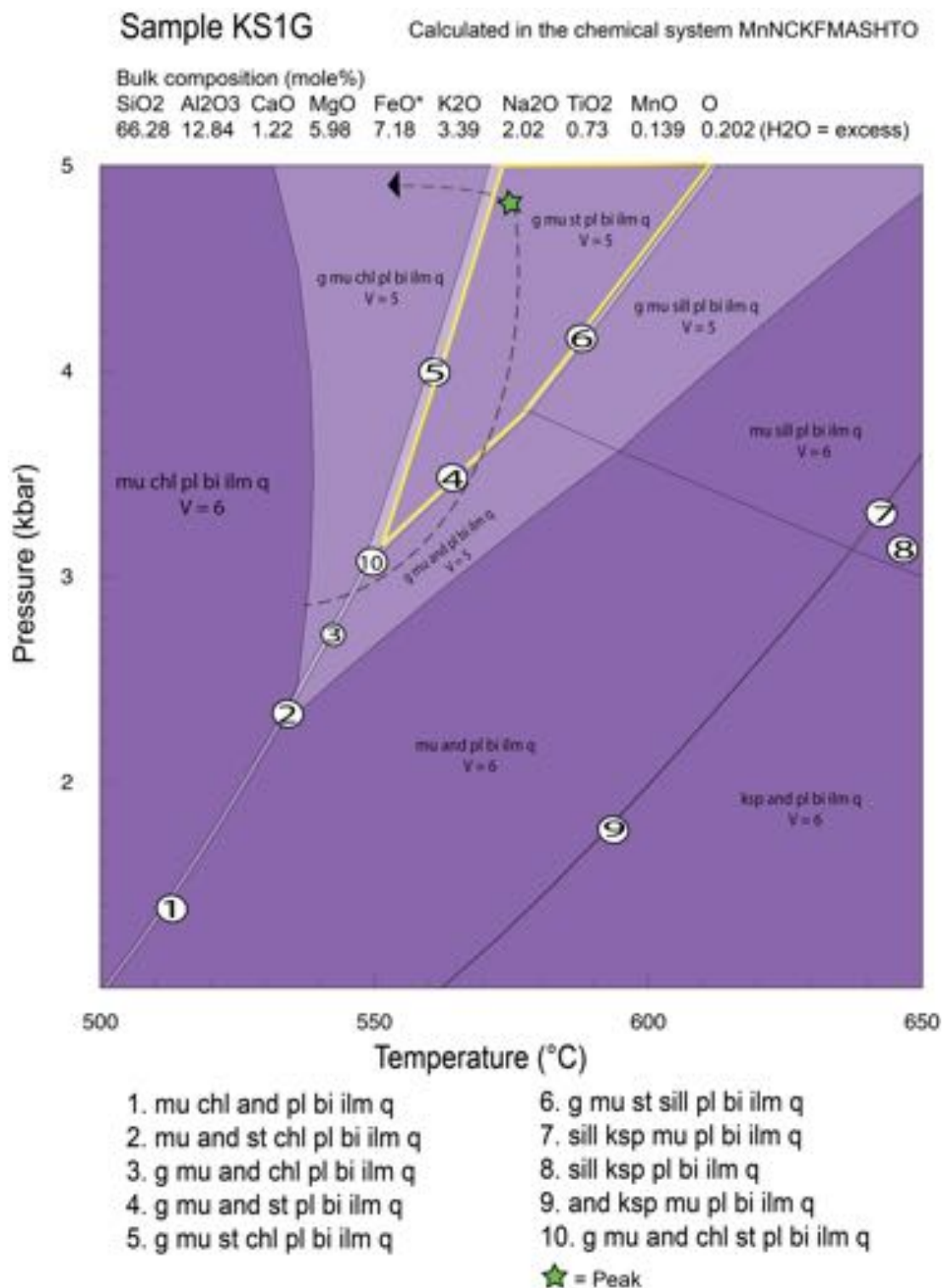
**Figure 12: Calculated P-T pseudosection for sample KS1G. All fields in the diagram additionally contain water, H₂O, as part of the equilibrium assemblage. Fields too small to be directly labelled are identified by numbered circles corresponding to the assemblage occurring within the field. Progressively darker tones are representative of increasing variance, V, where V = components – phases + 2 (components = 10). The composition in mole % used to calculate the diagram is provided above the diagram. The dashed line represents the interpreted P-T path. FeO\* = FeO + 2 x 'O'.**
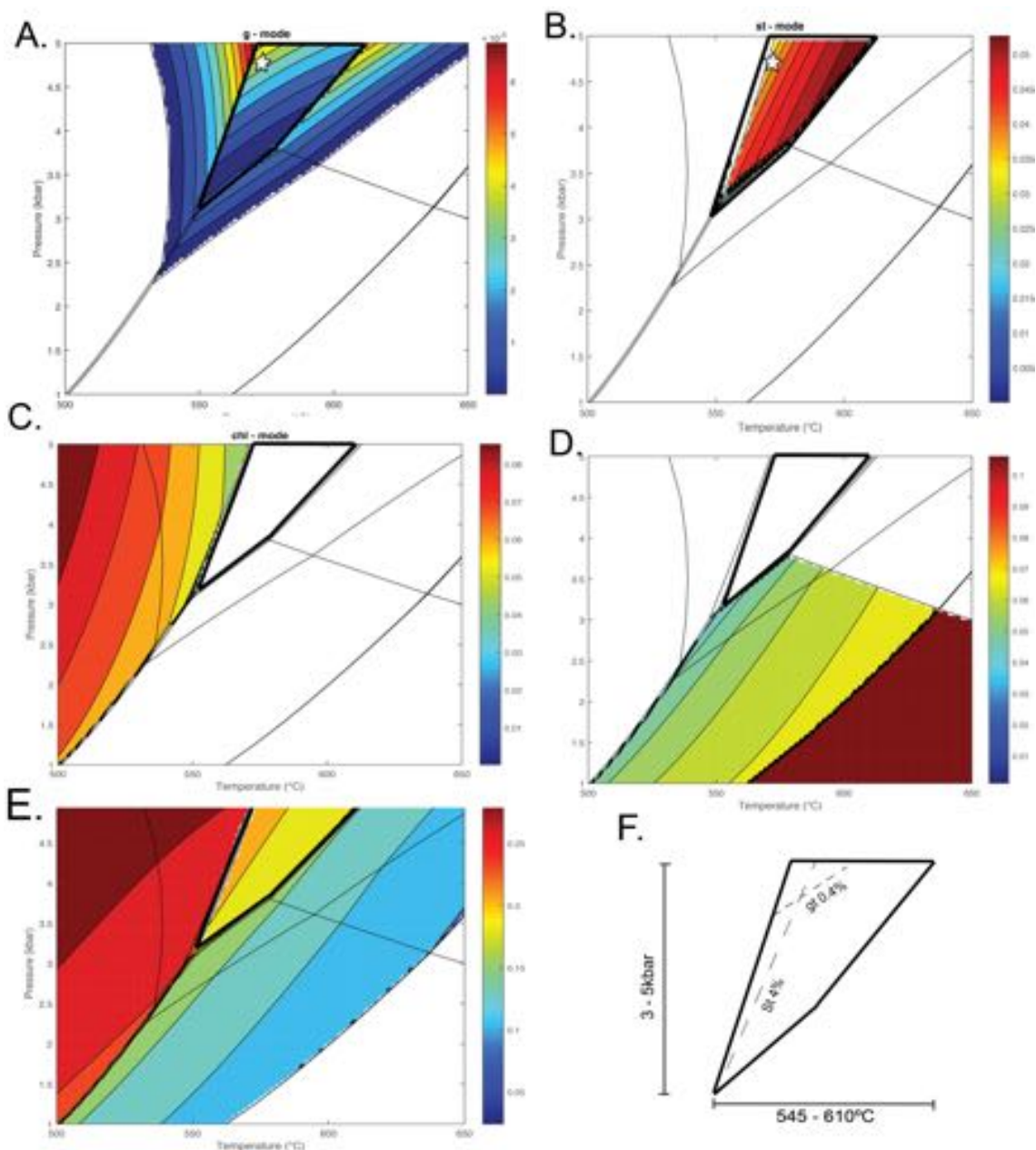
**Figure 13: Calculated P-T pseudosection for sample KS1G contoured for the abundance ('mode') of some minerals. The calculated abundances of phases in the peak assemblage (bold outline) were used in conjunction with the estimated abundances of minerals in the sample (Table 1) to constrain the peak P-T conditions experienced by the rock. Diagram F shows the detail of the peak assemblage field with calculated abundances of phase (combination of A and B), to further constrain the metamorphic conditions within the peak assemblage field.**
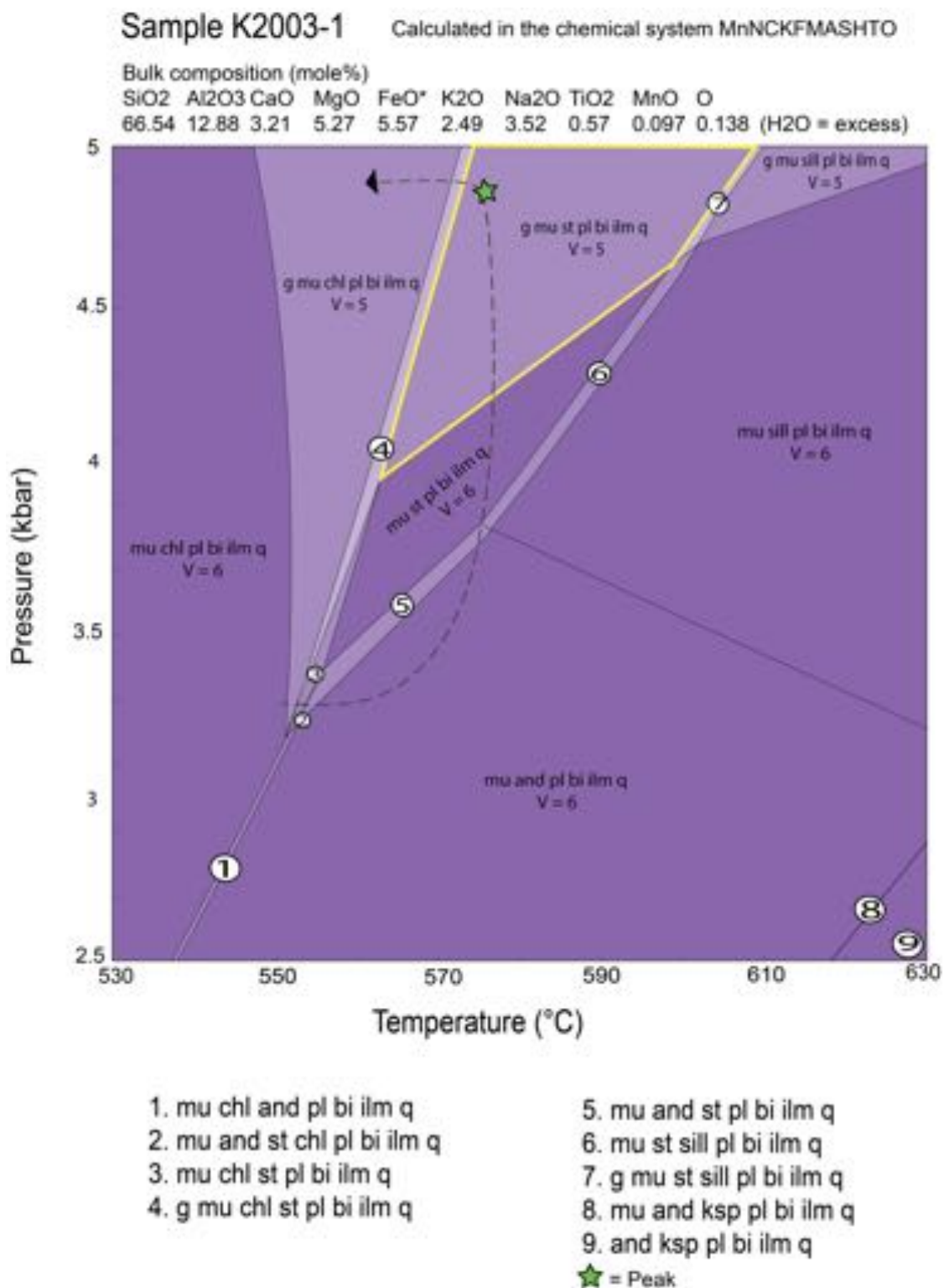
**Figure 14: Calculated P-T pseudosection for sample K2003-1. All fields in the diagram additionally contain water, H₂O, as part of the equilibrium assemblage. Fields too small to be directly labelled are identified by numbered circles corresponding to the assemblage occurring within the field. Progressively darker tones are representative of increasing variance, V, where V = components – phases + 2 (components = 10). The composition in mole % used to calculate the diagram is provided above the diagram. The dashed line represents the interpreted P-T path. FeO\* = FeO + 2 x 'O'.**
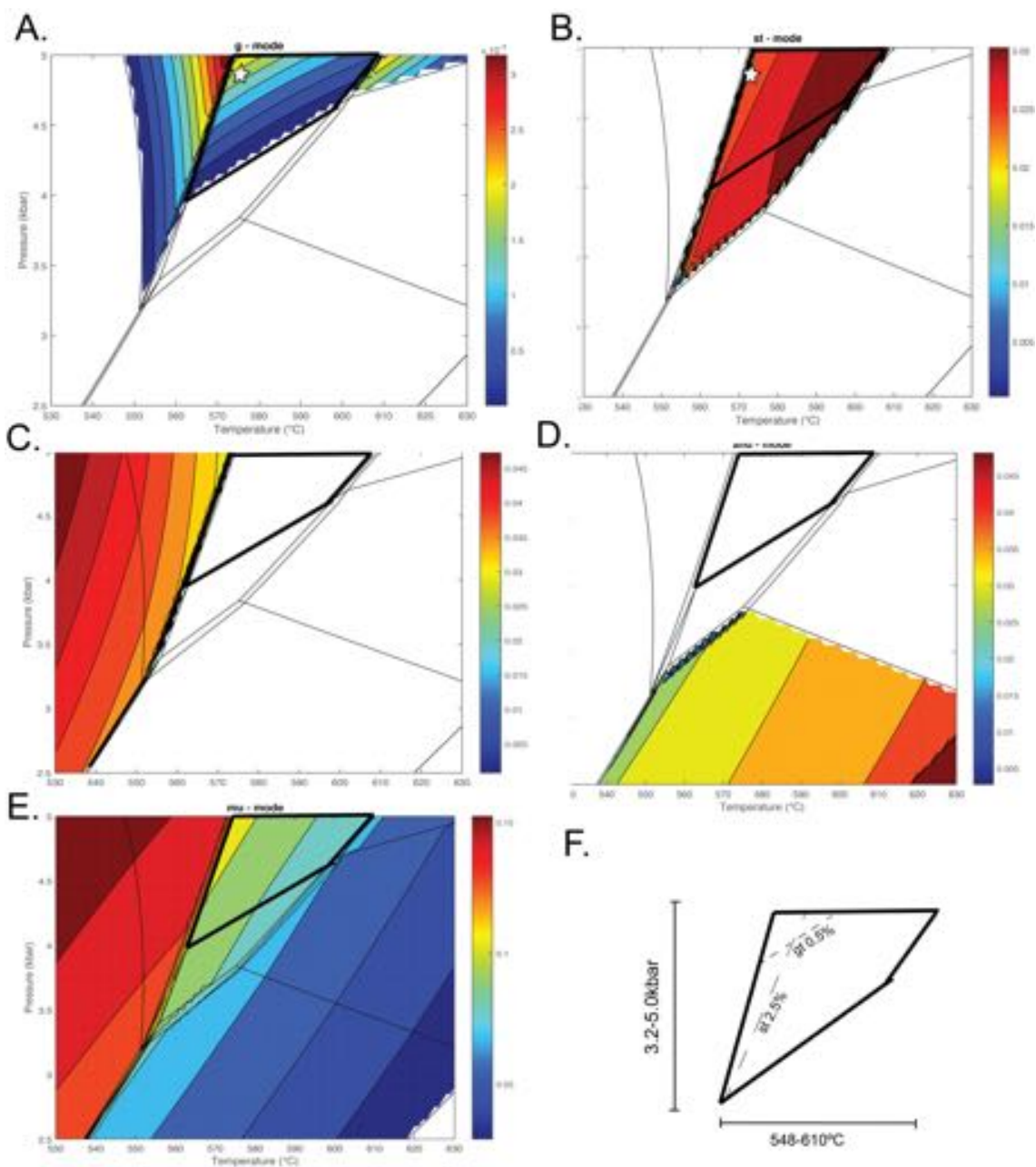
**Figure 15: Calculated P-T pseudosection for sample K2003-1 contoured for the abundance ('mode') of some phases. The calculated abundances of phases in the peak assemblage (bold outline) were used in conjunction with the estimated abundances of minerals in the sample (Table 1) to constrain the peak P-T conditions experienced by the rock. Diagram F shows the detail of the peak assemblage field with calculated abundances of phase (combination of A and B), to further constrain the metamorphic conditions within the peak assemblage field.**
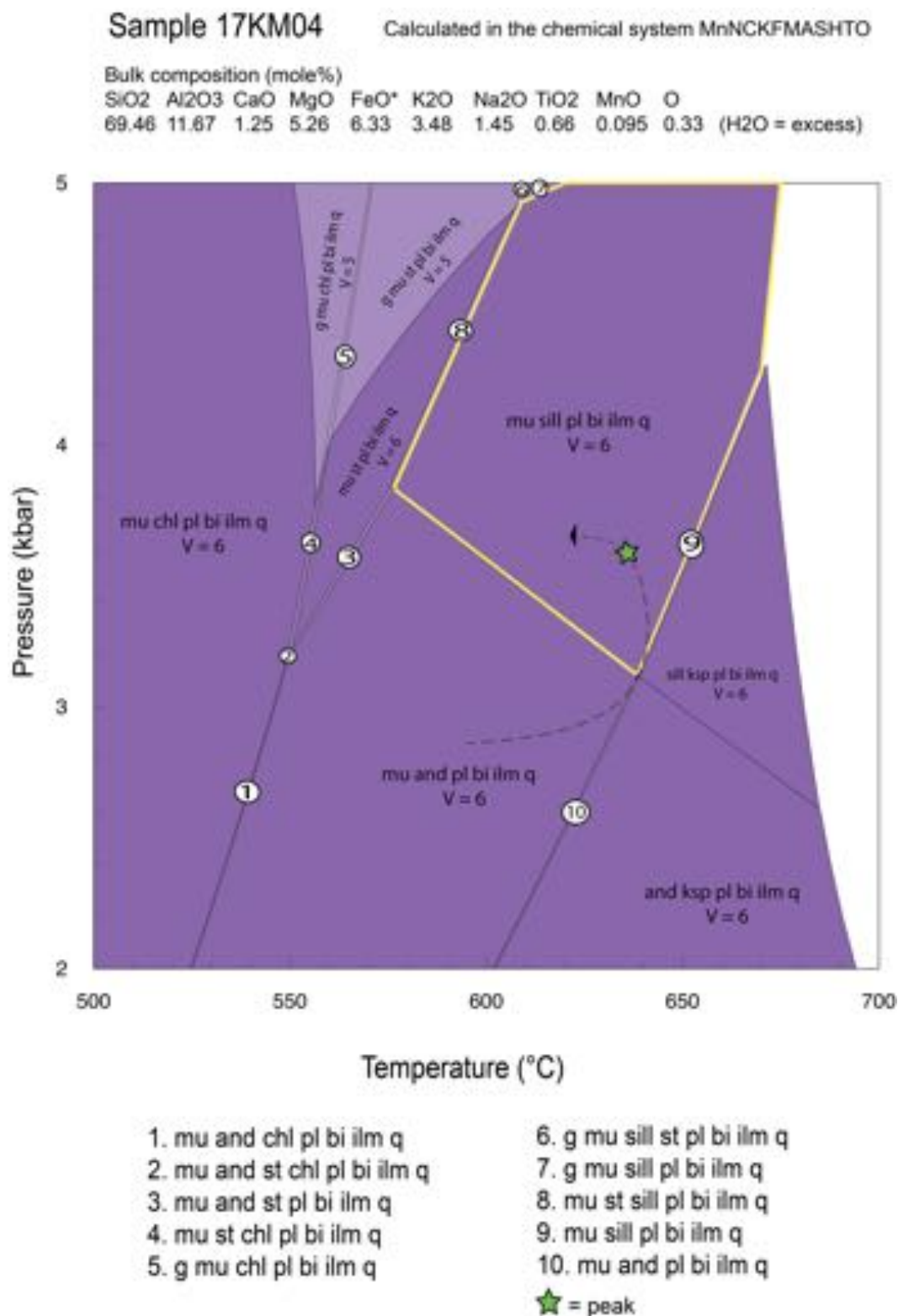
**Figure 16: Calculated P-T pseudosection for sample 17KM04. All fields in the diagram additionally contain water, H₂O, as part of the equilibrium assemblage. Fields too small to be directly labelled are identified by numbered circles corresponding to the assemblage occurring within the field. Progressively darker tones are representative of increasing variance, V, where V = components – phases + 2 (components = 10). The composition in mole % used to calculate the diagram is provided above the diagram. The dashed line represents the interpreted P-T path. FeO\* = FeO + 2 x 'O'.**
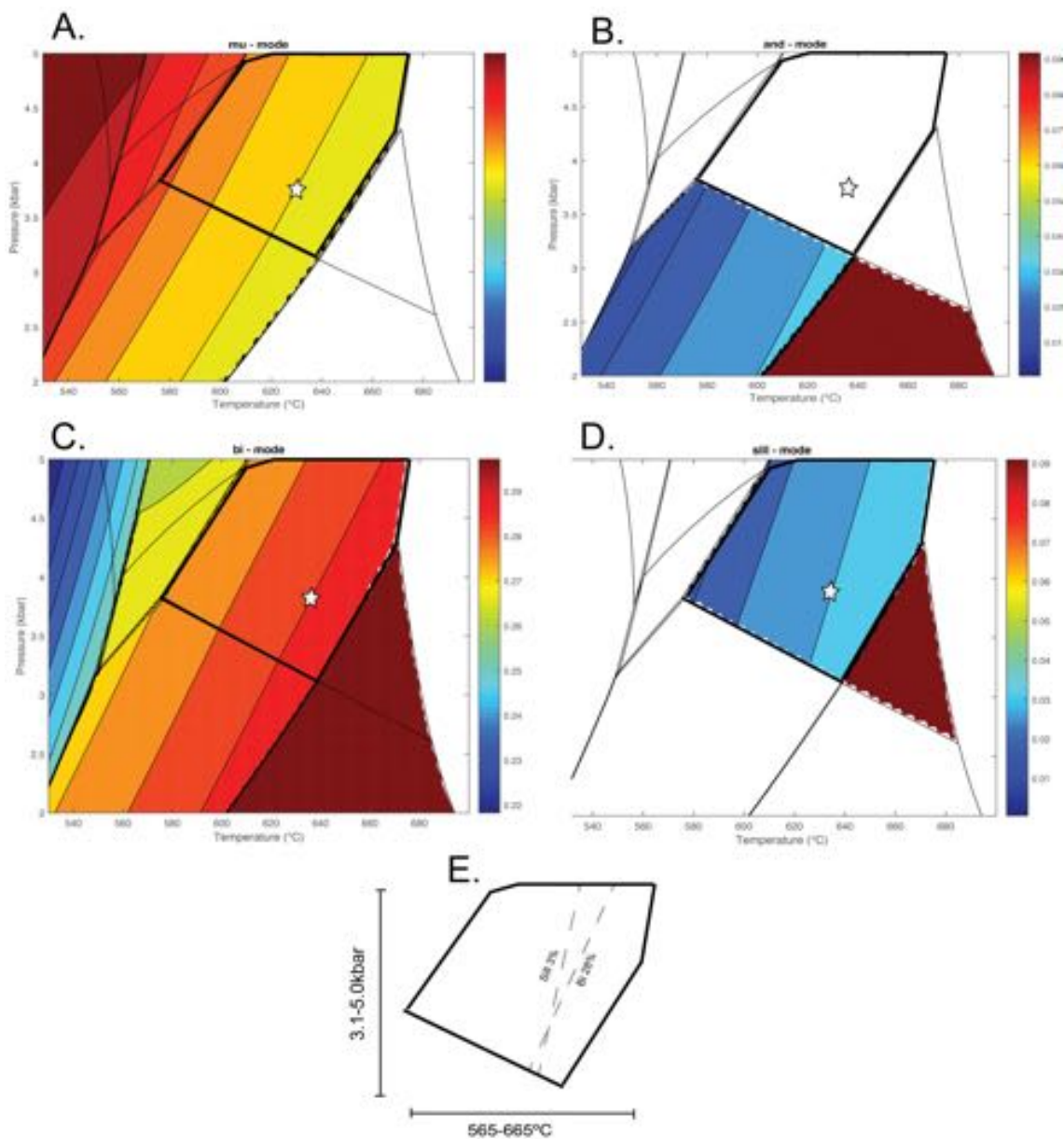
**Figure 17: Calculated P-T pseudosection for sample 17KM04 contoured for the abundance ('mode') of some minerals. The calculated abundances of phases in the peak assemblage (bold outline) were used in conjunction with the estimated abundances of minerals in the sample (Table 1) to constrain the peak P-T conditions experienced by the rock. Diagram F shows the detail of the peak assemblage field with calculated abundances of phase (combination of C and D), to further constrain the metamorphic conditions within the peak assemblage field.**
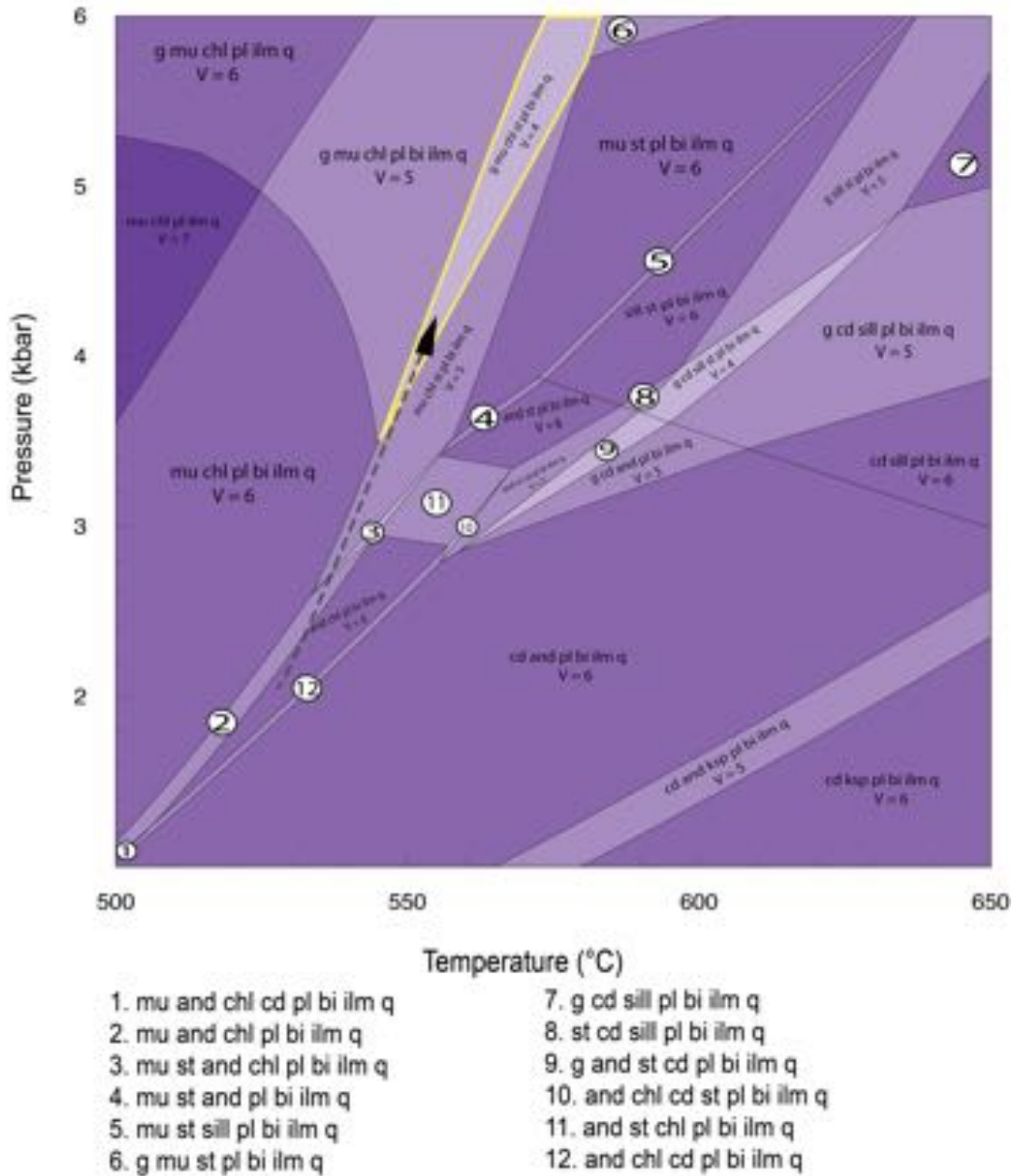
**Figure 18: Calculated P-T pseudosection for sample KI-25. All fields in the diagram additionally contain water, H₂O, as part of the equilibrium assemblage. Fields too small to be directly labelled are identified by numbered circles corresponding to the assemblage occurring within the field. Progressively darker tones are representative of increasing variance, V, where V = components – phases + 2 (components = 10). The composition in mole % used to calculate the diagram is provided above the diagram. The dashed line represents the interpreted P-T path. FeO\* = FeO + 2 x 'O'.**
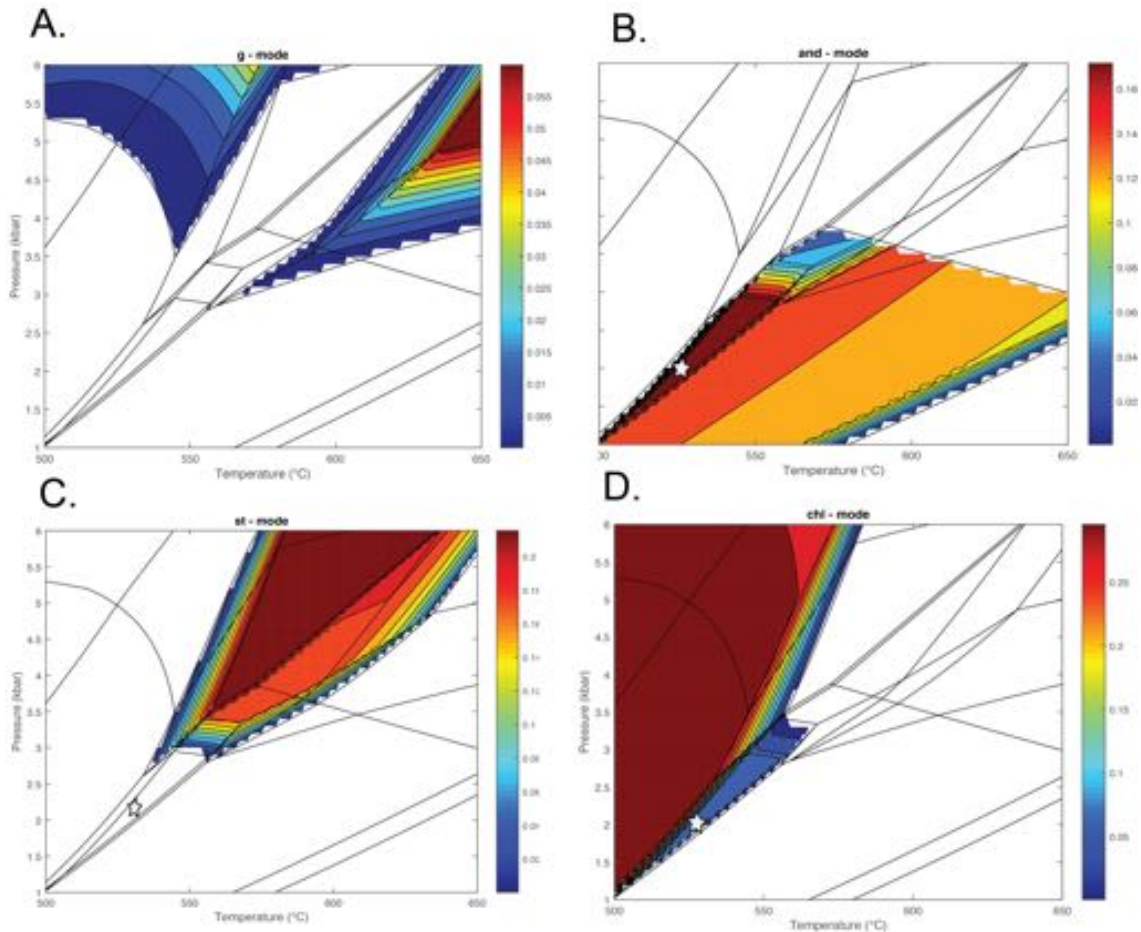
**Figure 19: Calculated P-T pseudosection for sample KI-25 contoured for the abundances ('mode')
of some minerals. The calculated abundances of phases in the peak assemblage (bold outline) were
used in conjunction with the estimated abundances of minerals in the sample (Table 1) to constrain
the peak P-T conditions experienced by the rock.**

## DISCUSSION

The aim of this study is to refine the timing of metamorphism and thermal character of

metapelites within the Delamerian Orogen, for the purpose of providing constraints on

its tectonic evolution.

## U-Pb monazite geochronology

SIGNIFICANCE OF U-PB GEOCHRONOLOGY

The $^{206}$Pb/$^{238}$U monazite ages presented in this study are in-situ monazite analyses. As

samples in this study are low-grade, monazites are typically ~20μm in size, thus

mounted monazite analyses would be difficult to obtain.  In-situ analysis also has the benefit of retaining accessory phase textural relationships.  The $^{206}$Pb/$^{238}$U monazite ages in this study are presented as concordia ages or as weighted mean averages.  As the Delamerian-aged metamorphism is recognised as a continuous process approaching 30 million years, no single 'age' of metamorphism is likely to be obtained.

GEOCHRONOLOGY

Monazite is a widely used geochronometer for understanding high-temperature processes (Spear & Pyle, 2002; Taylor *et al*, 2016) as diffusion rates of elements in monazite is slow, and has a high resistance to lead loss (Foster *et al*, 2000).  Thus, monazite can record previous geologic conditions Monazite commonly starts to grow in metasedimentary rocks during prograde metamorphism at temperatures of ~400-500°C (Smith & Barreiro, 1990), and is understood to have mostly reacted or recrystallized to form metamorphic monazite by ~350°C (Williams *et al*, 2007).  .  Monazite was chosen as the appropriate geochronometer in this study as the rock samples are subsolidus, where metamorphic zircon typically does not grow.  All samples preserve mid-amphibolite facies mineral assemblages (garnet + staurolite etc.), indicating temperatures >550°C, thus monazite age data in this study are presumably the result of: (1) a single metamorphic event or (2) poly-metamorphism.  The spread of data along a discord in KS1G is attributed to common Pb as the upper intercept approaches the age of the Earth.  The monazite geochronology from KS1G, K2003-1, MAC-2, 17-KM-04 and 17-KM-05 are in agreement with the monazite age of 493.3 ± 3.2 Ma from the high-grade core of the orogen (Foden *et al*, 2006).  The $^{206}$Pb/$^{238}$U weighted average ages presented in this study coincide with the abrupt change from I- and S-type granites to A-type granites at 493.3 ± 3.2 Ma (Foden *et al*, 2006) within the Delamerian Orogen,

which has been interpreted to mark the cessation of deformation.    The youngest

monazite ages imply that the A-type granites likely provided the heat for metamorphism

once deformation ceased.

The monazite geochronology of sample RDC-02 is complex.  Arguably a population

occurs at 523.6-507Ma, with a concordia age of 515.1 ± 16Ma.  Sample RDC-04

defines a concordia age of 483.5 ± 4.3Ma.  As Reedy Creek area (Fig. 1) records

significantly younger monazite ages than all other samples in this study, and has

evidence of granulite facies metamorphism (Aleisso *et al*, 2017) (Fig. 17a), it is

conceivable that either (1) the Reedy Creek area experienced the hottest temperatures

within the orogen, and hence took the longest time to cool or (2) the Delamerian Orogen

constitutes a patchwork of metamorphic sub-domains.

Garnet is the major repository of yttrium in metamorphic rocks (Williams *et* al, 2007).

The timing of garnet growth and/or breakdown strongly affects the yttrium distribution

in metamorphic monazite (Foster *et* al, 2000; Spear *et al,* 2009).  Typically, if monazite

growth begins prior to garnet growth, it will be enriched in yttrium than if monazite

growth post-dates garnet, as yttrium will partition into garnet as soon as it nucleates

(Spear & Pyle, 2002; Williams *et al*, 2007; Zhu & O'Nions, 1999).  The relationship

between yttrium content in monazite and garnet can link metamorphism to U-Pb ages

(Taylor *et al*, 2016; Zhu & O'Nions, 1999); however, this relationship does not always

exist and thus varies from study to study.  No measurable relationship is observed

between the U-Pb age of monazite inclusions and yttrium content of monazite in

samples MAC-2, K2003-1 and KS1G.  The random distribution of monazite ages with

respect to garnet indicates that potentially monazite growth began prior to garnet growth. Monazites in Samples K2003-1 and MAC-2 have high yttrium contents around 480Ma, and then yttrium content generally drops as the age increases as shown in Fig. 7. Potentially in these samples, there was a small amount of garnet breakdown associated with monazite growth at ~480Ma, and then the garnet stopped breaking down.

## Sm/Nd geochronology

Garnet-whole rock Sm/Nd data from Kangaroo Island indicates that peak metamorphism in the Kangaroo Island region began much earlier than metamorphism as recorded by monazite U-Pb on mainland South Australia. Sample KI-25 yields an age of $513 \pm 4$Ma, an age that is in agreement with the zircon age obtained by Foden *et al* (2006) from the Rathjen Gneiss. This age implies that peak metamorphism on Kangaroo Island was reached early in the deformation history, potentially due to heat from surrounding granitic intrusions.

## Pressure-temperature conditions

LIMITATIONS OF PHASE EQUILIBRIA MODELLING

The chemical system MnNCKFMASHTO was chosen as the appropriate system for phase equilibria modelling in this thesis. Manganese is important to stabilize garnet to low pressures to coexist with andalusite (Johnson *et al*, 2003), as evident in petrological observations of samples in this thesis. The model chemical system MnNCKFMASHTO has been used to represent a complex natural system, and it is acknowledged that there are a number of limitations. Some samples used in this study are low-temperature with

large porphyroblasts of andalusite, resulting in bulk composition fractionation (Clarke & Hand, 2010), where the surrounding composition becomes depleted in alumina as andalusite grows; altering the overall bulk composition of the rock (Alias *et al*, 2002). To minimize the effect of this limitation, samples with the smallest porphyroblasts were chosen.

PURPOSE OF PHASE EQUILIBRIA MODELLING

Phase equilibria modelling has been used to determine the thermal character recorded by the samples for constraining their P-T history throughout the Delamerian Orogeny. 'Clockwise' P-T paths are typically associated with convergent settings where the crust is thickened, suggesting that metamorphism occurs as a conductive response to thickening (e.g Collins & Vernon, 1991; Jamieson *et al*, 1998). Alternatively, 'anticlockwise' P-T paths are generated when the thermal peak is reached in the early stages of deformation and are more typically associated with magmatic heating (e.g Alias *et al,* 2002; Collins & Vernon, 1991).

In sample MAC-2, the peak assemblage biotite + muscovite + staurolite + garnet +quartz + plagioclase + ilmenite is preserved, therefore the abundances of minerals in thin section (Table 1) may be used in conjunction with calculated abundances to constrain the peak P-T conditions. The region with the peak assemblage field that corresponds most closely with the observed and calculated mineral modes (Fig. 11f) is in the P-T range ~4.7 kbar and 570°C. Inferring a P-T path for sample MAC-2 is difficult. The prograde evolution could not be directly constrained on the pseudosection (Fig.10). To determine the prograde evolution of the rock; it would be necessary to model a more aluminous bulk composition corresponding to the composition of

andalusite; however progressively modelling each sample as the bulk composition

changes is beyond the scope of this thesis. The lack of andalusite in this rock probably

precludes the prograde P-T path from passing through andalusite stability fields, as

andalusite is difficult to nucleate (Alias *et al*, 2002; Pattison & Tinkham, 2009). Thus,

if the prograde path had passed through andalusite stability fields to the peak

(andalusite-absent), one would expect to see relic andalusite surviving in the rock.

As relic andalusite occurs in samples KS1G and K2003-1, and is interpreted to pre-date

staurolite, the prograde P-T path likely passed through andalusite stability fields prior to

the metamorphic peak. The retrograde path is marked by the initial growth of chlorite.

The sequence of mineral growth interpreted from petrological observations and the

calculated pseudosection suggests that samples KS1G and K2003-1 followed an

'anticlockwise' P-T evolution (Figs. 11 & 13 respectively).

In sample 17KM04, the region within the peak assemblage field (Fig. 15; biotite +

muscovite + plagioclase + sillimanite + quartz + ilmenite + water) that corresponds

most closely with the observed and calculated modes is in the P-T range 3.7 kbar and

635 degrees. The retrograde path is poorly constrained, as the only evidence of

retrogression is retrograde muscovite cross-cutting the foliation. Sillimanite occurring

as fibrolite is interpreted to have pseudomorphed relic andalusite; hence the prograde

path is interpreted to have passed through the andalusite stability field. The calculated

pseudosection, coupled with petrological observations suggests that sample 17KM04

also followed an 'anticlockwise' P-T evolution.

Interpreting a P-T path for sample KI-25 is difficult. The interpreted P-T path (Fig.18) is based on the low abundances of garnet and staurolite (Fig. 19). There is very little evidence of retrogression, suggesting that KI-5 may have ran out of a reactant, possibly water.

Sample RDC-04 from Reedy Creek reached granulite facies metamorphism, and was modelled by Aleisso *et al* (2017) (Fig. 17a). The interpreted peak assemblage of RDC-04 of plagioclase + biotite + orthopyroxene + cordierite + spinel + magnetite + ilmenite occurs at 1.0-4.4kbar and 790-860°C, significantly higher temperatures than all samples modelled in this study. The granulite facies metamorphism reached at Reedy Creek may be explained by the close proximity of the Reedy Creek Granodiorite intruding the crust between ~490-480Ma (Foden *et al*, 2006), perturbing the thermal regime, inducing partial melting and providing the extreme heat for metamorphism to reach granulite facies.
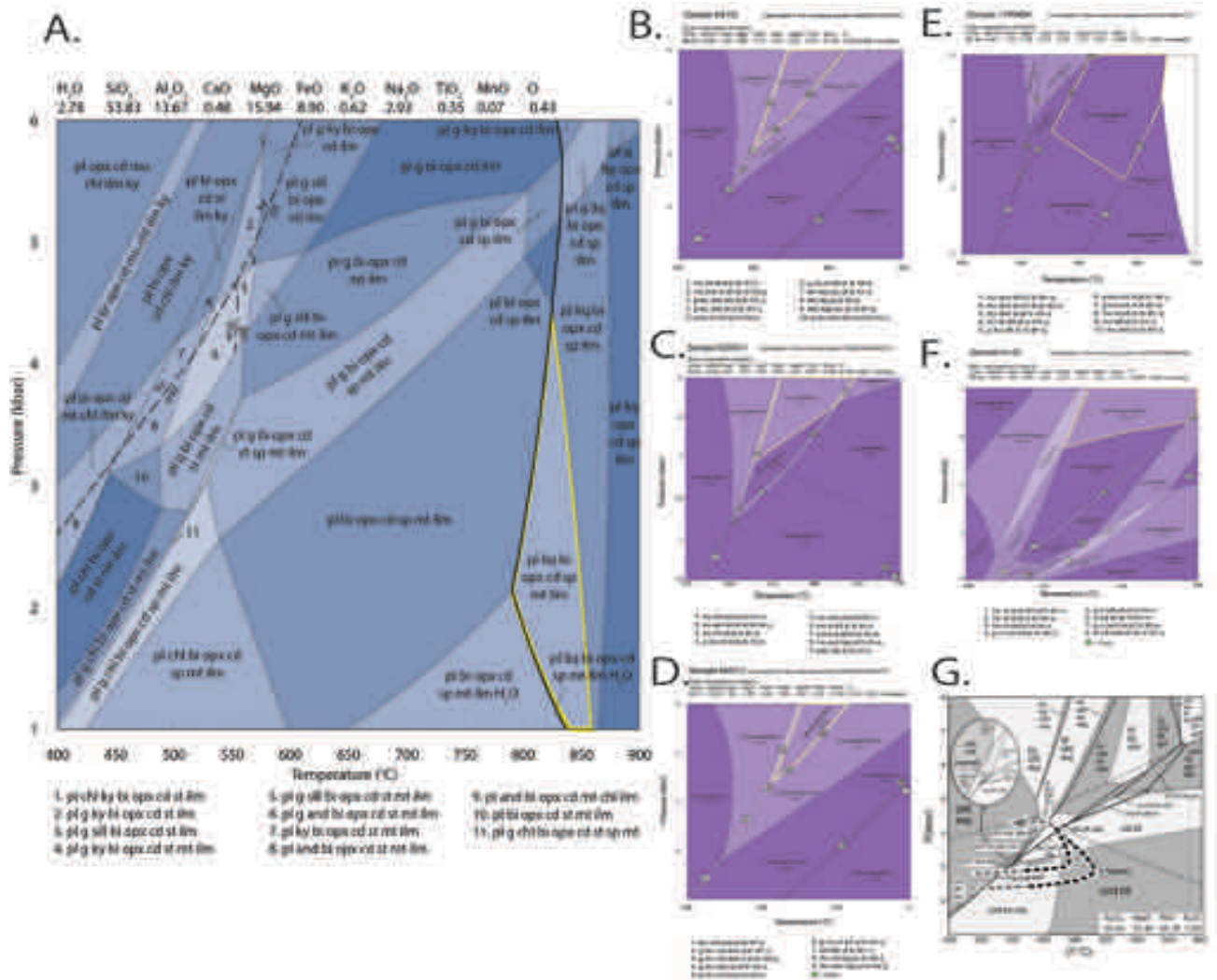
**Figure 20: All P-T pseudosections for sample discussed in this thesis. (A) RDC-04 P-T pseudosection (Aleisso *et al*, 2017); (B) Sample KS1G; (C) Sample K2003-1; (D) Sample MAC-2; (E) Sample 17KM04; (F) Sample KI-25; (G) Petrel Cove P-T pseudosection (Alias *et al*, 2002).**

The calculated P-T pseudosection for porphyroblastic schists at Petrel Cove (Alias *et al*, 2002) shows evidence for an 'anticlockwise' P-T evolution within the thermal aureole of the Victor Harbour Granite. This interpretation, as well as the 'anticlockwise' P-T paths proposed for the modelled samples in this thesis, is consistent with the thermal effects of granitic intrusions, and appears to be regionally representative of the Delamerian Orogen.

**P-T evolution**

Considering the petrographic observations described in previous sections, it can be concluded that the sequence of mineral growth in the Delamerian Orogeny on mainland South Australia was garnet → andalusite → staurolite, and Kangaroo Island was andalusite → staurolite → garnet . Based on petrographic observations and textural relationships, an overall 'anticlockwise' P-T evolution is proposed for the Delamerian Orogen. 'Anticlockwise' P-T paths are not typical of convergent settings. Sandiford & Powell (1991) propose that 'anticlockwise' P-T paths in convergent settings are a natural consequence of strain localization due to



**Figure 21: A model for generating 'anticlockwise' P-T paths in a convergent setting (Collins & Vernon, 1991).**

thermally weakened crust associated with magma ascent through the crust. Collins & Vernon (1991) suggest that low-P, high-T metamorphism, and 'anticlockwise' P-T paths can be induced by the repeated granitic intrusions that generate large metamorphic aureoles, thermally weakening the crust, and resulting in discrete low-P, high-T terranes that are localized around abundant granites (Fig. 19). The 'anticlockwise' P-T paths proposed in this study indicate that the granitic intrusions that span the Delamerian Orogen focused the generated heat in the crust, providing the high geothermal gradients for low-P, high-T metamorphism as metamorphic sub-domains as suggested by various

46

authors including, but not limited to, Alias *et* al (2002), Jenkins & Sandiford (1992), Oliver & Zakowski (1995) and Sandiford *et al* (1995). However, granitic intrusions are not observed in close proximity to all samples (eg. MAC-2) therefore the intrusions cannot account for all 'anticlockwise' P-T paths generated in the orogen. For samples that do not lie close to granitic intrusions, the 'anticlockwise' path may be a result of magmatic advection of heat due in the crust as suggested by Sandiford & Powell (1991), due to the emplacement of melts after the cessation of thrusting (Wakabayashi, 2004). The older metamorphic ages on Kangaroo Island from Sm/Nd geochronology (this study), Rb-Sr geochronology (Foden *et al*, 2002) and $^{207}Pb/^{206}Pb$ monazite geochronology (Weinberg *et al*, 2013), and younger ages on mainland South Australia (this study) (Fig. 20) suggest that the thermal locus moved northwards over time. This resulted in a metamorphic terrain of regionally similar style but consisting of discrete metamorphic sub-domains with the highest grade occurring late in the evolution in the vicinity of I- to S-type granites.
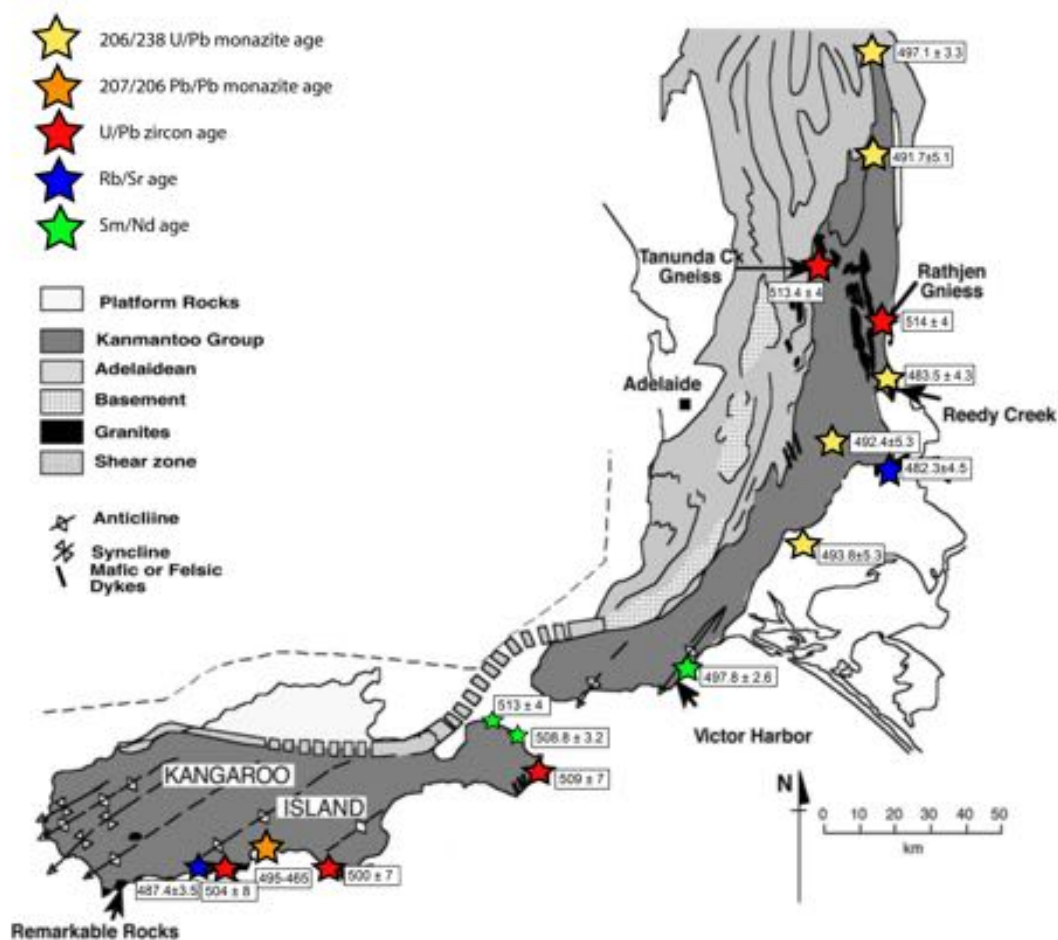
**Figure 22: Spatial age map of the Delamerian Orogen. Ages from this study, Burtt & Fanning (2001), Fanning (1990), Foden *et al* (1999), Foden *et al* (2002), Foden *et al* (2006), Turner & Foden (1996), and Weinberg *et al* (2013).**

## CONCLUSIONS

This study provides the first comprehensive monazite age data coupled to detailed P-T estimates to unravel the P-T history within the Southern Adelaide Fold-Thrust Belt portion of the Delamerian Orogen. In-situ monazite geochronology indicates that metamorphism was protracted until ~480Ma. Calculated phase equilibria modelling constrains the metamorphism of garnet-staurolite-andalusite bearing schists to ~4.6kbar and 570°C, and sillimanite-bearing schists to 3.7kbar and 635°C. Results from this study indicate that the Delamerian Orogen follows an 'anticlockwise' trajectory.

Granulites at Reedy Creek experienced much higher temperatures and younger ages,

suggesting that the Reedy Creek may have been the hottest part of the orogen and

therefore took the longest time to cool.  The older metamorphic ages on Kangaroo

Island and younger metamorphic ages on mainland South Australia indicate that the

thermal locus moved northwards over time, resulting in a metamorphic terrain that gives

the appearance of a patchwork orogen of discrete metamorphic sub-domains, with the

highest grades in the vicinity of I- and S-type granitic intrusions occurring late in the

evolution.

## ACKNOWLEDGMENTS

## REFERENCES

ALESSIO, K., HAND, M., MORRISSEY, L., KELSEY, D., & PAYNE, J. (2017).  Melt reintegration modelling: Testing against a subsolidus reference assemblage.  *Geosciences, 7*(75), doi: 10.3390/geosciences7030075.

ALIAS, G., SANDIFORD, M., HAND, M., & WORLEY, B. (2002). The P-T record of synchronous magmatism, metamorphism and deformation at Petrel Cove, southern Adelaide fold belt. *Journal of Metamorphic Geology, 20,* 351-363.

BOGER, S., & MILLER, J. (2004). Terminal suturing of Gondwana and the onset of the Ross–Delamerian Orogeny: the cause and effect of an Early Cambrian reconfiguration of plate motions. *Earth and Planetary Science Letters, 219*(1), 35-48.

BURTT, A. C., ABBOT, P. J., & FANNING, C. M. (2001).  Definition of Teal Flat and Marne River Volcanic and associatied shear zone.  *Minerals and Exploration in South Australia Journal, 17,* 37-43.

CARTWRIGHT, I., VRY, J., & SANDIFORD, M. (1995). Changes in stable isotope ratios of metapelites and marbles during regional metamorphism, Mount Lofty Ranges, South Australia: implications for crustal scale fluid flow. *Contributions to Mineralogy and Petrology, 120*(3-4), 292-310.

CLARK, C., & HAND, M. (2010).  Decoding Mesoproterozoic and Cambrian metamorphic events in Willyama Complex metapelites through the application of Sm-Nd garnet geochronology and P-T pseudosection analysis. *Gondwana Research, 17,* 59-74.

COLLINS, W. J., & VERNON, R. H. (1991). Orogeny associated with anticklockwise P-T-t paths: Evidence from low-P, high-T metamorphic terranes in the Arunta inlier, Central Australia. *Geology, 19,* 835-838.

COOPER, J. A., JENKINS, R. J. F., COMPSTON, W., & WILLIAMS, I. S. (1992). Ion-probe zircon dating of a mid-Early Cambrian tuff in South Australia. *Journal of the Geological Society of London, 149,* 185-192.

DIREEN, N. G., BROCK, D., & HAND, M. (2005). Geophysical testing of balanced cross-sections of fold-thrust belts with potential field data: an example from the Fleurieu Arc of the Delamerian Orogen, South Australia. *Journal of Structual Geology, 27*, 964-984.

DYMOKE, P., & SANDIFORD, M. (1992). Phase relationships in Buchan facies series pelitic assemblages: calculations with application to andalusite-staurolite parageneses in the Mount Lofty Ranges, South Australia. *Contributions to Mineralogy and Petrology, 110*(1), 121-132.

FANNING, C. M. (1990). Single grain dating of a granite sample from Cape Willoughby, Kangaroo Island. *Australian National University Progress Report, 89,* 29-32.

FLÖTTMANN, T., JAMES, P., MENPES, R., CESARE, P., TWINING, M., FAIRCLOUGH, M., MARSHAL, S. (1995). The structure of Kangaroo Island, South Australia: strain and kinematic partitioning during Delamerian basin and platform reactivation. *Australian Journal of Earth Sciences, 42*(1), 35-49.

FODEN, J., SANDIFORD, M., DOUGHERTY-PAGE, J., & WILLIAMS, I. (1999). Geochemistry and geochronology of the Rathjen Gneiss: implications for the early tectonic evolution of the Delamerian Orogen. *Australian Journal of Earth Sciences, 46*(3), 377-389.

FODEN, J., ELBURG, M. A., TURNER, S., SANDIFORD, M., O'CALLAGHAN, J., & MITCHELL, S. (2002). Granite production in the Delamerian orogen, South Australia. *Journal of the Geological Society, 159*(5), 557-575

FODEN, J., ELBURG, M. A., DOUGHERTY-PAGE, J., & BURTT, A. (2006). The timing and duration of the Delamerian Orogeny: correlation with the Ross Orogen and implications for Gondwana assembly. *The Journal of Geology, 114*(2), 189-210.

FOSTER, G., KINNY, P., VANCE, D., PRINCE, C., & HARRIS, N. (2000). The significance of monazite U-Th-Pb age data in metamorphic assemblages; a combined study of monazite and garnet chronometry. *Earth and Planetary Science Letters, 181,* 327-340.

GOUDIE, D. J., FISHER, C. M., HANCHAR, J. M., CROWLEY, J. L., & AYERS, J. C. (2014). Simultaneous in situ determination of U-Pb and Sm-Nd isotopes in monazite by laser ablation ICP-MS. *Geochemistry, Geophysics, Geosystems, 15*, 2575-2600, doi: 10.1002/2014GC005431

HAINES, P. W., & FLÖTTMANN, T. (1998). Delamerian Orogeny and potential foreland sedimentation: a review of age and stratigraphic constraints. *Australian Journal of Earth Sciences, 45*(4), 559-570.

HOLLAND, T.J.B., & POWELL, R. (2011). An improved and extended internally consistent thermodynamic dataset for phases of petrological interest, involving a new equation of state for solids. *Journal of Metamorphic Geology*, *29,* 333-383.

JAGO, J. B., GUM, J. C., BURTT, A. C., & HAINES, P. W. (2003). Stratigraphy of the Kanmantoo Group: a citical element of the Adelaide Fold Belt and the Palaeo-Pacific plate margin, Eastern Gondwana. *Australia Journal of Earth Sciences, 50*, 343-363.

JAMIESON, R. A., BEAUMONT, C., FULLSACK, P., & LEE, B. (1998). Barrovian regional metamorphism: where's the heat? *Geological Society of London Special publications, 138,* 23-51.

JENKINS, R. J., & SANDIFORD, M. (1992). Observations on the tectonic evolution of the southern Adelaide Fold Belt. *Tectonophysics, 214*(1-4), 27-36.

JOHNSON, T. E., BROWN, M., & SOLAR, G. S. (2003). Low-pressure subsolidus and suprasolidus phase equilibria in the MnNCKFMASH system: Constraints on conditions of regional metamorphism in western Maine, nothern Appalachians. *American Mineralogist, 88*, 624-638.

KELSEY, D. E., & HAND, M. (2015). On ultrahigh temperature crustal metamorphism: Phase equilibria, trace element thermometry, bulk composition, heat sources, timescales and tectonic settings. *Geoscience Frontiers, 6*, 311-356.

MARSHAK, S., & FLÖTTMANN, T. (1996). Structure and origin of the Fleurieu and Nackara Arcs in the Adelaide fold-thrust belt, South Australia: salient and recess development in the Delamerian Orogen. *Journal of Structural Geology, 18*(7), 891-908.

MORRISEY, L. J., HAND, M., WADE, B. P., & SZPUNAR, M. (2013). Early Mesoproterozoic metamorphism in the Barossa Comples, South Australia: links with the eastern margin of Proterozoic Australia. *Australian Journal of Earth Sciences, 60*, 769-795.

OFFLER, R., FLEMING, P. (1968). A synthesis of folding and metamorphism in the Mt Lofty Ranges, South Australia. *Geological Socierty of Australia, 15*, 245-266.

OLIVER, N., & ZAKOWSKI, S. (1995). Timing and geometry of deformation, low-pressure metamorphism and anatexis in the eastern Mt Lofty Ranges: the possible role of extension. *Australian Journal of Earth Sciences, 42*(5), 501-507.

PATON, C., HELLSTROM, J., PAUL, B., WOODHEAD, J., & HERGT, J. (2011). Iolite: Freeware for the visualisation and processing of mass spectrometric data. *Journal of Analytical Atomic Spectrometry, 26*(12), 2508-2518.

PATTISON, D., & TINKHAM, D. (2009). Interplay between equilibrium and kinetics in prograde metamorphism of pelites: an example from the Nelson aureole, British Columbia. *Journal of Metamorphic Geology, 27*(4)m 249-279.

PAYNE, J. L., HAND, M., BAROVICH, K. M., & WADE, B. P. (2008). Temporal constraints on the timing of high-grade metamorphism in the northern Gawler Craton: implications for assembly of the Australian Proterozoic. *An International Geoscience Journal of the Geological Society of Australia, 55*(5), 623-640. doi:10.1080/08120090801982595.

PEARCE, M., WHITE, A., GAZLEY, M. (2015). TCInvestigator: Automated calculation of mineral mode and composition contours for thermocalc pseudosections. *Journal of Metamorphic Geology, 33,* 413-425.

POWELL, R., WHITE, R., GREEN, E., HOLLAND, T. J. B., & DIENER, J. F. A. (2014). On parameterizing thermodynamic descriptions of minerals for petrological calculations. *Journal of Metamorphic Geology, 32*(3), 245-260.

SANDIFORD, M., & POWELL, R. (1991). Some remarks on high-temerature-low-pressure metamorphism in convergent orogens. *Journal of Metamorphic Geology, 9,* 333-340.

SANDIFORD, M., FODEN, J., ZHOU, S., & TURNER, S. (1992b). Granite genesis and the mechanics of convergent orogenic belts with application to the southern Adelaide Fold Belt. *Geological Society of America Special Papers, 272*, 83-94.

SANDIFORD, M., ERASER, G., ARNOLD, J., FODEN, J., & FARROW, T. (1995). Some causes and consequences of high-temperature, low-pressure metamorphism in the eastern Mt Lofty Ranges, South Australia. *Australian Journal of Earth Sciences, 42*(3), 233-240.

SMITH, H. A., & BARREIRO, B. (1990). Monazite U-Pb dating of staurolite grade metamorphism in pelitic schists. *Contributions to Mineralogy and Petrology, 105*(5), 602-615.

SPEAR, F. S., & PYLE, J. M. (2002). Apatite, monazite, and xenotime in metamorphic rocks. *Reviews in mineralogy and geochemistry, 48*(1), 293-335.

SPEAR, F. S., PYLE, J. M., & CHERNIAK, D. (2009). Limitations of chemical dating monazite. *Chemical Geology, 266*(3), 218-230.

TAYLOR, R. J., KIRKLAND, C. L., & CLARK, C. (2016). Accessories after the facts: Constraining the timing, duration and conditions of high-temperature metamorphic processes. *LITHOS, 264*, 239-257.

TURNER, S., SANDIFORD, M., FLÖTTMANN, T., & FODEN, J. (1994). Rb/Sr dating of differentiated cleavage from the upper Adelaidean metasediments at Hallett Cove, southern Adelaide fold belt. *Journal of Structural Geology, 16*(9), 1233-1241.

TURNER, N. J., & FODEN, J. D. (1996). Petrogenesis of late-Delamerian A-type granites and granophyre, South Australia: magma mingling in the Mannum granite, South Australia. *Contributions of Mineralogology and Petrology, 56,* 147-169.

TURNER, S., HAINES, P., FOSTER, D., POWELL, R., SANDIFORD, M., & OFFLER, R. (2009). Did the Delamerian Orogeny start in the Neoproterozoic? *The Journal of Geology, 117*(5), 575-583.

WAKABAYASHI, J. (2004). Tectonic mechanisms associated with P-T paths of regional metamorphism: alternatives to single-cycle thrusting and heating. *Tectonophysics, 392,* 193-218.

WEINBERG, R. F., HASALOVÁ, P., WARD, L., & FANNING, C. M. (2013). Interaction between deformation and magma extraction in migmatites: Examples from Kangaroo Island, South Australia. *Geological Society of America Bulletin, 125*(7-8), 1282-1300.

WHITE, R., POWELL, R., & JOHNSON, T. (2014a). The effect of Mn on mineral stability in metapelites revisited: New a-x relations for manganese-bearing minerals. *Journal of Metamorphic Geology, 32(3),* 261-286.

WHITE, R. W., POWELL, R., HOLLAND, T. J. B., JOHNSON, T. E., & GREEN, E. C. R. (2014b). New mineral activity-composition relations for thermodynamic calculatiosn in metapelitic systems. *Journal of Metamorphic Geology, 32*(3), 261-286.

WILLIAMS, M. L., JERCINOVIC, M. J., & HETHERINGTON, C. J. (2007). Microprobe monazite
geochronology: understanding geologic processes by integrating composition and chronology.
*Annu. Rev. Earth Planet. Sci., 35*, 137-175.

ZHU, X, K., & O'NIONS, R. K. (1999). Monazite chemical composition: some implications for monazite
geochronology. *Contributions to Mineral Petrology, 137,* 351-363.

## APPENDIX A: EXTENDED GEOCHRONOLOGY METHODS

### U-Pb isotopic dating of monazite

In-situ monazite grains were imaged using a Quanta 600 Scanning Electron Microscope (SEM) at Adelaide Microscopy, University of Adelaide. Monazites were identified on the basis of brightness (monazite being the brightest observable grains), using a back-scattered electron (BSE) detector to determine their microstructural locations. Monazite grains are commonly $\leq 20 \mu m$ for samples KS1G, MAC-2 and K2003-1, and commonly 25-35 $\mu m$ for samples 17-KM-04 and 17-KM-05. All errors are quoted at the $2\sigma$ level of precision. All ages are quoted as $^{206}Pb/^{238}U$.

### U-Pb data acquisition

U-Pb isotopic data were collected using Laser Ablation-Inductively Coupled Plasma-Mass Spectrometry (LA-ICP-MS) on in-situ (thin section) monazite grains. LA-ICP-MS monazite analyses were acquired on the Resonetics 193 - Agilent 7900 at Adelaide Microscopy within the University of Adelaide (spot size 13$\mu m$, ablation in a He atmosphere and a laser frequency of 5Hz). Monazite acquisition was undertaken with 30 seconds of background measurement and 30 seconds of sample ablation.

### Data reduction and processing

Monazite isotopic analyses were reduced using Iolite software. Elemental fractionation and mass bias for monazite geochronology was corrected using the primary standard MADel ($^{207/206}Pb = 490.7$ Ma, $^{206}Pb/^{238}U = 518.4$ Ma and $^{207}Pb/^{235}U = 510.4$ Ma, from Payne *et al* (2008)). Data accuracy was monitored by the use of secondary standards, including Ambat (~525Ma), 222 and NIST610.

Ages quoted in this study are in $^{206}Pb/^{238}U$ as all ages are <1000Ma. All errors are at the $2\sigma$ level unless stated otherwise. Concordance was calculated using the ratio ($^{206}Pb/^{238}U$)/($^{207}Pb/^{206}Pb$). Weighted averages of standard analyses in this study for the primary (MADel) and in-house (222 and Ambat) monazite standards are provided in Appendix C.

## APPENDIX B: WHOLE-ROCK GEOCHEMISTRY (WT %)

| Sample | KS1G | K2003-1 | MAC-2 | 17KM04 | 17KM05 | KI-25 |
|--------|------|---------|-------|--------|--------|-------|
| $SiO_2$ | 57.5 | 59.90 | 58.68 | 61.70 | 58.40 | 52.40 |
| $TiO_2$ | 0.845 | 0.68 | 0.97 | 0.78 | 0.97 | 1.44 |
| $Al_2O_3$ | 18.9 | 19.68 | 21.99 | 17.60 | 17.10 | 23.66 |
| Fe2O3T | 8.28 | 6.66 | 6.44 | 7.47 | 7.90 | 10.94 |

| | | | | | |
|---|---|---|---|---|---|
| **MnO** | 0.14 | 0.10 | 0.17 | 0.10 | 0.16 | 0.16 |
| **MgO** | 3.48 | 3.18 | 2.89 | 3.14 | 2.81 | 4.48 |
| **CaO** | 0.99 | 2.70 | 1.52 | 1.04 | 0.50 | 1.48 |
| **Na$_2$O** | 1.81 | 3.02 | 2.67 | 1.33 | 1.36 | 1.10 |
| **K$_2$O** | 4.61 | 3.49 | 4.17 | 4.85 | 8.95 | 3.53 |
| **P$_2$O$_5$** | 0.14 | 0.31 | 0.40 | 0.18 | 0.24 | 0.35 |
| **Total** | 88.415 | 99.72 | 99.90 | 98.19 | 98.39 | 99.54 |
| **FeO** | - | 4.56 | 4.42 | - | - | 6.98 |
| **Fe$_2$O$_3$** | - | 1.59 | 1.53 | 7.47 | 7.90 | 3.18 |
| **LOI** | 1.9 | 2.14 | 2.22 | 1.45 | 1.10 | 2.04 |
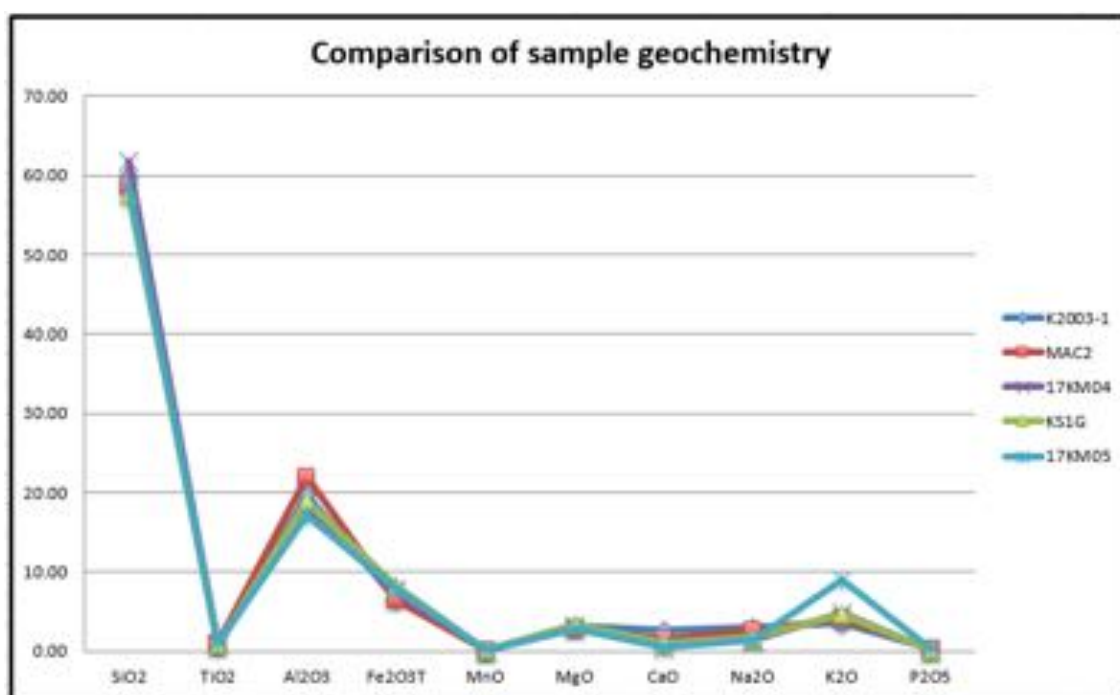


## APPENDIX C: U-PB GEOCHRONOLOGY MONAZITE STANDARD ANALYSES

| Analysis | $^{207}$Pb/$^{206}$Pb | 2σ | $^{207}$Pb/$^{235}$U | 2σ | $^{206}$Pb/$^{238}$U | 2σ | $^{207}$Pb/$^{206}$Pb Age(Ma) | 2σ | $^{206}$Pb/$^{238}$U Age(Ma) | 2σ | $^{207}$Pb/$^{235}$U Age(Ma) | 2σ |
|---|---|---|---|---|---|---|---|---|---|---|---|---|
| **Analysis date: 13/06/2017** | | | | | | | | | | | | |
| Madel-1 | 0.0569 | 0.0017 | 0.652 | 0.021 | 0.08275 | 0.0013 | 487 | 63 | 512.5 | 7.6 | 511 | 13 |
| Madel-2 | 0.0574 | 0.0016 | 0.653 | 0.021 | 0.08393 | 0.0013 | 515 | 61 | 519.5 | 7.9 | 511.3 | 13 |
| Madel-3 | 0.0575 | 0.0017 | 0.663 | 0.022 | 0.0838 | 0.0014 | 512 | 63 | 518.6 | 8.3 | 515.8 | 13 |
| Madel-4 | 0.0563 | 0.0017 | 0.654 | 0.021 | 0.08443 | 0.0013 | 463 | 68 | 522.5 | 7.5 | 510.3 | 13 |
| Madel-5 | 0.0572 | 0.0018 | 0.653 | 0.023 | 0.08329 | 0.0012 | 482 | 70 | 515.7 | 7.4 | 510.6 | 14 |
| Madel-6 | 0.0571 | 0.0017 | 0.65 | 0.021 | 0.08295 | 0.0013 | 494 | 63 | 513.6 | 7.5 | 509.1 | 13 |
| Madel-7 | 0.056 | 0.0016 | 0.65 | 0.023 | 0.084 | 0.0014 | 456 | 65 | 520.8 | 8.2 | 507.6 | 14 |
| Madel-8 | 0.0578 | 0.0016 | 0.671 | 0.021 | 0.0839 | 0.0013 | 518 | 61 | 519.2 | 8 | 521.1 | 13 |
| Madel-9 | 0.0574 | 0.0018 | 0.656 | 0.023 | 0.08337 | 0.0013 | 499 | 68 | 516.2 | 7.8 | 513 | 14 |
| Madel-10 | 0.0569 | 0.0017 | 0.663 | 0.024 | 0.0846 | 0.0014 | 480 | 67 | 523.6 | 8.2 | 519 | 15 |
| Madel-11 | 0.0565 | 0.0017 | 0.652 | 0.022 | 0.08389 | 0.0012 | 463 | 68 | 519.3 | 7.1 | 510.2 | 13 |

| Analysis | $^{207}Pb/^{206}Pb$ | $2\sigma$ | $^{207}Pb/^{235}U$ | $2\sigma$ | $^{206}Pb/^{238}U$ | $2\sigma$ | $^{207}Pb/^{206}Pb$ Age(Ma) | $2\sigma$ | $^{206}Pb/^{238}U$ Age(Ma) | $2\sigma$ | $^{207}Pb/^{235}U$ Age(Ma) | $2\sigma$ |
|---|---|---|---|---|---|---|---|---|---|---|---|---|
| Madel-12 | 0.0567 | 0.0016 | 0.655 | 0.021 | 0.084 | 0.0014 | 479 | 64 | 520.1 | 8 | 511.2 | 13 |
| Madel-13 | 0.0559 | 0.0017 | 0.659 | 0.022 | 0.0843 | 0.0012 | 460 | 68 | 521.7 | 7.4 | 513.3 | 14 |
| Madel-14 | 0.0585 | 0.0019 | 0.685 | 0.024 | 0.0853 | 0.0015 | 541 | 72 | 527.7 | 8.6 | 531 | 15 |
| Madel-15 | 0.0564 | 0.0018 | 0.652 | 0.022 | 0.08404 | 0.0013 | 471 | 66 | 520.2 | 7.7 | 509.2 | 14 |
| Madel-16 | 0.0572 | 0.0017 | 0.657 | 0.022 | 0.08321 | 0.0013 | 497 | 65 | 515.2 | 7.8 | 513.6 | 14 |
| Madel-17 | 0.0568 | 0.0017 | 0.664 | 0.022 | 0.0837 | 0.0013 | 491 | 65 | 519.1 | 7.9 | 516.8 | 13 |
| Madel-18 | 0.0566 | 0.0018 | 0.65 | 0.023 | 0.0829 | 0.0014 | 481 | 67 | 514.3 | 8.2 | 508.7 | 14 |
| Madel-19 | 0.0573 | 0.0017 | 0.649 | 0.024 | 0.083 | 0.0014 | 495 | 65 | 513.9 | 8.2 | 512 | 14 |
| Madel-20 | 0.0568 | 0.0016 | 0.652 | 0.022 | 0.08337 | 0.0013 | 479 | 60 | 516.2 | 7.9 | 509.4 | 13 |
| Madel-21 | 0.0569 | 0.0016 | 0.662 | 0.023 | 0.0838 | 0.0014 | 489 | 62 | 518.9 | 8.5 | 516 | 14 |
| Madel-22 | 0.0572 | 0.0017 | 0.649 | 0.022 | 0.083 | 0.0014 | 501 | 63 | 514 | 8.4 | 508.9 | 14 |
| Madel-23 | 0.0567 | 0.0017 | 0.667 | 0.023 | 0.0845 | 0.0014 | 476 | 67 | 522.7 | 8.3 | 518.5 | 14 |
| Madel-24 | 0.0579 | 0.0016 | 0.675 | 0.022 | 0.0838 | 0.0014 | 520 | 64 | 518.5 | 8.3 | 523 | 14 |
| Madel-25 | 0.056 | 0.0017 | 0.643 | 0.024 | 0.08336 | 0.0013 | 453 | 67 | 516.1 | 7.8 | 505 | 15 |
| Madel-26 | 0.0571 | 0.0016 | 0.657 | 0.022 | 0.08353 | 0.0012 | 492 | 64 | 517.1 | 7 | 512.2 | 14 |
| Madel-27 | 0.0572 | 0.0016 | 0.664 | 0.023 | 0.08338 | 0.0013 | 499 | 66 | 516.2 | 7.9 | 517.3 | 14 |
| Madel-28 | 0.0564 | 0.0017 | 0.661 | 0.025 | 0.0841 | 0.0014 | 467 | 72 | 520.6 | 8.4 | 514 | 15 |
| Madel-29 | 0.0571 | 0.0017 | 0.664 | 0.024 | 0.0836 | 0.0015 | 498 | 65 | 517.3 | 8.7 | 517.7 | 15 |
| Madel-30 | 0.0569 | 0.0017 | 0.658 | 0.024 | 0.08405 | 0.0013 | 487 | 64 | 520.2 | 7.8 | 512.8 | 15 |
| Madel-31 | 0.0566 | 0.0017 | 0.657 | 0.023 | 0.0845 | 0.0015 | 473 | 69 | 523 | 9 | 511.7 | 14 |
| Madel-32 | 0.0595 | 0.0016 | 0.681 | 0.022 | 0.0839 | 0.0014 | 581 | 59 | 519.4 | 8.1 | 528 | 13 |
| Madel-33 | 0.0568 | 0.0018 | 0.649 | 0.022 | 0.083 | 0.0013 | 475 | 68 | 514 | 7.5 | 507 | 13 |
| Madel-34 | 0.0571 | 0.0017 | 0.645 | 0.023 | 0.0827 | 0.0014 | 496 | 64 | 512.2 | 8.5 | 506.3 | 14 |
| Madel-35 | 0.0553 | 0.0017 | 0.637 | 0.023 | 0.08515 | 0.0013 | 418 | 66 | 526.7 | 7.6 | 501.1 | 14 |
| Madel-36 | 0.0583 | 0.0017 | 0.673 | 0.022 | 0.08334 | 0.0013 | 540 | 65 | 516 | 7.7 | 522.9 | 13 |
| Madel-37 | 0.0561 | 0.0018 | 0.641 | 0.024 | 0.0831 | 0.0013 | 437 | 73 | 514.8 | 8 | 502 | 15 |
| Madel-38 | 0.05674 | 0.0015 | 0.66 | 0.021 | 0.0842 | 0.0014 | 484 | 63 | 521.2 | 8.3 | 514.2 | 13 |
| Madel-39 | 0.0559 | 0.0017 | 0.639 | 0.024 | 0.0833 | 0.0015 | 435 | 69 | 516 | 8.7 | 501 | 15 |
| Madel-40 | 0.0576 | 0.0018 | 0.661 | 0.023 | 0.08416 | 0.0013 | 499 | 67 | 520.8 | 8 | 514.4 | 14 |
| **Analysis** | $^{207}Pb/^{206}Pb$ | $2\sigma$ | $^{207}Pb/^{235}U$ | $2\sigma$ | $^{206}Pb/^{238}U$ | $2\sigma$ | $^{207}Pb/^{206}Pb$ Age(Ma) | $2\sigma$ | $^{206}Pb/^{238}U$ Age(Ma) | $2\sigma$ | $^{207}Pb/^{235}U$ Age(Ma) | $2\sigma$ |
| Ambat-1 | 0.05739 | 0.0014 | 0.674 | 0.021 | 0.08546 | 0.0013 | 505 | 57 | 528.6 | 7.5 | 524.7 | 13 |
| Ambat-2 | 0.05748 | 0.0015 | 0.669 | 0.022 | 0.0846 | 0.0013 | 503 | 57 | 523.5 | 7.5 | 519.4 | 13 |
| Ambat-3 | 0.0583 | 0.0016 | 0.68 | 0.023 | 0.08403 | 0.0012 | 547 | 60 | 520.1 | 7.1 | 527.1 | 14 |
| Ambat-4 | 0.0572 | 0.0092 | 0.683 | 0.14 | 0.0855 | 0.0022 | 489 | 190 | 529 | 13 | 527 | 62 |
| Ambat-5 | 0.05792 | 0.0015 | 0.676 | 0.021 | 0.08481 | 0.0011 | 523 | 58 | 524.8 | 6.7 | 523.8 | 13 |
| Ambat-6 | 0.05692 | 0.0015 | 0.662 | 0.021 | 0.08436 | 0.0012 | 486 | 58 | 522.1 | 7.4 | 516.4 | 12 |
| Ambat-7 | 0.05788 | 0.0015 | 0.676 | 0.021 | 0.0837 | 0.0013 | 527 | 59 | 518.2 | 7.6 | 523.8 | 13 |
| Ambat-8 | 0.05765 | 0.0015 | 0.666 | 0.021 | 0.08358 | 0.0012 | 514 | 58 | 517.4 | 7.4 | 517.9 | 13 |
| Ambat-9 | 0.0572 | 0.0015 | 0.673 | 0.022 | 0.08495 | 0.0013 | 507 | 56 | 525.6 | 7.5 | 522.1 | 13 |
| Ambat-10 | 0.05737 | 0.0014 | 0.663 | 0.02 | 0.0831 | 0.0014 | 499 | 56 | 514.8 | 8.1 | 516 | 13 |
| Ambat-11 | 0.05664 | 0.0015 | 0.672 | 0.022 | 0.08597 | 0.0013 | 479 | 57 | 531.6 | 7.6 | 522.3 | 14 |
| Ambat-12 | 0.0575 | 0.0016 | 0.663 | 0.021 | 0.08385 | 0.0012 | 507 | 60 | 519 | 7.4 | 518.1 | 13 |
| Ambat-13 | 0.05686 | 0.0015 | 0.659 | 0.021 | 0.0843 | 0.0014 | 487 | 59 | 521.8 | 8 | 513.8 | 13 |
| Ambat-14 | 0.05723 | 0.0015 | 0.676 | 0.021 | 0.08538 | 0.0012 | 497 | 58 | 528.1 | 7.3 | 524 | 13 |
| Ambat-15 | 0.0566 | 0.0016 | 0.662 | 0.021 | 0.08472 | 0.0013 | 475 | 65 | 524.2 | 7.6 | 516.3 | 13 |
| Ambat-16 | 0.05648 | 0.0014 | 0.6566 | 0.02 | 0.08384 | 0.0013 | 474 | 51 | 519 | 7.5 | 513 | 13 |
| Ambat-17 | 0.05682 | 0.0015 | 0.661 | 0.021 | 0.08414 | 0.0012 | 486 | 56 | 520.8 | 7.4 | 515.6 | 13 |
| Ambat-18 | 0.05737 | 0.0015 | 0.655 | 0.02 | 0.08321 | 0.0012 | 504 | 55 | 515.2 | 7.4 | 510.9 | 12 |
| Ambat-19 | 0.05672 | 0.0015 | 0.655 | 0.02 | 0.08523 | 0.0012 | 478 | 59 | 527.3 | 7.2 | 512.2 | 12 |
| Ambat-20 | 0.05707 | 0.0015 | 0.663 | 0.021 | 0.08446 | 0.0012 | 486 | 59 | 522.6 | 7.4 | 516.2 | 13 |
| **Analysis** | $^{207}Pb/^{206}Pb$ | $2\sigma$ | $^{207}Pb/^{235}U$ | $2\sigma$ | $^{206}Pb/^{238}U$ | $2\sigma$ | $^{207}Pb/^{206}Pb$ Age(Ma) | $2\sigma$ | $^{206}Pb/^{238}U$ Age(Ma) | $2\sigma$ | $^{207}Pb/^{235}U$ Age(Ma) | $2\sigma$ |
| 222-1 | 0.05638 | 0.0018 | 0.565 | 0.02 | 0.07275 | 0.0018 | 458 | 69 | 452.6 | 11 | 454.3 | 13 |
| 222-2 | 0.05539 | 0.0018 | 0.5606 | 0.022 | 0.07361 | 0.0017 | 435 | 68 | 457.8 | 10 | 451.6 | 14 |
| 222-3 | 0.05725 | 0.0015 | 0.5698 | 0.018 | 0.07181 | 0.0011 | 502 | 59 | 447 | 6.5 | 457.5 | 12 |
| 222-4 | 0.0553 | 0.0015 | 0.556 | 0.018 | 0.07233 | 0.0011 | 426 | 61 | 450.1 | 6.4 | 449.4 | 12 |
| 222-5 | 0.0564 | 0.0016 | 0.562 | 0.018 | 0.07233 | 0.0011 | 460 | 61 | 450.2 | 6.6 | 452.4 | 12 |
| 222-6 | 0.05577 | 0.0015 | 0.5574 | 0.018 | 0.07193 | 0.0011 | 439 | 59 | 447.8 | 6.5 | 451.2 | 12 |
| 222-7 | 0.05618 | 0.0014 | 0.5626 | 0.018 | 0.07164 | 0.0011 | 458 | 55 | 446 | 6.7 | 452.9 | 12 |

| Analysis | $^{207}Pb/^{206}Pb$ | 2σ | $^{207}Pb/^{235}U$ | 2σ | $^{206}Pb/^{238}U$ | 2σ | $^{207}Pb/^{206}Pb$ Age(Ma) | 2σ | $^{206}Pb/^{238}U$ Age(Ma) | 2σ | $^{207}Pb/^{235}U$ Age(Ma) | 2σ |
|---|---|---|---|---|---|---|---|---|---|---|---|---|
| 222-8 | 0.05589 | 0.0015 | 0.557 | 0.019 | 0.07262 | 0.0011 | 439 | 60 | 452.6 | 6.8 | 450.1 | 13 |
| 222-9 | 0.0571 | 0.0016 | 0.57 | 0.019 | 0.07265 | 0.0011 | 492 | 61 | 452.1 | 6.8 | 457.4 | 13 |
| 222-10 | 0.05716 | 0.0014 | 0.569 | 0.017 | 0.07227 | 0.0011 | 492 | 55 | 449.8 | 6.3 | 457.8 | 11 |
| 222-11 | 0.05693 | 0.0015 | 0.5682 | 0.018 | 0.07308 | 0.0012 | 492 | 61 | 454.7 | 7.3 | 457.4 | 12 |
| 222-12 | 0.05622 | 0.0015 | 0.5594 | 0.017 | 0.07169 | 0.0011 | 458 | 58 | 446.3 | 6.3 | 450.9 | 11 |
| 222-13 | 0.0553 | 0.0016 | 0.562 | 0.019 | 0.07279 | 0.0012 | 420 | 66 | 452.9 | 7.2 | 453.3 | 13 |
| 222-14 | 0.0572 | 0.0016 | 0.569 | 0.019 | 0.07248 | 0.0011 | 494 | 61 | 451.1 | 6.6 | 457.6 | 12 |
| 222-15 | 0.0565 | 0.0017 | 0.567 | 0.019 | 0.07299 | 0.0011 | 459 | 65 | 454.1 | 6.5 | 455.5 | 12 |
| 222-16 | 0.05711 | 0.0015 | 0.575 | 0.019 | 0.07304 | 0.0011 | 487 | 60 | 454.4 | 6.8 | 461.8 | 12 |
| 222-17 | 0.0569 | 0.0016 | 0.57 | 0.019 | 0.07298 | 0.0011 | 487 | 65 | 454 | 6.9 | 457.3 | 12 |
| 222-18 | 0.0556 | 0.0016 | 0.556 | 0.018 | 0.07258 | 0.0012 | 430 | 63 | 451.6 | 7.2 | 449.5 | 12 |
| 222-19 | 0.05607 | 0.0015 | 0.567 | 0.019 | 0.07354 | 0.0011 | 446 | 61 | 457.4 | 6.8 | 456.5 | 12 |
| 222-20 | 0.0563 | 0.0016 | 0.568 | 0.018 | 0.07328 | 0.0012 | 463 | 62 | 455.9 | 7.1 | 456.5 | 12 |
| Analysis | $^{207}Pb/^{206}Pb$ | 2σ | $^{207}Pb/^{235}U$ | 2σ | $^{206}Pb/^{238}U$ | 2σ | $^{207}Pb/^{206}Pb$ Age(Ma) | 2σ | $^{206}Pb/^{238}U$ Age(Ma) | 2σ | $^{207}Pb/^{235}U$ Age(Ma) | 2σ |
| **Analysis date: 26/06/17** | | | | | | | | | | | | |
| Madel-1 | 0.05713 | 0.0012 | 0.657 | 0.013 | 0.08314 | 0.0012 | 495 | 47 | 514.8 | 4.7 | 512.7 | 7.9 |
| Madel-2 | 0.05627 | 0.0012 | 0.657 | 0.013 | 0.08436 | 0.0013 | 461 | 47 | 522 | 5.3 | 512.6 | 7.7 |
| Madel-3 | 0.05681 | 0.0013 | 0.659 | 0.013 | 0.08461 | 0.0013 | 481 | 50 | 523.6 | 5.2 | 513.6 | 8.1 |
| Madel-4 | 0.0573 | 0.0014 | 0.657 | 0.015 | 0.0826 | 0.0015 | 512 | 52 | 511.4 | 6.8 | 511.9 | 9.3 |
| Madel-5 | 0.05689 | 0.0013 | 0.657 | 0.014 | 0.0834 | 0.0013 | 483 | 52 | 516.3 | 5.2 | 513.1 | 8.8 |
| Madel-7 | 0.0578 | 0.0014 | 0.662 | 0.015 | 0.08363 | 0.0012 | 510 | 55 | 517.7 | 4.3 | 517.3 | 8.5 |
| Madel-8 | 0.0566 | 0.0015 | 0.654 | 0.015 | 0.08419 | 0.0013 | 474 | 57 | 521 | 5.4 | 511.3 | 9.2 |
| Madel-9 | 0.0572 | 0.0014 | 0.658 | 0.015 | 0.08426 | 0.0013 | 490 | 53 | 521.5 | 5.5 | 513.9 | 8.8 |
| Madel-10 | 0.0577 | 0.0013 | 0.657 | 0.013 | 0.08368 | 0.0013 | 513 | 51 | 518 | 5.4 | 513.1 | 7.9 |
| Madel-11 | 0.0578 | 0.0013 | 0.659 | 0.014 | 0.08332 | 0.0012 | 518 | 50 | 515.9 | 4.7 | 513.5 | 8.4 |
| Madel-12 | 0.0577 | 0.0014 | 0.657 | 0.014 | 0.08378 | 0.0013 | 519 | 53 | 518.6 | 5.1 | 512.6 | 8.6 |
| Madel-13 | 0.05619 | 0.0012 | 0.654 | 0.014 | 0.08422 | 0.0012 | 471 | 47 | 521.2 | 4.6 | 510.8 | 8.5 |
| Madel-14 | 0.0573 | 0.0015 | 0.659 | 0.015 | 0.08356 | 0.0013 | 503 | 57 | 517.3 | 5.2 | 514.9 | 9.6 |
| Madel-15 | 0.05783 | 0.0012 | 0.664 | 0.015 | 0.08395 | 0.0013 | 517 | 47 | 519.6 | 5.7 | 517.8 | 9.6 |
| Madel-16 | 0.05697 | 0.0013 | 0.655 | 0.013 | 0.08317 | 0.0012 | 487 | 48 | 515 | 4.5 | 511.2 | 7.9 |
| Madel-17 | 0.05549 | 0.0013 | 0.654 | 0.013 | 0.08405 | 0.0013 | 428 | 50 | 520.2 | 5.3 | 510.7 | 8.1 |
| Madel-18 | 0.05682 | 0.0013 | 0.66 | 0.014 | 0.08354 | 0.0012 | 487 | 53 | 517.2 | 4.3 | 514 | 8.3 |
| Madel-19 | 0.0583 | 0.0024 | 0.667 | 0.031 | 0.0841 | 0.0015 | 493 | 57 | 520.3 | 6.9 | 517 | 17 |
| Madel-21 | 0.0577 | 0.0013 | 0.658 | 0.014 | 0.08407 | 0.0013 | 521 | 48 | 520.3 | 5.1 | 515.2 | 8.3 |
| Madel-22 | 0.05772 | 0.0013 | 0.661 | 0.015 | 0.08361 | 0.0012 | 521 | 49 | 517.6 | 4.6 | 514.8 | 9 |
| Madel-23 | 0.05628 | 0.0013 | 0.651 | 0.013 | 0.08329 | 0.0013 | 460 | 51 | 515.7 | 5.2 | 508.9 | 8.2 |
| Madel-24 | 0.05612 | 0.0012 | 0.6595 | 0.012 | 0.0839 | 0.0012 | 454 | 50 | 519.3 | 5 | 514 | 7.4 |
| Madel-25 | 0.05674 | 0.0012 | 0.658 | 0.014 | 0.08331 | 0.0013 | 484 | 45 | 515.8 | 5.3 | 513.7 | 8.1 |
| Madel-26 | 0.0566 | 0.0013 | 0.6574 | 0.012 | 0.08411 | 0.0013 | 479 | 49 | 520.6 | 5.2 | 512.8 | 7.4 |
| Madel-27 | 0.0569 | 0.0013 | 0.659 | 0.014 | 0.0836 | 0.0013 | 482 | 54 | 517.6 | 5.1 | 513.3 | 8.5 |
| Madel-28 | 0.0567 | 0.0012 | 0.657 | 0.013 | 0.08386 | 0.0013 | 473 | 48 | 519.1 | 5.7 | 512.2 | 8.2 |
| Madel-29 | 0.05781 | 0.0013 | 0.659 | 0.014 | 0.08394 | 0.0013 | 515 | 48 | 519.6 | 5.6 | 514.8 | 8.9 |
| Madel-30 | 0.05677 | 0.0012 | 0.655 | 0.013 | 0.08381 | 0.0012 | 485 | 44 | 519.4 | 4.1 | 511 | 7.9 |
| Madel-31 | 0.0571 | 0.0014 | 0.663 | 0.014 | 0.0844 | 0.0012 | 491 | 54 | 522.3 | 4.4 | 515.8 | 8.8 |
| Madel-32 | 0.0568 | 0.0013 | 0.655 | 0.013 | 0.08258 | 0.0012 | 496 | 47 | 511.4 | 5 | 511.2 | 8.3 |
| Madel-33 | 0.05718 | 0.0013 | 0.658 | 0.015 | 0.08351 | 0.0013 | 501 | 54 | 517 | 5.7 | 514.1 | 9.4 |
| Madel-34 | 0.0575 | 0.0013 | 0.657 | 0.015 | 0.08398 | 0.0013 | 513 | 51 | 519.8 | 5.7 | 512.2 | 9.3 |
| Analysis | $^{207}Pb/^{206}Pb$ | 2σ | $^{207}Pb/^{235}U$ | 2σ | $^{206}Pb/^{238}U$ | 2σ | $^{207}Pb/^{206}Pb$ Age(Ma) | 2σ | $^{206}Pb/^{238}U$ Age(Ma) | 2σ | $^{207}Pb/^{235}U$ Age(Ma) | 2σ |
| Ambat-1 | 0.0569 | 0.0013 | 0.662 | 0.014 | 0.0847 | 0.0014 | 484 | 53 | 524.2 | 8.4 | 515.6 | 8.5 |
| Ambat-2 | 0.0578 | 0.0013 | 0.662 | 0.013 | 0.08402 | 0.0013 | 524 | 50 | 520 | 7.9 | 516.2 | 7.8 |
| Ambat-3 | 0.0569 | 0.0014 | 0.674 | 0.016 | 0.0847 | 0.0014 | 488 | 54 | 523.9 | 8.5 | 522.5 | 10 |
| Ambat-4 | 0.0572 | 0.0014 | 0.674 | 0.017 | 0.08405 | 0.0013 | 512 | 55 | 520.2 | 7.8 | 524.9 | 11 |
| Ambat-5 | 0.0573 | 0.0014 | 0.658 | 0.014 | 0.08452 | 0.0013 | 493 | 53 | 523 | 8 | 513.8 | 8.6 |
| Ambat-6 | 0.0581 | 0.0014 | 0.67 | 0.015 | 0.08504 | 0.0013 | 535 | 54 | 526.1 | 7.5 | 519.9 | 9.1 |
| Ambat-7 | 0.057 | 0.0015 | 0.678 | 0.016 | 0.086 | 0.0014 | 493 | 56 | 531.7 | 8.2 | 524.8 | 9.9 |
| Ambat-8 | 0.0569 | 0.0014 | 0.676 | 0.017 | 0.0847 | 0.0014 | 496 | 58 | 524.3 | 8.2 | 523.4 | 10 |
| Ambat-9 | 0.0579 | 0.0015 | 0.628 | 0.015 | 0.08225 | 0.0013 | 512 | 57 | 509.5 | 7.6 | 495.7 | 9.6 |
| Ambat-10 | 0.0567 | 0.0014 | 0.617 | 0.015 | 0.08303 | 0.0013 | 481 | 57 | 514.1 | 7.7 | 487.2 | 9.2 |
| Ambat-11 | 0.05758 | 0.0013 | 0.684 | 0.013 | 0.0852 | 0.0014 | 512 | 47 | 526.9 | 8.3 | 528.5 | 8.1 |
| Ambat-12 | 0.0575 | 0.0015 | 0.682 | 0.015 | 0.08548 | 0.0013 | 497 | 58 | 528.7 | 7.5 | 528.7 | 9.3 |
| Ambat-13 | 0.0574 | 0.0016 | 0.665 | 0.016 | 0.08369 | 0.0013 | 507 | 61 | 518 | 7.9 | 516.7 | 9.8 |
| Ambat-14 | 0.0569 | 0.0015 | 0.664 | 0.017 | 0.08457 | 0.0012 | 475 | 59 | 523.3 | 7.3 | 516.6 | 10 |
| Ambat-15 | 0.0564 | 0.0014 | 0.659 | 0.016 | 0.08439 | 0.0013 | 458 | 54 | 522.3 | 7.6 | 513.6 | 9.7 |

| Analysis | $^{207}Pb/^{206}Pb$ | 2σ | $^{207}Pb/^{235}U$ | 2σ | $^{206}Pb/^{238}U$ | 2σ | $^{207}Pb/^{206}Pb$ Age(Ma) | 2σ | $^{206}Pb/^{238}U$ Age(Ma) | 2σ | $^{207}Pb/^{235}U$ Age(Ma) | 2σ |
|---|---|---|---|---|---|---|---|---|---|---|---|---|
| Ambat-16 | 0.05709 | 0.0013 | 0.669 | 0.015 | 0.08415 | 0.0013 | 487 | 50 | 520.8 | 8 | 519.8 | 9.2 |
| Ambat-17 | 0.0573 | 0.0015 | 0.663 | 0.016 | 0.0847 | 0.0013 | 495 | 56 | 524.1 | 7.7 | 516.9 | 9.6 |
| Ambat-18 | 0.0563 | 0.0014 | 0.647 | 0.015 | 0.08554 | 0.0013 | 457 | 57 | 529.1 | 7.9 | 506.1 | 9.2 |
| Analysis | $^{207}Pb/^{206}Pb$ | 2σ | $^{207}Pb/^{235}U$ | 2σ | $^{206}Pb/^{238}U$ | 2σ | $^{207}Pb/^{206}Pb$ Age(Ma) | 2σ | $^{206}Pb/^{238}U$ Age(Ma) | 2σ | $^{207}Pb/^{235}U$ Age(Ma) | 2σ |
| 222-1 | 0.05662 | 0.0012 | 0.558 | 0.012 | 0.07178 | 0.0012 | 484 | 48 | 446.8 | 7.1 | 450 | 8 |
| 222-2 | 0.0556 | 0.0016 | 0.549 | 0.016 | 0.07229 | 0.0012 | 435 | 66 | 449.9 | 7.1 | 444 | 10 |
| 222-3 | 0.0561 | 0.0014 | 0.565 | 0.013 | 0.07182 | 0.001 | 453 | 55 | 447.1 | 6.1 | 454.5 | 8.7 |
| 222-5 | 0.0558 | 0.0013 | 0.5441 | 0.011 | 0.07217 | 0.0011 | 453 | 54 | 449.2 | 6.8 | 440.8 | 7.4 |
| 222-6 | 0.05597 | 0.0013 | 0.55 | 0.012 | 0.07233 | 0.0011 | 442 | 52 | 450.1 | 6.8 | 444.6 | 7.9 |
| 222-7 | 0.05635 | 0.0011 | 0.5731 | 0.011 | 0.07226 | 0.0011 | 465 | 46 | 449.7 | 6.8 | 459.8 | 6.9 |
| 222-8 | 0.05742 | 0.0012 | 0.5766 | 0.012 | 0.07121 | 0.001 | 502 | 45 | 443.4 | 6.1 | 461.9 | 7.5 |
| 222-9 | 0.0561 | 0.0015 | 0.524 | 0.012 | 0.07093 | 0.0011 | 470 | 59 | 441.7 | 6.6 | 429.2 | 8.1 |
| 222-10 | 0.0565 | 0.0018 | 0.516 | 0.015 | 0.07085 | 0.0012 | 466 | 70 | 441.2 | 7.2 | 421.5 | 10 |
| 222-11 | 0.0574 | 0.0017 | 0.587 | 0.015 | 0.07202 | 0.0012 | 503 | 63 | 448.2 | 7.5 | 468 | 9.8 |
| 222-12 | 0.0573 | 0.0018 | 0.581 | 0.017 | 0.07197 | 0.0012 | 490 | 71 | 448 | 7 | 465.7 | 10 |
| 222-13 | 0.0549 | 0.0019 | 0.552 | 0.02 | 0.0722 | 0.0014 | 403 | 83 | 449.6 | 8.7 | 445 | 13 |
| 222-14 | 0.0563 | 0.0015 | 0.554 | 0.016 | 0.07162 | 0.0012 | 470 | 63 | 445.9 | 7.4 | 446.7 | 10 |
| 222-15 | 0.05541 | 0.0013 | 0.559 | 0.012 | 0.07257 | 0.0012 | 425 | 52 | 451.6 | 7.3 | 451.4 | 7.8 |
| 222-16 | 0.0554 | 0.0014 | 0.562 | 0.013 | 0.07277 | 0.0011 | 418 | 55 | 452.8 | 6.8 | 454.4 | 8.6 |
| 222-17 | 0.0566 | 0.0016 | 0.559 | 0.015 | 0.07374 | 0.0011 | 476 | 65 | 458.6 | 6.9 | 452.9 | 9.2 |
| 222-18 | 0.0549 | 0.0014 | 0.546 | 0.014 | 0.07272 | 0.001 | 410 | 54 | 452.5 | 6.1 | 441.5 | 8.8 |

| Analysis | $^{207}Pb/^{206}Pb$ | 2σ | $^{207}Pb/^{235}U$ | 2σ | $^{206}Pb/^{238}U$ | 2σ | $^{207}Pb/^{206}Pb$ Age(Ma) | 2σ | $^{206}Pb/^{238}U$ Age(Ma) | 2σ | $^{207}Pb/^{235}U$ Age(Ma) | 2σ |
|---|---|---|---|---|---|---|---|---|---|---|---|---|
| **Analysis date: 18/08/17** | | | | | | | | | | | | |
| Madel-1 | 0.0561 | 0.0022 | 0.636 | 0.034 | 0.0836 | 0.0024 | 447 | 88 | 517.3 | 14 | 499.2 | 21 |
| Madel-2 | 0.0595 | 0.0024 | 0.691 | 0.04 | 0.084 | 0.0024 | 579 | 87 | 520 | 14 | 533 | 24 |
| Madel-3 | 0.05651 | 0.002 | 0.66 | 0.034 | 0.0837 | 0.0023 | 467 | 80 | 518 | 14 | 514.3 | 21 |
| Madel-4 | 0.0569 | 0.0022 | 0.655 | 0.035 | 0.0837 | 0.0024 | 476 | 87 | 517.9 | 14 | 511.3 | 21 |
| Madel-5 | 0.0573 | 0.0021 | 0.689 | 0.038 | 0.0839 | 0.0025 | 507 | 83 | 519.1 | 15 | 531 | 23 |
| Madel-6 | 0.0579 | 0.0023 | 0.671 | 0.036 | 0.08366 | 0.0023 | 524 | 81 | 517.9 | 14 | 520.3 | 22 |
| Madel-7 | 0.0558 | 0.0022 | 0.638 | 0.035 | 0.08367 | 0.0022 | 436 | 94 | 518 | 13 | 500 | 22 |
| Madel-8 | 0.0571 | 0.0023 | 0.647 | 0.035 | 0.0838 | 0.0023 | 477 | 88 | 518.7 | 14 | 506.1 | 21 |
| Madel-9 | 0.0572 | 0.0023 | 0.659 | 0.036 | 0.0837 | 0.0024 | 486 | 90 | 517.9 | 14 | 513.5 | 22 |
| Madel-10 | 0.05732 | 0.0021 | 0.663 | 0.035 | 0.0839 | 0.0023 | 496 | 78 | 519.2 | 14 | 516.1 | 21 |
| Madel-11 | 0.05678 | 0.002 | 0.653 | 0.034 | 0.08363 | 0.0023 | 476 | 80 | 517.7 | 13 | 510.2 | 21 |
| Madel-12 | 0.05674 | 0.002 | 0.654 | 0.034 | 0.08376 | 0.0023 | 480 | 75 | 518.5 | 14 | 510.3 | 21 |
| Analysis | $^{207}Pb/^{206}Pb$ | 2σ | $^{207}Pb/^{235}U$ | 2σ | $^{206}Pb/^{238}U$ | 2σ | $^{207}Pb/^{206}Pb$ Age(Ma) | 2σ | $^{206}Pb/^{238}U$ Age(Ma) | 2σ | $^{207}Pb/^{235}U$ Age(Ma) | 2σ |
| Ambat-1 | 0.05619 | 0.0021 | 0.661 | 0.035 | 0.08535 | 0.0023 | 457 | 84 | 527.9 | 14 | 514.8 | 21 |
| Ambat-2 | 0.0572 | 0.0021 | 0.672 | 0.036 | 0.08407 | 0.0023 | 487 | 83 | 520.3 | 14 | 521.2 | 22 |
| Ambat-3 | 0.0564 | 0.0021 | 0.656 | 0.035 | 0.08664 | 0.0024 | 466 | 81 | 535.6 | 14 | 511.8 | 22 |
| Ambat-4 | 0.05596 | 0.002 | 0.654 | 0.035 | 0.08716 | 0.0024 | 448 | 79 | 538.7 | 14 | 510.2 | 21 |
| Analysis | $^{207}Pb/^{206}Pb$ | 2σ | $^{207}Pb/^{235}U$ | 2σ | $^{206}Pb/^{238}U$ | 2σ | $^{207}Pb/^{206}Pb$ Age(Ma) | 2σ | $^{206}Pb/^{238}U$ Age(Ma) | 2σ | $^{207}Pb/^{235}U$ Age(Ma) | 2σ |
| 222-1 | 0.0564 | 0.0021 | 0.558 | 0.029 | 0.07372 | 0.0021 | 459 | 83 | 458.5 | 12 | 449.8 | 19 |
| 222-2 | 0.05595 | 0.0021 | 0.555 | 0.029 | 0.07349 | 0.002 | 441 | 83 | 457.1 | 12 | 448.1 | 19 |
| 222-3 | 0.0556 | 0.0021 | 0.555 | 0.03 | 0.07409 | 0.002 | 424 | 86 | 460.7 | 12 | 447.6 | 19 |
| 222-4 | 0.05615 | 0.002 | 0.567 | 0.03 | 0.07504 | 0.002 | 452 | 80 | 466.4 | 12 | 455.7 | 19 |

## APPENDIX D: U-PB GEOCHRONOLOGY MONAZITE RESULTS

| Analysis | $^{207}Pb/^{206}Pb$ | 2σ | $^{207}Pb/^{235}U$ | 2σ | $^{206}Pb/^{238}U$ | 2σ | $^{207}Pb/^{206}Pb$ Age(Ma) | 2σ | $^{206}Pb/^{238}U$ Age(Ma) | 2σ | $^{207}Pb/^{235}U$ Age(Ma) | 2σ |
|---|---|---|---|---|---|---|---|---|---|---|---|---|

| | | | | | | | | | | | | |
|---|---|---|---|---|---|---|---|---|---|---|---|---|
| KS1G-2 | 0.0798 | 0.0035 | 0.881 | 0.05 | 0.0796 | 0.0027 | 1185 | 89 | 494 | 16 | 644 | 27 |
| KS1G-3 | 0.0676 | 0.0034 | 0.745 | 0.03 | 0.0788 | 0.002 | 872 | 99 | 489 | 12 | 565 | 18 |
| KS1G-4 | 0.0568 | 0.0018 | 0.625 | 0.038 | 0.0793 | 0.0039 | 495 | 73 | 492.1 | 23 | 492.7 | 24 |
| KS1G-7 | 0.0618 | 0.0044 | 0.668 | 0.026 | 0.0774 | 0.0029 | 673 | 160 | 480.7 | 18 | 522 | 16 |
| KS1G-8 | 0.0579 | 0.0018 | 0.636 | 0.023 | 0.0802 | 0.0014 | 522 | 67 | 499 | 9.3 | 499.8 | 14 |
| KS1G-10 | 0.0706 | 0.0028 | 0.802 | 0.048 | 0.0823 | 0.0031 | 940 | 82 | 510 | 19 | 597 | 27 |
| KS1G-11 | 0.0577 | 0.0017 | 0.649 | 0.027 | 0.0808 | 0.0023 | 511 | 67 | 500.9 | 14 | 507.6 | 16 |
| KS1G-12 | 0.0954 | 0.0035 | 1.103 | 0.046 | 0.0853 | 0.0025 | 1548 | 79 | 528 | 15 | 754 | 23 |
| KS1G-13 | 0.0588 | 0.0026 | 0.647 | 0.025 | 0.0795 | 0.0015 | 562 | 94 | 493.2 | 9.1 | 506 | 15 |
| KS1G-14 | 0.0607 | 0.0021 | 0.66 | 0.025 | 0.0791 | 0.0019 | 621 | 77 | 490.4 | 11 | 514.5 | 15 |
| KS1G-15 | 0.0589 | 0.002 | 0.666 | 0.026 | 0.0819 | 0.0019 | 557 | 74 | 507.6 | 11 | 518 | 16 |
| KS1G-16 | 0.1017 | 0.0049 | 1.183 | 0.061 | 0.088 | 0.0044 | 1648 | 91 | 551 | 23 | 792 | 28 |
| KS1G-17 | 0.0579 | 0.002 | 0.633 | 0.028 | 0.0787 | 0.0024 | 521 | 72 | 488.1 | 14 | 497.9 | 18 |
| KS1G-18 | 0.0609 | 0.0028 | 0.664 | 0.028 | 0.0802 | 0.0021 | 627 | 97 | 497.2 | 13 | 516.8 | 17 |
| KS1G-19 | 0.0645 | 0.0029 | 0.714 | 0.032 | 0.0802 | 0.0014 | 748 | 97 | 497.4 | 8.5 | 546.7 | 19 |
| KS1G-20 | 0.1122 | 0.0064 | 1.265 | 0.062 | 0.0819 | 0.0023 | 1827 | 100 | 507.5 | 14 | 829 | 28 |
| KS1G-21 | 0.0631 | 0.0035 | 0.689 | 0.04 | 0.0793 | 0.0026 | 699 | 120 | 491.6 | 16 | 531 | 24 |
| KS1G-22 | 0.064 | 0.0043 | 0.695 | 0.054 | 0.078 | 0.0028 | 722 | 110 | 484.2 | 17 | 535 | 29 |
| KS1G-23 | 0.0571 | 0.01 | 0.626 | 0.14 | 0.0793 | 0.0033 | 490 | 280 | 491.7 | 20 | 493.3 | 75 |
| KS1G-26 | 0.076 | 0.0024 | 0.851 | 0.033 | 0.0807 | 0.0019 | 1089 | 61 | 500.3 | 12 | 625 | 18 |
| KS1G-27 | 0.0621 | 0.0027 | 0.677 | 0.035 | 0.07921 | 0.002 | 677 | 84 | 491.4 | 12 | 526.2 | 21 |
| KS1G-28 | 0.0621 | 0.0023 | 0.682 | 0.029 | 0.0796 | 0.0027 | 683 | 78 | 493.7 | 16 | 528 | 17 |
| KS1G-29 | 0.075 | 0.0062 | 0.857 | 0.068 | 0.0822 | 0.0034 | 1090 | 150 | 509 | 20 | 627 | 37 |
| KS1G-30 | 0.0555 | 0.002 | 0.617 | 0.03 | 0.0806 | 0.0023 | 420 | 81 | 499.8 | 14 | 487.3 | 19 |
| KS1G-31 | 0.0588 | 0.0027 | 0.638 | 0.026 | 0.0794 | 0.0014 | 554 | 110 | 492.5 | 8.3 | 500.7 | 17 |
| KS1G-32 | 0.0622 | 0.0023 | 0.676 | 0.025 | 0.0793 | 0.0015 | 675 | 75 | 491.7 | 9.2 | 525.8 | 15 |
| KS1G-33 | 0.0896 | 0.0045 | 1.064 | 0.056 | 0.0844 | 0.0022 | 1440 | 110 | 523 | 13 | 735 | 28 |
| KS1G-34 | 0.0575 | 0.0021 | 0.627 | 0.022 | 0.0793 | 0.0016 | 510 | 77 | 491.8 | 9.8 | 493.8 | 14 |
| KS1G-35 | 0.0636 | 0.0025 | 0.673 | 0.029 | 0.0777 | 0.0019 | 737 | 73 | 482.3 | 11 | 522.3 | 18 |
| KS1G-36 | 0.068 | 0.0024 | 0.735 | 0.027 | 0.0788 | 0.0019 | 871 | 70 | 489 | 12 | 559.3 | 16 |
| KS1G-38 | 0.0804 | 0.0038 | 0.942 | 0.045 | 0.0846 | 0.0039 | 1195 | 94 | 523 | 23 | 673 | 23 |
| KS1G-39 | 0.0794 | 0.0027 | 0.913 | 0.034 | 0.0828 | 0.0022 | 1177 | 66 | 513 | 13 | 658 | 18 |
| KS1G-40 | 0.0652 | 0.0054 | 0.724 | 0.069 | 0.0802 | 0.0027 | 805 | 160 | 497.4 | 16 | 552.5 | 40 |
| KS1G-41 | 0.0651 | 0.0028 | 0.71 | 0.039 | 0.0795 | 0.0023 | 780 | 89 | 493.2 | 14 | 547 | 23 |
| KS1G-42 | 0.0702 | 0.0035 | 0.744 | 0.034 | 0.0762 | 0.0024 | 945 | 98 | 473.5 | 15 | 564 | 20 |
| KS1G-46 | 0.0759 | 0.0045 | 0.854 | 0.06 | 0.0821 | 0.003 | 1080 | 120 | 509 | 18 | 625 | 32 |

| Analysis | $^{207}Pb/^{206}Pb$ | 2σ | $^{207}Pb/^{235}U$ | 2σ | $^{206}Pb/^{238}U$ | 2σ | $^{207}Pb/^{206}Pb$ Age(Ma) | 2σ | $^{206}Pb/^{238}U$ Age(Ma) | 2σ | $^{207}Pb/^{235}U$ Age(Ma) | 2σ |
|---|---|---|---|---|---|---|---|---|---|---|---|---|
| K2003-1 | 0.0626 | 0.003 | 0.727 | 0.04 | 0.085 | 0.0024 | 684 | 99 | 525.7 | 14 | 554 | 24 |
| K2003-2 | 0.05745 | 0.0019 | 0.609 | 0.022 | 0.07653 | 0.0013 | 506 | 71 | 475.3 | 7.8 | 482.6 | 15 |
| K2003-3 | 0.0909 | 0.0047 | 0.912 | 0.056 | 0.0727 | 0.0027 | 1434 | 96 | 452 | 16 | 657 | 30 |
| K2003-4 | 0.0589 | 0.0021 | 0.623 | 0.023 | 0.07746 | 0.0017 | 560 | 83 | 480.9 | 10 | 491.2 | 15 |
| K2003-5 | 0.0572 | 0.0018 | 0.634 | 0.024 | 0.07947 | 0.0014 | 492 | 70 | 492.9 | 8.5 | 497.9 | 15 |
| K2003-6 | 0.0623 | 0.0025 | 0.662 | 0.026 | 0.0774 | 0.0018 | 674 | 87 | 480.6 | 11 | 515 | 17 |
| K2003-7 | 0.0625 | 0.0017 | 0.625 | 0.022 | 0.07287 | 0.0016 | 691 | 59 | 453.4 | 9.9 | 492.6 | 14 |

| Analysis | $^{207}Pb/^{206}Pb$ | 2σ | $^{207}Pb/^{235}U$ | 2σ | $^{206}Pb/^{238}U$ | 2σ | $^{207}Pb/^{206}Pb$ Age(Ma) | 2σ | $^{206}Pb/^{238}U$ Age(Ma) | 2σ | $^{207}Pb/^{235}U$ Age(Ma) | 2σ |
|---|---|---|---|---|---|---|---|---|---|---|---|---|
| K2003-8 | 0.0573 | 0.0023 | 0.682 | 0.026 | 0.0862 | 0.0021 | 498 | 90 | 532.7 | 12 | 528.9 | 16 |
| K2003-9 | 0.0603 | 0.0027 | 0.668 | 0.026 | 0.0802 | 0.002 | 613 | 100 | 497.2 | 12 | 519 | 16 |
| K2003-11 | 0.0883 | 0.0053 | 1.179 | 0.076 | 0.0943 | 0.0037 | 1380 | 130 | 581 | 20 | 794 | 34 |
| K2003-12 | 0.065 | 0.0025 | 0.717 | 0.034 | 0.0787 | 0.0017 | 779 | 82 | 488.5 | 10 | 550 | 20 |
| K2003-13 | 0.0672 | 0.0058 | 0.816 | 0.062 | 0.089 | 0.0032 | 826 | 170 | 549 | 19 | 606 | 35 |
| K2003-15 | 0.05948 | 0.0017 | 0.647 | 0.022 | 0.07851 | 0.0012 | 587 | 59 | 487.2 | 7.2 | 506.2 | 15 |
| K2003-16 | 0.0612 | 0.004 | 0.67 | 0.043 | 0.0799 | 0.0019 | 649 | 150 | 495.3 | 11 | 520 | 26 |
| K2003-17 | 0.0571 | 0.0021 | 0.648 | 0.021 | 0.0824 | 0.0017 | 487 | 82 | 510 | 10 | 506 | 13 |
| K2003-19 | 0.0567 | 0.0021 | 0.63 | 0.029 | 0.0808 | 0.0019 | 484 | 79 | 500.6 | 11 | 495 | 13 |
| K2003-20 | 0.0587 | 0.002 | 0.625 | 0.023 | 0.0775 | 0.0019 | 553 | 76 | 481.4 | 11 | 492.8 | 15 |
| K2003-21 | 0.0569 | 0.0022 | 0.601 | 0.028 | 0.07655 | 0.0022 | 487 | 82 | 475.4 | 13 | 477.1 | 18 |
| K2003-22 | 0.0568 | 0.002 | 0.625 | 0.024 | 0.0796 | 0.0018 | 493 | 87 | 493.9 | 11 | 492.5 | 15 |
| K2003-23 | 0.0575 | 0.0023 | 0.639 | 0.035 | 0.08 | 0.0018 | 509 | 98 | 497.2 | 11 | 501.1 | 21 |
| K2003-24 | 0.0575 | 0.0024 | 0.648 | 0.025 | 0.08089 | 0.0018 | 518 | 110 | 501.4 | 11 | 506.8 | 16 |
| K2003-26 | 0.0565 | 0.003 | 0.577 | 0.034 | 0.0739 | 0.002 | 494 | 100 | 460 | 12 | 462 | 22 |
| K2003-27 | 0.0686 | 0.004 | 0.789 | 0.051 | 0.085 | 0.0033 | 869 | 120 | 526 | 20 | 590 | 29 |
| K2003-28 | 0.0564 | 0.0027 | 0.619 | 0.032 | 0.0784 | 0.0018 | 464 | 100 | 486.2 | 11 | 489 | 21 |
| K2003-29 | 0.0592 | 0.002 | 0.695 | 0.024 | 0.0837 | 0.0015 | 565 | 71 | 518.2 | 9.2 | 535.5 | 15 |
| K2003-30 | 0.0629 | 0.0019 | 0.671 | 0.033 | 0.0773 | 0.002 | 698 | 66 | 480 | 12 | 521 | 20 |
| K2003-31 | 0.05712 | 0.0017 | 0.617 | 0.027 | 0.07895 | 0.0017 | 496 | 63 | 489.8 | 9.9 | 487.8 | 16 |
| K2003-32 | 0.05966 | 0.002 | 0.71 | 0.028 | 0.086 | 0.0023 | 585 | 74 | 531.8 | 13 | 544.1 | 17 |
| K2003-33 | 0.0579 | 0.002 | 0.662 | 0.024 | 0.0818 | 0.0019 | 531 | 76 | 506.6 | 11 | 515.2 | 15 |
| K2003-34 | 0.07 | 0.0025 | 0.797 | 0.041 | 0.0823 | 0.0023 | 936 | 71 | 510 | 14 | 595 | 22 |
| K2003-36 | 0.0584 | 0.0022 | 0.65 | 0.025 | 0.0812 | 0.0017 | 534 | 84 | 503.5 | 10 | 508 | 15 |
| K2003-37 | 0.0582 | 0.0016 | 0.597 | 0.022 | 0.0734 | 0.0022 | 542 | 61 | 456.5 | 13 | 475.1 | 14 |
| K2003-38 | 0.0614 | 0.0037 | 0.668 | 0.052 | 0.0791 | 0.0023 | 647 | 120 | 490.4 | 14 | 519 | 31 |
| K2003-39 | 0.0592 | 0.0015 | 0.636 | 0.022 | 0.07744 | 0.0016 | 582 | 56 | 480.8 | 9.6 | 499.7 | 14 |
| K2003-40 | 0.05839 | 0.0016 | 0.64 | 0.023 | 0.0805 | 0.0013 | 541 | 59 | 499.1 | 7.9 | 502.1 | 14 |
| K2003-41 | 0.0684 | 0.0031 | 0.799 | 0.03 | 0.0851 | 0.0027 | 877 | 99 | 526.7 | 16 | 596 | 17 |
| K2003-42 | 0.05728 | 0.0018 | 0.615 | 0.024 | 0.07759 | 0.0024 | 499 | 69 | 481.7 | 14 | 486.7 | 15 |
| K2003-43 | 0.0676 | 0.0029 | 0.755 | 0.035 | 0.0807 | 0.0023 | 855 | 94 | 500.3 | 14 | 570.5 | 20 |

| Analysis | $^{207}Pb/^{206}Pb$ | 2σ | $^{207}Pb/^{235}U$ | 2σ | $^{206}Pb/^{238}U$ | 2σ | $^{207}Pb/^{206}Pb$ Age(Ma) | 2σ | $^{206}Pb/^{238}U$ Age(Ma) | 2σ | $^{207}Pb/^{235}U$ Age(Ma) | 2σ |
|---|---|---|---|---|---|---|---|---|---|---|---|---|
| MAC1-1 | 0.0608 | 0.0037 | 0.671 | 0.035 | 0.0804 | 0.0022 | 632 | 130 | 498.5 | 13 | 522.5 | 22 |
| MAC1-2 | 0.0617 | 0.0022 | 0.682 | 0.029 | 0.08012 | 0.0017 | 662 | 78 | 496.8 | 9.9 | 527.2 | 17 |
| MAC1-3 | 0.0622 | 0.0029 | 0.668 | 0.038 | 0.0781 | 0.0021 | 660 | 100 | 485 | 13 | 518 | 22 |
| MAC1-4 | 0.0545 | 0.0033 | 0.598 | 0.033 | 0.0784 | 0.0016 | 397 | 130 | 486.5 | 9.5 | 475 | 21 |
| MAC1-7 | 0.0618 | 0.0026 | 0.677 | 0.031 | 0.0791 | 0.0025 | 668 | 93 | 491 | 15 | 528 | 19 |
| MAC1-8 | 0.0565 | 0.0019 | 0.624 | 0.028 | 0.0809 | 0.0018 | 474 | 75 | 501.5 | 11 | 492 | 17 |
| MAC1-9 | 0.0597 | 0.0029 | 0.715 | 0.037 | 0.0864 | 0.0023 | 593 | 99 | 534 | 14 | 547 | 22 |
| MAC1-10 | 0.057 | 0.0024 | 0.615 | 0.029 | 0.0786 | 0.0027 | 494 | 93 | 487.5 | 16 | 486 | 18 |

| | | | | | | | | | | | | |
|---|---|---|---|---|---|---|---|---|---|---|---|---|
| MAC1-11 | 0.0597 | 0.0037 | 0.616 | 0.043 | 0.0763 | 0.0029 | 570 | 140 | 474 | 17 | 486 | 27 |
| MAC1-12 | 0.0641 | 0.0026 | 0.681 | 0.03 | 0.0772 | 0.002 | 747 | 88 | 479.2 | 12 | 527 | 18 |
| MAC1-14 | 0.0573 | 0.002 | 0.629 | 0.026 | 0.07876 | 0.0015 | 506 | 74 | 489.5 | 8.8 | 495.3 | 16 |
| MAC1-15 | 0.0608 | 0.0022 | 0.657 | 0.033 | 0.0781 | 0.0021 | 633 | 79 | 484.6 | 13 | 512 | 20 |
| MAC1-17 | 0.0575 | 0.0019 | 0.661 | 0.03 | 0.0833 | 0.0019 | 501 | 76 | 515.5 | 11 | 515 | 17 |
| MAC1-19 | 0.0658 | 0.0037 | 0.702 | 0.036 | 0.0775 | 0.0027 | 805 | 120 | 481 | 18 | 539 | 21 |
| MAC1-20 | 0.06 | 0.0042 | 0.646 | 0.041 | 0.0779 | 0.0025 | 590 | 140 | 483.4 | 15 | 506 | 25 |
| MAC1-22 | 0.0645 | 0.0031 | 0.7 | 0.034 | 0.0777 | 0.0026 | 755 | 100 | 482 | 16 | 541 | 21 |
| MAC1-23 | 0.0577 | 0.002 | 0.6391 | 0.022 | 0.0808 | 0.0019 | 512 | 77 | 500.9 | 11 | 501.6 | 14 |
| MAC1-24 | 0.0584 | 0.0018 | 0.652 | 0.026 | 0.0804 | 0.0015 | 531 | 68 | 498.2 | 9 | 508.9 | 16 |
| MAC1-25 | 0.0576 | 0.0027 | 0.62 | 0.036 | 0.07736 | 0.0023 | 516 | 100 | 480.3 | 14 | 490 | 22 |
| MAC1-26 | 0.0575 | 0.0026 | 0.634 | 0.034 | 0.07918 | 0.002 | 506 | 110 | 491.2 | 12 | 498.3 | 21 |
| MAC1-27 | 0.0586 | 0.0017 | 0.655 | 0.023 | 0.0816 | 0.0019 | 548 | 62 | 505.4 | 11 | 511.3 | 14 |
| MAC1-28 | 0.0582 | 0.0022 | 0.616 | 0.023 | 0.077 | 0.0026 | 533 | 84 | 478.4 | 15 | 486.9 | 14 |
| MAC1-29 | 0.0584 | 0.0028 | 0.644 | 0.03 | 0.0796 | 0.0023 | 534 | 110 | 493.7 | 14 | 506.6 | 18 |
| MAC1-30 | 0.0599 | 0.0034 | 0.628 | 0.04 | 0.0755 | 0.0021 | 584 | 120 | 468.9 | 13 | 494 | 25 |
| MAC1-34 | 0.0597 | 0.0051 | 0.724 | 0.036 | 0.0891 | 0.0049 | 579 | 200 | 550.2 | 29 | 553 | 22 |
| MAC1-35 | 0.0577 | 0.0028 | 0.639 | 0.029 | 0.08021 | 0.0022 | 518 | 110 | 497.3 | 13 | 502.3 | 18 |
| MAC1-37 | 0.0587 | 0.004 | 0.663 | 0.042 | 0.079 | 0.003 | 563 | 140 | 490 | 18 | 516 | 25 |
| MAC1-38 | 0.0576 | 0.0018 | 0.665 | 0.025 | 0.0831 | 0.0019 | 518 | 73 | 514.4 | 11 | 517.4 | 15 |
| MAC1-39 | 0.0639 | 0.0026 | 0.691 | 0.031 | 0.0783 | 0.0017 | 727 | 85 | 486.1 | 10 | 535 | 18 |
| MAC1-40 | 0.0575 | 0.0021 | 0.627 | 0.028 | 0.0781 | 0.0024 | 511 | 81 | 485 | 15 | 494 | 18 |
| MAC1-41 | 0.05869 | 0.0022 | 0.651 | 0.027 | 0.0799 | 0.0023 | 556 | 84 | 495.7 | 14 | 508.6 | 16 |
| MAC1-43 | 0.0562 | 0.0018 | 0.643 | 0.022 | 0.0822 | 0.0016 | 461 | 72 | 509.2 | 9.7 | 503.6 | 16 |
| MAC1-45 | 0.0621 | 0.0027 | 0.681 | 0.035 | 0.0793 | 0.0018 | 685 | 87 | 491.8 | 11 | 527 | 21 |
| MAC1-46 | 0.05715 | 0.0015 | 0.613 | 0.02 | 0.07751 | 0.0013 | 515 | 57 | 481.2 | 7.6 | 485.1 | 13 |

| Analysis | $^{207}Pb/^{206}Pb$ | $2\sigma$ | $^{207}Pb/^{235}U$ | $2\sigma$ | $^{206}Pb/^{238}U$ | $2\sigma$ | $^{207}Pb/^{206}Pb$ Age(Ma) | $2\sigma$ | $^{206}Pb/^{238}U$ Age(Ma) | $2\sigma$ | $^{207}Pb/^{235}U$ Age(Ma) | $2\sigma$ |
|---|---|---|---|---|---|---|---|---|---|---|---|---|
| 17-KM-04-1 | 0.05676 | 0.0012 | 0.5986 | 0.011 | 0.0783 | 0.0012 | 475 | 48 | 485.9 | 6.9 | 476.1 | 7.1 |
| 17-KM-04-2 | 0.057 | 0.0013 | 0.602 | 0.013 | 0.07802 | 0.0013 | 493 | 48 | 484.3 | 7.8 | 478.4 | 7.9 |
| 17-KM-04-3 | 0.0591 | 0.0014 | 0.661 | 0.021 | 0.083 | 0.0022 | 574 | 47 | 516 | 13 | 514 | 13 |
| 17-KM-04-4 | 0.059 | 0.0021 | 0.645 | 0.027 | 0.0815 | 0.002 | 558 | 79 | 505 | 12 | 505 | 17 |
| 17-KM-04-5 | 0.05752 | 0.0013 | 0.611 | 0.013 | 0.0784 | 0.0015 | 519 | 51 | 486.7 | 8.8 | 484.2 | 8 |
| 17-KM-04-6 | 0.06 | 0.0014 | 0.653 | 0.014 | 0.08105 | 0.0012 | 593 | 51 | 502.3 | 7.3 | 510.5 | 8.8 |
| 17-KM-04-7 | 0.05609 | 0.0012 | 0.6049 | 0.012 | 0.08017 | 0.0012 | 453 | 46 | 497.1 | 7 | 480 | 7.3 |
| 17-KM-04-8 | 0.0597 | 0.0017 | 0.651 | 0.016 | 0.0811 | 0.0016 | 597 | 57 | 502.4 | 9.6 | 508.7 | 9.6 |
| 17-KM-04-9 | 0.0678 | 0.0025 | 0.72 | 0.026 | 0.07814 | 0.0012 | 834 | 77 | 485 | 7.1 | 549 | 15 |
| 17-KM-04-10 | 0.0584 | 0.0016 | 0.606 | 0.016 | 0.0777 | 0.0019 | 538 | 62 | 482 | 11 | 480.5 | 10 |
| 17-KM-04-12 | 0.0663 | 0.0023 | 0.696 | 0.023 | 0.0784 | 0.0014 | 804 | 73 | 486.5 | 8.6 | 538 | 13 |
| 17-KM-04-13 | 0.05637 | 0.0012 | 0.5889 | 0.011 | 0.07728 | 0.0012 | 465 | 46 | 479.8 | 7.2 | 469.9 | 6.8 |
| 17-KM-04-14 | 0.0652 | 0.0023 | 0.728 | 0.027 | 0.0824 | 0.0019 | 780 | 76 | 510.5 | 11 | 554 | 16 |
| 17-KM-04-15 | 0.0636 | 0.0019 | 0.662 | 0.024 | 0.0763 | 0.0013 | 718 | 62 | 474.1 | 7.9 | 514 | 14 |
| 17-KM-04-16 | 0.0634 | 0.0017 | 0.689 | 0.017 | 0.0775 | 0.0014 | 711 | 56 | 481.3 | 8.3 | 531.9 | 10 |
| 17-KM-04-17 | 0.0776 | 0.002 | 0.881 | 0.022 | 0.08038 | 0.0012 | 1137 | 50 | 498.4 | 7.4 | 641 | 12 |
| 17-KM-04-18 | 0.0621 | 0.0024 | 0.685 | 0.031 | 0.0781 | 0.0016 | 660 | 83 | 484.6 | 9.3 | 529 | 18 |
| 17-KM-04-19 | 0.0955 | 0.0044 | 1.119 | 0.052 | 0.083 | 0.0014 | 1516 | 85 | 513.7 | 8.1 | 758 | 25 |
| 17-KM-04-20 | 0.05682 | 0.0011 | 0.629 | 0.012 | 0.07802 | 0.0013 | 487 | 43 | 484.2 | 7.6 | 495.2 | 7.5 |
| 17-KM-04-21 | 0.05716 | 0.0013 | 0.634 | 0.013 | 0.07831 | 0.0011 | 508 | 51 | 486 | 6.8 | 499 | 8 |
| 17-KM-04-24 | 0.05846 | 0.0012 | 0.622 | 0.014 | 0.07592 | 0.0011 | 550 | 49 | 471.7 | 6.9 | 490.9 | 8.5 |
| 17-KM-04-25 | 0.06106 | 0.0013 | 0.652 | 0.014 | 0.0767 | 0.0013 | 640 | 48 | 476.4 | 7.5 | 510.4 | 9.1 |
| 17-KM-04-26 | 0.0611 | 0.0017 | 0.697 | 0.019 | 0.0819 | 0.0017 | 645 | 60 | 507.7 | 10 | 538 | 11 |
| 17-KM-04-27 | 0.0626 | 0.0017 | 0.668 | 0.017 | 0.07607 | 0.0012 | 693 | 54 | 472.6 | 7.4 | 519.2 | 10 |
| 17-KM-04-29 | 0.0573 | 0.0012 | 0.6067 | 0.012 | 0.07672 | 0.0011 | 497 | 46 | 476.5 | 6.7 | 482 | 7.4 |
| 17-KM-04-30 | 0.06077 | 0.0013 | 0.666 | 0.014 | 0.07856 | 0.0012 | 640 | 48 | 487.5 | 7.2 | 517.8 | 8.4 |
| 17-KM-04-31 | 0.058 | 0.0014 | 0.634 | 0.015 | 0.0811 | 0.0013 | 522 | 55 | 502.9 | 8 | 498.1 | 9 |

| Analysis | $^{207}Pb/^{206}Pb$ | $2\sigma$ | $^{207}Pb/^{235}U$ | $2\sigma$ | $^{206}Pb/^{238}U$ | $2\sigma$ | $^{207}Pb/^{206}Pb$ Age(Ma) | $2\sigma$ | $^{206}Pb/^{238}U$ Age(Ma) | $2\sigma$ | $^{207}Pb/^{235}U$ Age(Ma) | $2\sigma$ |
|---|---|---|---|---|---|---|---|---|---|---|---|---|
| 17-KM-04-32 | 0.0635 | 0.0018 | 0.695 | 0.02 | 0.0804 | 0.0016 | 737 | 60 | 498.6 | 9.3 | 535 | 12 |
| 17-KM-04-33 | 0.0611 | 0.0024 | 0.656 | 0.032 | 0.0805 | 0.002 | 628 | 83 | 499 | 12 | 511 | 20 |
| 17-KM-04-34 | 0.05675 | 0.0011 | 0.613 | 0.013 | 0.07933 | 0.0013 | 476 | 44 | 492.1 | 7.8 | 487 | 7.7 |
| 17-KM-04-35 | 0.0562 | 0.0011 | 0.607 | 0.012 | 0.07839 | 0.0013 | 457 | 42 | 486.4 | 7.8 | 481.3 | 7.6 |
| 17-KM-04-36 | 0.05615 | 0.0012 | 0.626 | 0.013 | 0.08137 | 0.0012 | 452 | 47 | 504.3 | 7.1 | 494.4 | 7.9 |
| 17-KM-04-37 | 0.0801 | 0.0025 | 0.901 | 0.031 | 0.0815 | 0.0016 | 1216 | 59 | 505.1 | 9.4 | 651 | 16 |
| 17-KM-04-38 | 0.062 | 0.0012 | 0.658 | 0.013 | 0.07801 | 0.0011 | 677 | 44 | 484.2 | 6.9 | 513.1 | 8.2 |
| 17-KM-04-39 | 0.0656 | 0.0025 | 0.72 | 0.028 | 0.0789 | 0.0014 | 797 | 85 | 489.6 | 8.2 | 553 | 15 |
| 17-KM-04-40 | 0.0693 | 0.002 | 0.777 | 0.023 | 0.0808 | 0.0017 | 898 | 59 | 500.8 | 9.9 | 583 | 13 |
| 17-KM-04-41 | 0.069 | 0.0023 | 0.764 | 0.028 | 0.0797 | 0.0015 | 886 | 70 | 494 | 9.1 | 574 | 17 |
| 17-KM-04-42 | 0.05711 | 0.0012 | 0.6286 | 0.012 | 0.07947 | 0.0011 | 494 | 44 | 492.9 | 6.7 | 494.9 | 7.3 |
| 17-KM-04-43 | 0.06437 | 0.0013 | 0.701 | 0.014 | 0.0786 | 0.0012 | 753 | 44 | 487.7 | 7.1 | 541.2 | 8.5 |
| 17-KM-04-44 | 0.0625 | 0.0016 | 0.669 | 0.017 | 0.07736 | 0.0013 | 682 | 54 | 480.3 | 7.7 | 519.4 | 10 |
| 17-KM-04-45 | 0.0639 | 0.0024 | 0.698 | 0.019 | 0.0788 | 0.0021 | 722 | 81 | 489 | 13 | 539 | 12 |
| 17-KM-04-46 | 0.0562 | 0.0014 | 0.626 | 0.014 | 0.07871 | 0.0012 | 451 | 54 | 489.2 | 7.3 | 494.3 | 8.4 |
| 17-KM-04-47 | 0.0642 | 0.0019 | 0.7 | 0.022 | 0.0761 | 0.0017 | 771 | 62 | 473 | 10 | 538 | 13 |
| 17-KM-04-48 | 0.0605 | 0.0019 | 0.659 | 0.026 | 0.0761 | 0.0018 | 612 | 68 | 473 | 11 | 513 | 16 |
| 17-KM-04-51 | 0.0596 | 0.0012 | 0.6583 | 0.012 | 0.07502 | 0.0011 | 596 | 40 | 466.3 | 6.7 | 513.3 | 7.2 |
| 17-KM-04-52 | 0.05698 | 0.0012 | 0.602 | 0.014 | 0.0711 | 0.0012 | 484 | 47 | 442.7 | 7.3 | 478.2 | 8.6 |
| 17-KM-04-53 | 0.0629 | 0.0028 | 0.749 | 0.038 | 0.0804 | 0.0026 | 688 | 94 | 499 | 16 | 566 | 22 |
| 17-KM-04-54 | 0.0576 | 0.0014 | 0.644 | 0.018 | 0.0761 | 0.0016 | 510 | 52 | 472.6 | 9.9 | 506.9 | 10 |
| 17-KM-04-55 | 0.0582 | 0.0015 | 0.632 | 0.018 | 0.07322 | 0.0012 | 541 | 56 | 455.5 | 7.5 | 497 | 11 |
| 17-KM-04-56 | 0.0598 | 0.0014 | 0.694 | 0.016 | 0.07734 | 0.0013 | 591 | 53 | 480.2 | 7.7 | 535.8 | 9.4 |
| 17-KM-04-57 | 0.05773 | 0.0012 | 0.621 | 0.013 | 0.07284 | 0.0013 | 522 | 45 | 453.2 | 7.6 | 490 | 8.2 |
| 17-KM-04-58 | 0.0603 | 0.0017 | 0.693 | 0.02 | 0.0782 | 0.0015 | 605 | 61 | 485.2 | 8.8 | 534 | 12 |
| 17-KM-04-59 | 0.0702 | 0.0073 | 0.784 | 0.079 | 0.0781 | 0.0019 | 870 | 190 | 485 | 11 | 580 | 41 |
| 17-KM-04-60 | 0.0616 | 0.002 | 0.689 | 0.035 | 0.0769 | 0.0026 | 651 | 67 | 478 | 16 | 531 | 20 |
| 17-KM-04-61 | 0.0587 | 0.0013 | 0.5491 | 0.011 | 0.07352 | 0.0011 | 549 | 50 | 457.3 | 6.9 | 444.2 | 7.2 |
| 17-KM-04-62 | 0.062 | 0.0018 | 0.636 | 0.024 | 0.081 | 0.0022 | 668 | 63 | 502 | 13 | 499 | 15 |
| 17-KM-04-63 | 0.0583 | 0.0015 | 0.591 | 0.013 | 0.0788 | 0.0013 | 543 | 56 | 488.7 | 8 | 470.9 | 8.6 |
| 17-KM-04-64 | 0.057 | 0.0013 | 0.57 | 0.014 | 0.07843 | 0.0013 | 489 | 47 | 486.7 | 7.6 | 457.8 | 8.8 |
| 17-KM-04-65 | 0.0627 | 0.0035 | 0.593 | 0.034 | 0.0746 | 0.0019 | 690 | 110 | 464 | 12 | 476 | 20 |

| Analysis | $^{207}Pb/^{206}Pb$ | $2\sigma$ | $^{207}Pb/^{235}U$ | $2\sigma$ | $^{206}Pb/^{238}U$ | $2\sigma$ | $^{207}Pb/^{206}Pb$ Age(Ma) | $2\sigma$ | $^{206}Pb/^{238}U$ Age(Ma) | $2\sigma$ | $^{207}Pb/^{235}U$ Age(Ma) | $2\sigma$ |
|---|---|---|---|---|---|---|---|---|---|---|---|---|
| 17-KM-05-1 | 0.05741 | 0.0012 | 0.5642 | 0.011 | 0.0776 | 0.0012 | 501 | 45 | 481.8 | 6.9 | 454 | 7.1 |
| 17-KM-05-2 | 0.0583 | 0.0021 | 0.619 | 0.023 | 0.0827 | 0.0021 | 518 | 79 | 512 | 13 | 488 | 14 |
| 17-KM-05-3 | 0.0584 | 0.0014 | 0.575 | 0.014 | 0.0777 | 0.0013 | 547 | 52 | 482.2 | 8 | 461 | 8.7 |
| 17-KM-05-4 | 0.0629 | 0.003 | 0.61 | 0.029 | 0.0777 | 0.0022 | 701 | 100 | 482 | 13 | 482 | 18 |
| 17-KM-05-5 | 0.05675 | 0.0012 | 0.569 | 0.013 | 0.0785 | 0.0015 | 474 | 48 | 486.9 | 8.7 | 456.8 | 8.6 |
| 17-KM-05-6 | 0.05755 | 0.0013 | 0.5803 | 0.011 | 0.07918 | 0.0012 | 521 | 49 | 491.2 | 7.2 | 464.3 | 7.3 |
| 17-KM-05-7 | 0.05803 | 0.0013 | 0.597 | 0.015 | 0.07973 | 0.0012 | 527 | 52 | 494.5 | 7.3 | 474.9 | 9.4 |
| 17-KM-05-8 | 0.05775 | 0.0012 | 0.579 | 0.012 | 0.07646 | 0.0012 | 518 | 47 | 475.6 | 7 | 463.3 | 7.8 |
| 17-KM-05-9 | 0.05802 | 0.0013 | 0.628 | 0.014 | 0.08224 | 0.0012 | 534 | 45 | 509.5 | 7.4 | 494.4 | 8.7 |
| 17-KM-05-13 | 0.0573 | 0.0016 | 0.724 | 0.02 | 0.0875 | 0.0018 | 513 | 63 | 540.6 | 11 | 552 | 12 |
| 17-KM-05-14 | 0.0586 | 0.0017 | 0.672 | 0.02 | 0.0796 | 0.0014 | 560 | 62 | 493.4 | 8.3 | 522 | 12 |
| 17-KM-05-15 | 0.0583 | 0.0018 | 0.715 | 0.025 | 0.086 | 0.002 | 551 | 67 | 532 | 12 | 551 | 15 |
| 17-KM-05-16 | 0.05729 | 0.0012 | 0.616 | 0.013 | 0.0754 | 0.0013 | 496 | 47 | 468.8 | 7.9 | 487.2 | 8.4 |
| 17-KM-05-17 | 0.0557 | 0.0013 | 0.647 | 0.015 | 0.0806 | 0.0014 | 448 | 56 | 499.4 | 8.4 | 507.4 | 9 |
| 17-KM-05-18 | 0.05614 | 0.0011 | 0.6065 | 0.012 | 0.07617 | 0.0012 | 457 | 47 | 473.2 | 7.3 | 481.1 | 7.4 |
| 17-KM-05-19 | 0.0577 | 0.0014 | 0.64 | 0.016 | 0.0785 | 0.0014 | 509 | 55 | 487.4 | 8.6 | 502.8 | 10 |
| 17-KM-05-20 | 0.058 | 0.0015 | 0.603 | 0.015 | 0.07327 | 0.0012 | 524 | 56 | 455.8 | 7.5 | 479.7 | 9.6 |
| 17-KM-05-21 | 0.05673 | 0.0013 | 0.598 | 0.016 | 0.0751 | 0.0015 | 475 | 51 | 466.6 | 9.2 | 475.7 | 10 |
| 17-KM-05-22 | 0.0562 | 0.0014 | 0.658 | 0.015 | 0.0831 | 0.0014 | 459 | 52 | 514.8 | 8.5 | 513 | 9.1 |
| 17-KM-05-23 | 0.0588 | 0.0014 | 0.63 | 0.017 | 0.076 | 0.0014 | 566 | 54 | 471.9 | 8.2 | 495.5 | 11 |
| 17-KM-05-25 | 0.0614 | 0.0014 | 0.739 | 0.017 | 0.0858 | 0.0015 | 645 | 48 | 530.7 | 9 | 562.7 | 9.9 |
| 17-KM-05-28 | 0.0749 | 0.004 | 0.876 | 0.077 | 0.087 | 0.0046 | 1050 | 110 | 538 | 27 | 635 | 42 |
| 17-KM-05-31 | 0.0623 | 0.0016 | 0.652 | 0.016 | 0.0776 | 0.0013 | 672 | 56 | 481.6 | 7.9 | 509.1 | 9.6 |
| 17-KM-05-32 | 0.0692 | 0.0022 | 0.765 | 0.03 | 0.0806 | 0.0014 | 895 | 61 | 499.7 | 8.6 | 575 | 17 |
| 17-KM-05-33 | 0.0722 | 0.0026 | 0.779 | 0.031 | 0.0815 | 0.0016 | 1004 | 71 | 505.3 | 9.4 | 585 | 17 |
| 17-KM-05-34 | 0.0708 | 0.0018 | 0.738 | 0.016 | 0.07851 | 0.0013 | 945 | 55 | 487.2 | 7.6 | 560.7 | 9.5 |
| 17-KM-05-37 | 0.0606 | 0.0015 | 0.647 | 0.016 | 0.0801 | 0.0014 | 633 | 59 | 496.5 | 8.6 | 507.6 | 10 |
| 17-KM-05-39 | 0.0659 | 0.0039 | 0.726 | 0.039 | 0.0842 | 0.0022 | 790 | 110 | 521 | 13 | 554 | 21 |

| 17-KM-05-40 | 0.0557 | 0.0013 | 0.591 | 0.013 | 0.07882 | 0.0012 | 437 | 53 | 489 | 7.4 | 471.9 | 8.7 |
|---|---|---|---|---|---|---|---|---|---|---|---|---|
| 17-KM-05-42 | 0.0585 | 0.0014 | 0.668 | 0.014 | 0.08191 | 0.0013 | 543 | 54 | 507.5 | 7.7 | 519 | 8.6 |
| 17-KM-05-43 | 0.0578 | 0.0014 | 0.63 | 0.015 | 0.07714 | 0.0012 | 521 | 56 | 479 | 6.9 | 495.4 | 9.2 |
| 17-KM-05-44 | 0.0587 | 0.0014 | 0.636 | 0.015 | 0.077 | 0.0013 | 549 | 50 | 478.1 | 7.8 | 499.6 | 9.2 |
| 17-KM-05-45 | 0.0609 | 0.0022 | 0.649 | 0.02 | 0.0755 | 0.0014 | 647 | 73 | 469.2 | 8.6 | 507 | 12 |
| 17-KM-05-46 | 0.0596 | 0.0014 | 0.669 | 0.013 | 0.07916 | 0.0013 | 582 | 50 | 491 | 7.6 | 520.6 | 7.8 |
| 17-KM-05-47 | 0.057 | 0.0016 | 0.643 | 0.017 | 0.08071 | 0.0012 | 474 | 63 | 500.3 | 7.4 | 504.5 | 11 |
| 17-KM-05-48 | 0.0577 | 0.0016 | 0.647 | 0.015 | 0.0803 | 0.0014 | 514 | 59 | 497.7 | 8.3 | 506.4 | 9 |
| 17-KM-05-49 | 0.0606 | 0.0018 | 0.648 | 0.018 | 0.0771 | 0.0013 | 607 | 63 | 479 | 8.1 | 507.8 | 11 |
| 17-KM-05-50 | 0.058 | 0.0016 | 0.653 | 0.016 | 0.081 | 0.0013 | 530 | 61 | 502.1 | 7.6 | 509.9 | 9.9 |
| 17-KM-05-51 | 0.063 | 0.002 | 0.709 | 0.021 | 0.0814 | 0.0016 | 717 | 68 | 504.3 | 9.7 | 543 | 13 |
| 17-KM-05-52 | 0.05742 | 0.0012 | 0.626 | 0.014 | 0.0782 | 0.0014 | 523 | 46 | 485 | 8.1 | 493 | 8.7 |
| 17-KM-05-53 | 0.0569 | 0.0015 | 0.64 | 0.015 | 0.0815 | 0.0015 | 481 | 57 | 505 | 8.7 | 501.7 | 9.3 |
| 17-KM-05-54 | 0.05679 | 0.0013 | 0.628 | 0.014 | 0.0813 | 0.0014 | 485 | 49 | 503.9 | 8.2 | 495.7 | 8.9 |
| 17-KM-05-55 | 0.0559 | 0.0015 | 0.639 | 0.016 | 0.0832 | 0.0014 | 434 | 60 | 515.3 | 8.4 | 501.3 | 9.9 |

| Analysis | $^{207}Pb/^{206}Pb$ | $2\sigma$ | $^{207}Pb/^{235}U$ | $2\sigma$ | $^{206}Pb/^{238}U$ | $2\sigma$ | $^{207}Pb/^{206}Pb$ Age(Ma) | $2\sigma$ | $^{206}Pb/^{238}U$ Age(Ma) | $2\sigma$ | $^{207}Pb/^{235}U$ Age(Ma) | $2\sigma$ |
|---|---|---|---|---|---|---|---|---|---|---|---|---|
| RDC mnz-1 | 0.05658 | 0.0021 | 0.605 | 0.031 | 0.07277 | 0.002 | 466 | 79 | 452.8 | 12 | 480 | 20 |
| RDC mnz-2 | 0.0561 | 0.0021 | 0.592 | 0.031 | 0.06783 | 0.0019 | 448 | 83 | 423 | 12 | 471.8 | 20 |
| RDC mnz-3 | 0.0559 | 0.0022 | 0.597 | 0.032 | 0.06857 | 0.002 | 434 | 88 | 427.5 | 12 | 474.7 | 20 |
| RDC mnz-4 | 0.0573 | 0.0022 | 0.626 | 0.034 | 0.06979 | 0.002 | 490 | 83 | 434.9 | 12 | 492.9 | 21 |
| RDC mnz-5 | 0.0564 | 0.0021 | 0.625 | 0.033 | 0.07102 | 0.002 | 455 | 83 | 442.2 | 12 | 492.7 | 21 |
| RDC mnz-6 | 0.0566 | 0.0023 | 0.598 | 0.033 | 0.0689 | 0.0022 | 465 | 88 | 429.5 | 14 | 475.3 | 21 |
| RDC mnz-7 | 0.0558 | 0.0024 | 0.635 | 0.036 | 0.075 | 0.0022 | 430 | 94 | 466.3 | 13 | 498 | 22 |
| RDC mnz-8 | 0.0564 | 0.0022 | 0.641 | 0.036 | 0.0846 | 0.0024 | 459 | 87 | 523.6 | 14 | 502 | 22 |
| RDC mnz-9 | 0.0571 | 0.0023 | 0.643 | 0.035 | 0.0844 | 0.0024 | 481 | 88 | 522.4 | 14 | 503.6 | 22 |
| RDC mnz-12 | 0.0559 | 0.0022 | 0.621 | 0.034 | 0.08262 | 0.0022 | 433 | 87 | 511.7 | 13 | 489.6 | 21 |
| RDC mnz-13 | 0.05584 | 0.002 | 0.616 | 0.034 | 0.0818 | 0.0027 | 439 | 80 | 507 | 16 | 486.6 | 21 |

## APPENDIX E: EXTENDED EMPA METHODS

Chemical compositions of garnet, andalusite, staurolite, chlorite, biotite, muscovite, sillimanite, ilmenite and potassium feldspar were acquired using a Cameca SXFive electron microprobe at the Adelaide Microscopy, University of Adelaide.  Calibration was undertaken on natural and synthetic mineral standards, following the standard protocols at Adelaide Microscopy.  For each spot analysis, a beam current of 20nA and accelerating voltage of 15kV was set, and a PAP correction was applied to all data. Each analysis resulted in measurements of $SiO_2$, $TiO_2$, $Cr_2O_3$, $Al_2O_3$, FeO, MnO, MgO, CaO, $Na_2O$, $K_2O$, ZnO, Cl and F using Wavelength Dispersive Spectrometers (WDS).

## APPENDIX F: RANGE OF CHEMISTRY OF MINERALS

| | KS1G | K2003-1 | MAC-2 | 17KM04 | 17KM05 |
|---|---|---|---|---|---|
| **Garnet core** $X_{alm}$ $X_{py}$ $X_{grs}$ $X_{sps}$ | 0.643-0.644 0.060-0.065 0.041-0.042 0.189-0.191 | 0.629-0.631 0.077-0.100 0.045-0.046 0.213-0.214 | 0.644 0.075-0.101 0.034 0.215-0.216 | - - - - | - - - - |
| **Garnet rim** $X_{alm}$ | 0.685-0.688 0.067-0.089 | 0.633-0.636 0.054-0.085 | 0.641-0.640 0.029-0.045 | - - | - - |

| | | | | | |
|---|---|---|---|---|---|
| $X_{py}$ | 0.033 | 0.047-0.048 | 0.033-0.035 | - | - |
| $X_{grs}$ | 0.173-0.176 | 0.210-0.224 | 0.211-0.217 | - | - |
| $X_{sps}$ | | | | | |
| **Biotite** | | | | | |
| F (wt%) | 0.192 | 0.083 | 0.221 | 0.264 | 0.222 |
| Cl (wt%) | 0.089 | 0.024 | 0.083 | 0.096 | 0.080 |
| $TiO_2$ (wt%) | 1.485 | 1.523 | 1.822 | 2.173 | 2.787 |
| Xbi | 0.520 | 0.511 | 0.511 | 0.478 | 0.436 |
| **Muscovite** | | | | | |
| n(mu) | 0.179 | - | 0.210 | 0.044 | - |
| c(mu) | 0.001 | - | 0.000 | 0.003 | - |
| p(mu) | 0.726 | - | 0.586 | 0.848 | - |
| p(cel) | 0.047 | - | 0.107 | 0.046 | - |
| p(fcel) | 0.047 | - | 0.097 | 0.059 | - |
| **Ilmenite** | | | | | |
| g(ilm) | - | - | 0.018 | - | - |
| m(ilm) | - | - | 0.044 | - | - |
| p(ilm) | - | - | 0.655 | - | - |
| p(hem) | - | - | 0.282 | - | - |
| MnO (wt%) | - | - | 1.566 | - | - |
| $TiO_2$ (wt%) | - | - | 28.526 | - | - |
| **Potassium Feldspar** | | | | | |
| na(ksp) | - | - | - | 0.103 | 0.66-0.78 |
| p(abh) | - | - | - | 0.103 | 0.66-0.78 |
| p(an) | - | - | - | 0.001 | 0.001 |
| p(san) | - | - | - | 0.897 | 0.921-0.933 |
| **Staurolite** | | | | | |
| $XFe^{2+}$ | 0.824 | 0.807 | 0.821 | - | - |
| Xmg | 0.176 | 0.193 | 0.179 | - | - |
| XFe(tot.) | 0.824 | 0.807 | 0.821 | - | - |

$X_{alm}=Fe^{2+}/(Fe^{2+}+Mg+Ca+Mn)$, $X_{py}=Mg/(Fe^{2+}+Mg+Ca+Mn)$, $X_{grs}=Ca/(Fe^{2+}+Mg+Ca+Mn)$, $X_{sps}=Mn/(Fe^{2+}+Mg+Ca+Mn)$, $X_{bi}=Fe/(Fe^{2+}+Mg)$

*Garnet*
Garnet in KS1G, K2003-1 and MAC-2 is predominantly almandine-spessartine mixtures.

*Biotite*
Biotite in all samples is relatively titanium-low, with $TiO_2$ values of 1.485-2.787 wt%. Sample 17KM05 is the most titanium-rich, 2.787 wt%. Sample K2003-1 has the lowest Cl content (0.024) and F content (0.083) compared to all other samples.

*Muscovite*
Muscovite is observed in all samples but only analysed in samples KS1G, MAC-2 and 17KM04.

*Ilmenite*
Ilmenite is observed in all samples but was only analysed in MAC-2, with 28.526 wt% titanium.

*Potassium Feldspar*
Potassium Feldspar is only observed in samples 17KM04 and 17KM05. Potassium Feldspar in sample 17KM04 is significantly more Na-rich (0.103) compared to sample 17KM05 (0.66-0.78).

## APPENDIX G: T-M$_0$ PSEUDOSECTION AND TCI RESULTS

Calculated TMo pseudosection for all samples. All fields in the diagram contain water, $H_2O$, as part of the equilibrium assemblage. Numbered circles corresponding to the assemblage occurring within the field identify fields too small to be directly labelled. Progressively darker tones are representative of increasing variance, V, where V = components – phases +2 (components = 10). The composition in mole % used to calculate the diagram, corresponding to that at M = 0 and M = 1, are provided above the diagram. FeO* = Fe + 2 x 'O'.

## Sample MAC-2

Calculated T-Mo pseudosection for sample MAC-2 contoured for the abundance ('mode') of some phases. The calculated abundance of phases in the peak assemblage field were used in conjunction with estimated abundances of minerals in the sample (Table 1) to choose an appropriate composition along the Mo axis for calculation of the P-T pseudosection. The composition used for the calculation of the P-T pseudosection, is that at Mo = 0.080, depicted as a dashed vertical line. This composition passes through the interpreted peak assemblage field.

Sample MAC-2 TMo

MnNCKFMASHTo   3.5kbar

Bulk composition (mole %)

| SiO2 | Al2O3 | CaO | MgO | FeO* | K2O | Na2O | TiO2 | MnO | O | %H2O | |
|------|-------|-----|-----|------|-----|------|------|-----|------|------|------|
| 61.18 | 13.51 | 1.70 | 4.49 | 5.05 | 2.77 | 2.70 | 0.76 | 0.15 | 0.03 | 7.72 | (x = 0) |
| 62.73 | 13.85 | 1.74 | 4.61 | 5.18 | 2.84 | 2.77 | 0.78 | 0.15 | 2.56 | 7.91 | (x = 1) |
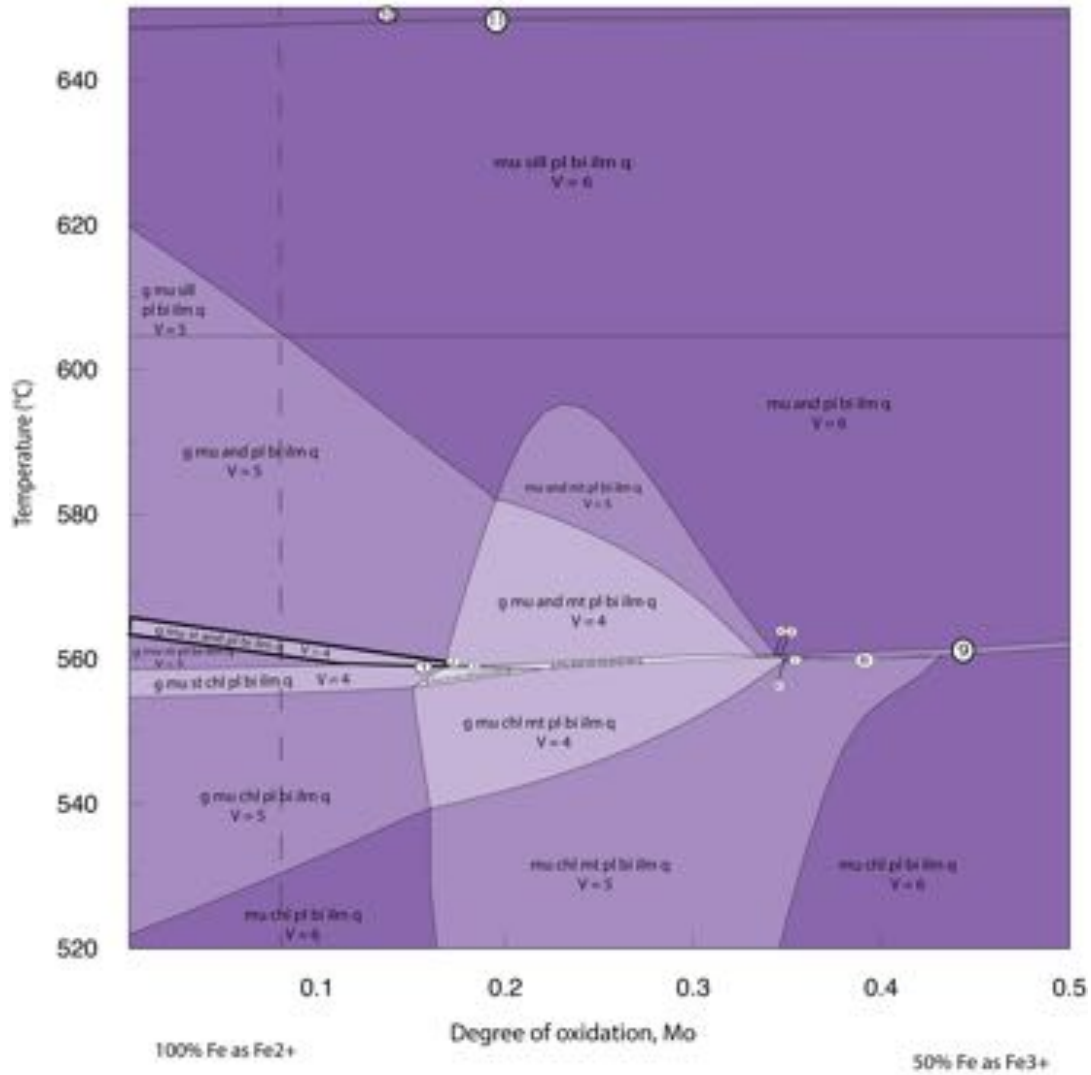
1. g mu st and chl pl bi ilm q
2. g mu st and mt pl bi ilm q
3. g mu st mt and chl pl bi ilm q
4. mu and chl mt pl bi ilm q
5. g mu and chl pl bi ilm q
6. g mu chl pl bi ilm q
7. mu chl pl bi ilm q
8. mu chl mt and pl bi ilm q
9. mu chl and pl bi ilm q
10. mu ksp sill pl bi ilm q
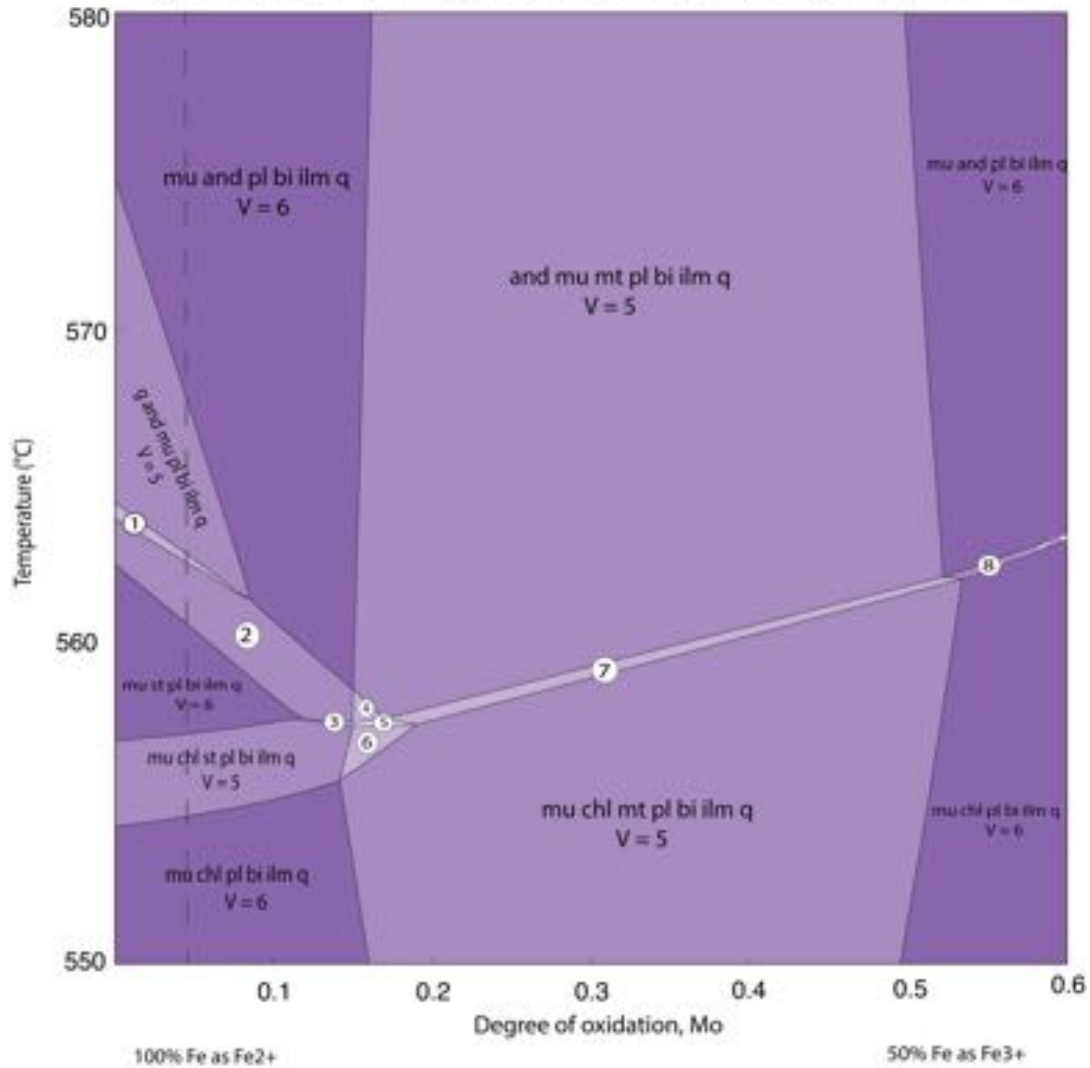11. ksp sill pl bi ilm q
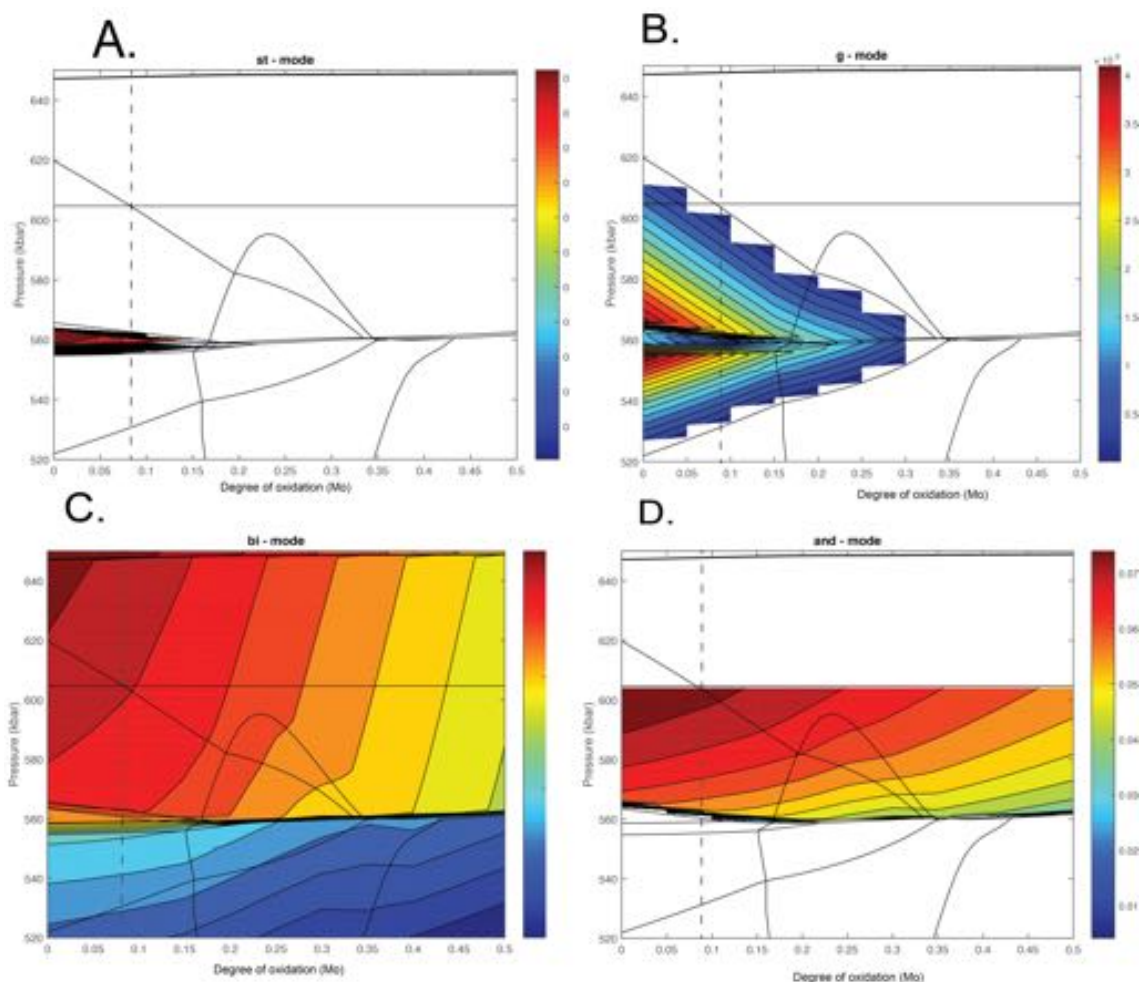
## Sample K2003-1

Calculated T-Mo pseudosection for sample K2003-1 contoured for the abundance ('mode') of some phases. The calculated abundance of phases in the peak assemblage field were used in conjunction with estimated abundances of minerals in the sample (Table 1) to choose an appropriate composition along the Mo axis for calculation of the P-T pseudosection. The composition used for the calculation of the P-T pseudosection, is that at Mo = 0.050, depicted as a dashed vertical line. This composition passes through the interpreted peak assemblage field.
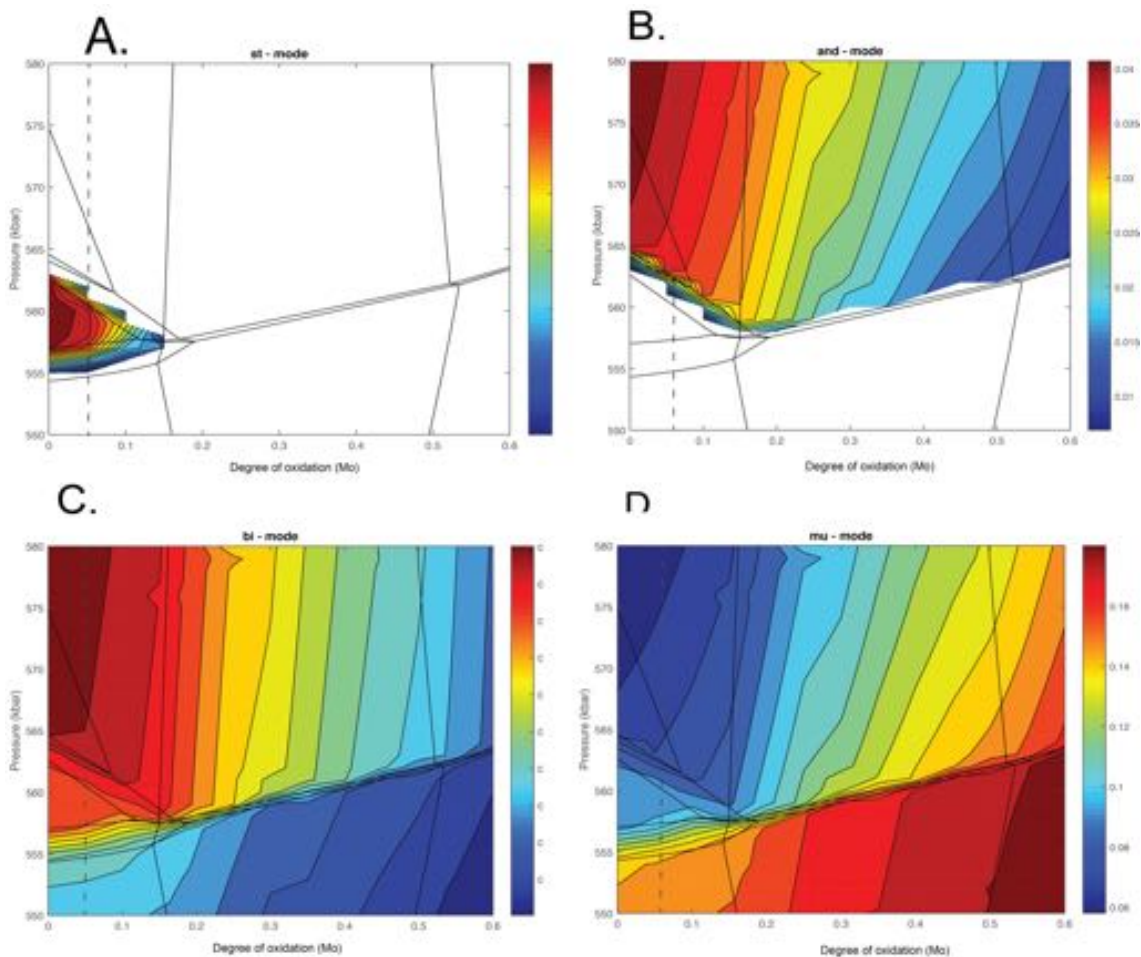
## Sample K2003-1 TMo

MnNCKFMASHTo    3.5kbar

Bulk composition (mole %)

| SiO2 | Al2O3 | CaO | MgO | FeO* | K2O | Na2O | TiO2 | MnO | O | %H2O | |
|------|-------|-----|-----|------|-----|------|------|-----|---|------|---|
| 61.75 | 11.95 | 2.98 | 4.89 | 5.17 | 2.29 | 3.02 | 0.53 | 0.09 | 0.03 | 7.36 | ( x = 0) |
| 63.35 | 12.27 | 3.06 | 5.01 | 5.30 | 2.35 | 3.10 | 0.54 | 0.09 | 2.62 | 7.55 | ( x = 1) |

1. g and mu st pl bi ilm q
2. and st mu pl bi ilm q
3. st mu chl and pl bi ilm q
4. and mu st mt pl bi ilm q
5. and mu st chl mt pl bi ilm q
6. mu st chl mt pl bi ilm q
7. mu chl and mt pl bi ilm q
8. mu chl and pl bi ilm q

## Sample 17KM04

Calculated T-Mo pseudosection for sample 17KM04 contoured for the abundance ('mode') of some phases.  The calculated abundance of phases in the peak assemblage field were used in conjunction with estimated abundances of minerals in the sample (Table 1) to choose an appropriate composition along the Mo axis for calculation of the P-T pseudosection.  The composition used for the calculation of the P-T pseudosection, is that at Mo = 0.050, depicted as a dashed vertical line.  This composition passes through the interpreted peak assemblage field.

## Sample 17KM04 TMo

MnNCKFMASHTo 3.5kbar

**Bulk composition (mole %)**

| SiO2 | Al2O3 | CaO | MgO | FeO* | K2O | Na2O | TiO2 | MnO | O | %H2O | |
|------|-------|-----|-----|------|-----|------|------|-----|---|------|---|
| 66.10 | 11.11 | 1.19 | 5.01 | 6.02 | 3.31 | 1.38 | 0.63 | 0.09 | 0.03 | 7.72 | ( x = 0) |
| 68.10 | 11.45 | 1.23 | 5.17 | 6.20 | 3.41 | 1.42 | 0.65 | 0.10 | 3.07 | 7.91 | ( x = 1) |
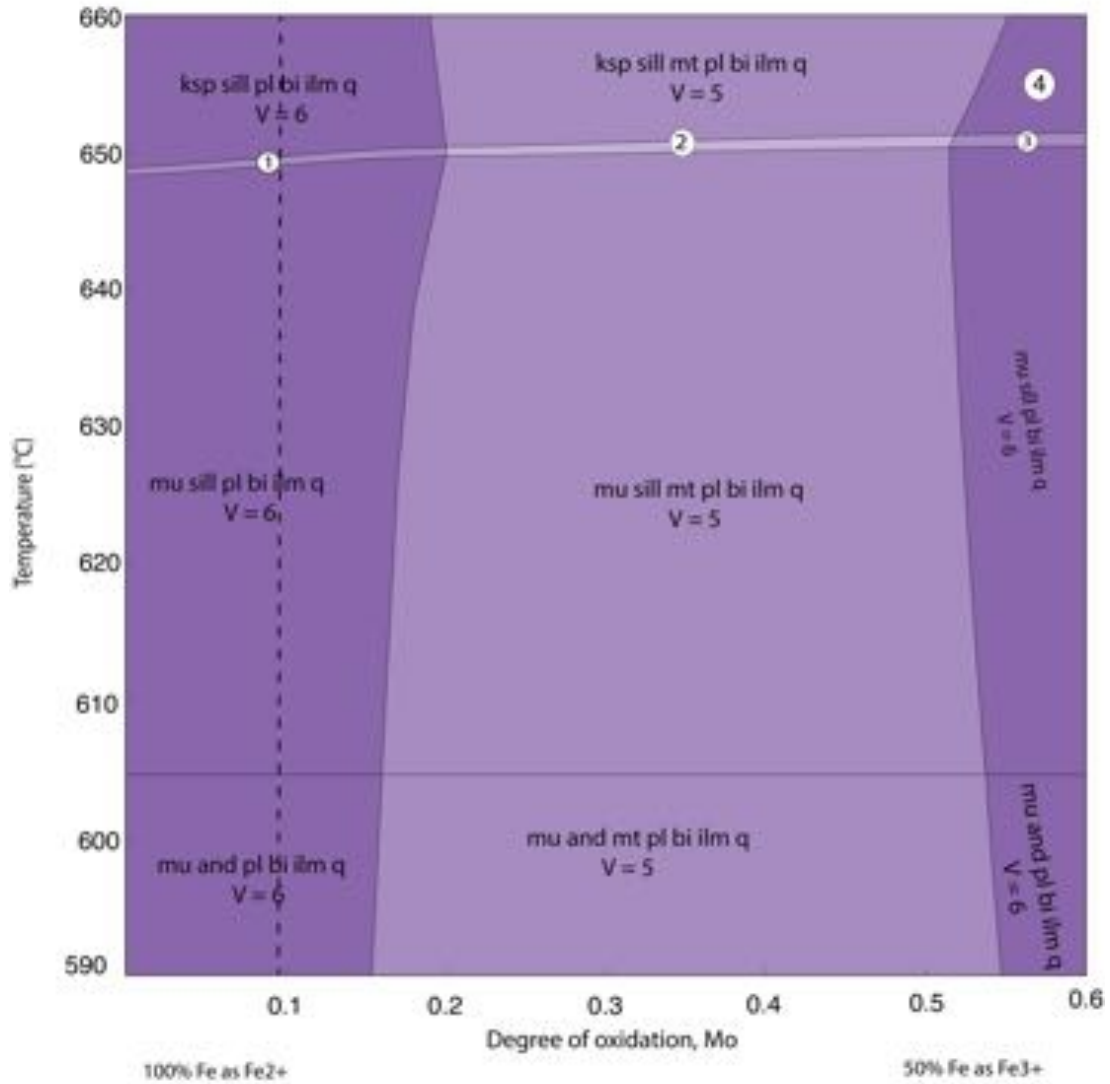
1. mu ksp sill pl bi ilm q
2. mu ksp sill mt pl bi ilm q
3. mu ksp sill pl bi ilm q
4. ksp sill pl bi ilm q